NORSAR

NORSAR Scientific Report No. 1-87/88

Semiannual Technical Summary

1 April — 30 September 1987

L.B. Loughran (ed.)

Kjeller, December 1987

REPORT DOCUMENTATION PAGE

Form Approved
OMB No. 0704-0188

1a. REPORT SECURITY CLASSIFICATION UNCLASSIFIED	1b. RESTRICTIVE MARKINGS NOT APPLICABLE
2a. SECURITY CLASSIFICATION AUTHORITY NOT APPLICABLE	3. DISTRIBUTION/AVAILABILITY OF REPORT APPROVED FOR PUBLIC RELEASE DISTRIBUTION UNLIMITED
2b. DECLASSIFICATION/DOWNGRADING SCHEDULE NOT APPLICABLE	

4. PERFORMING ORGANIZATION REPORT NUMBER(S) Scientific Report 1-87/88	5. MONITORING ORGANIZATION REPORT NUMBER(S) Scientific Report 1-87/88

6a. NAME OF PERFORMING ORGANIZATION NTNF/NORSAR	6b. OFFICE SYMBOL (If applicable) GSD	7a. NAME OF MONITORING ORGANIZATION HQ/AFTAC/TTS

6c. ADDRESS (City, State, and ZIP Code) POST BOX 51 N-2007 KJELLER, NORWAY	7b. ADDRESS (City, State, and ZIP Code) PATRICK AFB, FL 32925-6001

8a. NAME OF FUNDING/SPONSORING ORGANIZATION DEFENCE ADVANCED RESEARCH PROJECTS AGENCY	8b. OFFICE SYMBOL (If applicable)	9. PROCUREMENT INSTRUMENT IDENTIFICATION NUMBER CONTRACT NO. F08606-86-C-0004

8c. ADDRESS (City, State, and ZIP Code) 1400 WILSON BLVD. ARLINGTON, VA 22209-2308	10. SOURCE OF FUNDING NUMBERS			

		PROGRAM ELEMENT NO.	PROJECT NO.	TASK NO.	WORK UNIT ACCESSION NO.
		R&D	NORSAR PHASE 3	SOW TASK 5.0	SEQUENCE NO. 003A2

11. TITLE (Include Security Classification)
SEMIANNUAL TECHNICAL SUMMARY 1 APR - 30 SEP 1987   (UNCLASSIFIED)

12. PERSONAL AUTHOR(S)
L.B. LOUGHRAN (ED.)

13a. TYPE OF REPORT SCIENTIFIC SUMMARY	13b. TIME COVERED FROM 1 Apr TO 30 Sep 87	14. DATE OF REPORT (Year, Month, Day) Dec 1987	15. PAGE COUNT 129

16. SUPPLEMENTARY NOTATION
NOT APPLICABLE

17.	COSATI CODES		18. SUBJECT TERMS (Continue on reverse if necessary and identify by block number)
FIELD	GROUP	SUB-GROUP	NORSAR, NORWEGIAN SEISMIC ARRAY
8	11		

19. ABSTRACT (Continue on reverse if necessary and identify by block number)

This Semiannual Technical Summary describes the operation, maintenance and
research activities at the Norwegian Seismic Array (NORSAR) for the period
1 Apr - 30 Sep 87.

20. DISTRIBUTION/AVAILABILITY OF ABSTRACT ☒ UNCLASSIFIED/UNLIMITED ☐ SAME AS RPT. ☐ DTIC USERS	21. ABSTRACT SECURITY CLASSIFICATION UNCLASSIFIED
22a. NAME OF RESPONSIBLE INDIVIDUAL MAJOR JAMES A. ROBB	22b. TELEPHONE (Include Area Code) (305) 494-7665	22c. OFFICE SYMBOL AFTAC/TTS

DD Form 1473, JUN 86   *Previous editions are obsolete.*   SECURITY CLASSIFICATION OF THIS PAGE

Abstract (cont.)

The NORSAR Detection Processing system has operated throughout the reporting period with an average uptime of 98.9 per cent. A total of 1940 seismic events have been reported in the NORSAR monthly seismic bulletin. The performance of the continuous alarm system and the automatic bulletin transfer by telex to AFTAC have been satisfactory. Processing of requests for full NORSAR/NORESS data on magnetic tapes has progressed according to established schedules.

A new Detection Processing system has been implemented, providing improvements especially in the data quality checking and reduction in false detections caused by occasional data spikes. The NORSAR beam table and event processing algorithms remain unchanged. 'Processing code has been developed for on-line regional array analysis based on SUN 3 computer systems.

Field maintenance activity has included regular preventive maintenance at all subarrays and occasional corrective actions when required. No special problems have been noted in the performance of field systems. In addition, field maintenance personnel have participated in establishing the new regional array in Finnmark, Northern Norway.

A study of Pn scattering has been conducted, using as a data base NORESS recordings of six mining explosions in the Blåsjø area, at an epicentral distance of about 300 km. Wideband f-k analysis of these event recordings show a pronounced and consistent anomaly in the frequency range 2-4 Hz, which is also the frequency band of maximum Pn energy. This is found to be consistent with scattering by topographic relief of the Moho discontinuity, and the inferred location of the proposed topographic feature coincides with the border of the Oslo Graben.

A study of the effect of lateral heterogeneities on short period surface waves (T < 20 s), using numerical modelling with a coupled-mode scheme, has been initiated. So far it has been found that the coupled-local modes method can be applied to model wave propagation in realistic structures, needing a reasonable amount of lateral zones and local modes to achieve satisfactory precision in transmission and reflection coefficients. The plan is now to apply this method to laterally heterogeneous structures around Scandinavia, and compare the results of the numerical modelling to surface wave data recorded at NORSAR and NORESS.

The problem of threshold determination for regional event detection
has been investigated, addressing in particular the tradeoff between
detector sensitivity and false detections caused by noise fluctuations
of stochastic nature. It has been found that for the same false alarm
rate, thresholds of incoherent beams can be set at 4.5-7 dB lower than
for coherent beams. This implies that for Pn detection, coherent beams
will usually outperform incoherent beams, since the SNR gain is typi-
cally 8-15 dB. However, for secondary phase detection, the incoherent
beams will usually be the best, since the coherent beam gain in these
cases is much lower. A particularly promising result is that inco-
herent beamforming based on horizontal channels appears to provide
more effective noise variance reduction than is obtained using ver-
tical channels. Also a large number of noise detections can be iden-
tified as such using the slowness estimates provided by a small-
aperture array.

Initial data recorded at the new regional array in Finnmark, Northern
Norway, have been processed and compared to NORESS recordings. The
Finnmark array is found to provide the same excellent (better than $\sqrt{N}$)
noise suppression as NORESS in selected filter bands, using "optimum"
subgeometries for beamforming. The background noise level at Finnmark
is even lower than that of NORESS at high frequencies (greater than
2 Hz), but somewhat higher than for NORESS at the low frequency end,
due to closer distance from the coast. A feature of Finnmark recor-
dings not seen at NORESS is the presence of strong Rg phases for
mining explosions out to about 350 km epicentral distance. A two-week
test period of joint processing of the two arrays has shown that the
large majority of small events ($M_L < 2.0$) are detected by only one
array, whereas larger events ($M_L \geqslant 2.0$) detected by either array in most
cases have at least one confirming phase detection from the other
array.

Analysis of P coda and Lg phases recorded at NORSAR for a set of 72
large explosions from the Shagan River test area near Semipalatinsk,
USSR, has shown that such data can provide event magnitude estimates
comparable in stability to world-wide network m_b. A systematic dif-
ference in $m_b(P) - m_b(Lg)$ has been observed for the northeast and south-
west portion of the Shagan River test area. There are indications that
this is mainly due to a bias in $m_b(P)$ estimates, and if so, the $m_b(lg)$
values observed at NORSAR would be expected to give more reliable
relative yield estimates than can be obtained from P-wave data.

A large-scale study comprising NORESS recordings of 101 events from
the North Sea/western Norway region has been conducted with the aim to
determine optimum beam deployment for regional phase detection. The
study has reconfirmed that a number of narrow band filters applied in

parallel and in combination with array beams based on filter-dependent subgeometries produce the best detection performance. In particular, the study has demonstrated the usefulness of high-frequency (10-16 Hz) coherent beams for Pn phase detection. It has furthermore been shown that high frequency incoherent beams (10-16 Hz) formed from horizontal channels significantly enhance detectability of Sn phases. The best results in Lg phase detection are found for low frequency incoherent beams (1.5-4.5 Hz) combining both horizontal and vertical channels. Further work will in particular be directed toward analyzing events from other regions in order to determine a beam deployment that provides optimized detection in the entire regional distance range.

The local geology of the two regional array sites in Norway has been studied, with emphasis on compiling information that is considered relevant from a seismological viewpoint. At this stage, the main purpose has been to present results of various surveys conducted by the Norwegian Geological Survey and NORSAR scientists. In the future, this information is expected to become useful in explaining observed features in the recorded seismograms from the two arrays.

AFTAC Project Authorization   :   T/6141/B/PMP

ARPA Order No.   :   4138

Program Code No.   :   OF10

Name of Contractor   :   Royal Norwegian Council
for Scientific and
Industrial Research

Effective Date of Contract   :   1 October 1985

Contract Expiration Date   :   30 September 1987

Project Manager   :   Frode Ringdal (06) 81 71 21

Title of Work   :   The Norwegian Seismic Array
(NORSAR) Phase 3

Amount of Contract   : $ 1,509,253.00

Contract Period Covered by the Report   :   1 Apr - 30 Sep 1987

NORSAR Contribution No. 383

TABLE OF CONTENTS

I.   SUMMARY

This Semiannual Technical Summary describes the operation, maintenance
and research activities at the Norwegian Seismic Array (NORSAR) for
the period 1 April - 30 September 1987.

The uptime of the NORSAR online detection processor system has
averaged 98.9 per cent during the reporting period as compared to 99.6
for the previous period. 04C and 06C have been the most frequently
affected systems due to cable damage (04C) and synchronization
problems (06C). A total of 1940 seismic events were reported in the
NORSAR monthly seismic bulletins in this period, giving a daily
average of 10.6 events.

The new Detection Processor (DP) was put into routine operation on day
289. The detector program is executing on the IBM 4341/L01 computer
for the NORSAR array. There are no changes in the beam table. From day
320, the MODCOMP processor has been doing data acquisition only, as
the beamforming and filtering tasks have been moved to the IBM 4341.
The new detection process has lead to a significant reduction in load
on the event processor, due to a greatly reduced number of "spike"
detections. There are no changes in the event processor code. There
are also no changes in the 'online' RONAPP detection processing for
the NORESS array, but the new detector package now being used for
NORSAR has also been applied to NORESS data and is executing regularly
on tapes with data from the new Finnmark regional array.

A new program, SEGPRO - Segmented processing, has been developed to do
the onset determination as well as phase velocity and azimuth measure-
ments on detections reported from the new detector package, on a

routine basis. A new event processor code is under development to process NORESS and Finnmark array data.

The data acquisition and real-time processing systems for the new Finnmark array will be based on three Sun 3 computers. The IBM/PC currently used for controlling critical tasks in the NORSAR/NORESS systems will also be used for the new array.

Much time and effort has been spent by the field maintenance personnel on preparatory work in connection with the new array in Finnmark, and the actual installation of the array required extensive field work during the summer of 1987.

The research activity is summarized in section VII. Section VII.1 presents a scattering model of regional P_n wave propagation. Section VII.2 describes preliminary tests for surface waves in 2-D structures. In Section VII.3 false alarm statistics and threshold determination for regional event detection are presented. Section VII.4 gives initial results from analysis of data recorded at the new regional array in Finnmark. In Section VII.5 the potential of using NORSAR recorded P coda and Lg waves to obtain stable magnitude estimates of large Semipalatinsk explosions is investigated. Section VII.6 describes investigations of optimum beam deployment for NORESS using a North Sea/ western Norway data base. In Section VII.7 the local geology of the regional array sites in Norway is presented.

II.   OPERATION OF ALL SYSTEMS

II.1   Detection Processor (DP) Operation

There have been 88 breaks in the otherwise continuous operation of the NORSAR online system within the current 6-month reporting interval. The uptime percentage for the period is 98.9 as compared to 99.6 for the previous period.

Fig. II.1.1 and the accompanying Table II.1.1 both show the daily DP downtime for the days between 1 April and 30 September 1987. The monthly recording times and percentages are given in Table II.1.2.

The breaks can be grouped as follows:

a)   Hardware failure   4
b)   Stops related to program work or error   0
c)   Hardware maintenance stops   6
d)   Power jumps and breaks   5
e)   TOD error correction   6
f)   Communication lines   67

The total downtime for the period was 50 hours and 26 minutes. The mean-time-between-failures (MTBF) was 2.5 days, as compared to 2.0 for the previous period.

J. Torstveit

Month	DP uptime hours	DP uptime %	No. of DP breaks	No. of days with breaks	DP MTBF* (days)
APR	713.60	99.1	37	13	0.8
MAY	718.35	96.5	7	6	3.7
JUN	714.27	99.2	14	8	2.0
JUL	743.75	99.9	8	6	3.4
AUG	738.40	99.3	13	8	2.2
SEP	713.20	99.1	9	8	3.0
		98.9	88	49	2.5

* Mean-time-between-failures = total uptime/no. of up intervals.

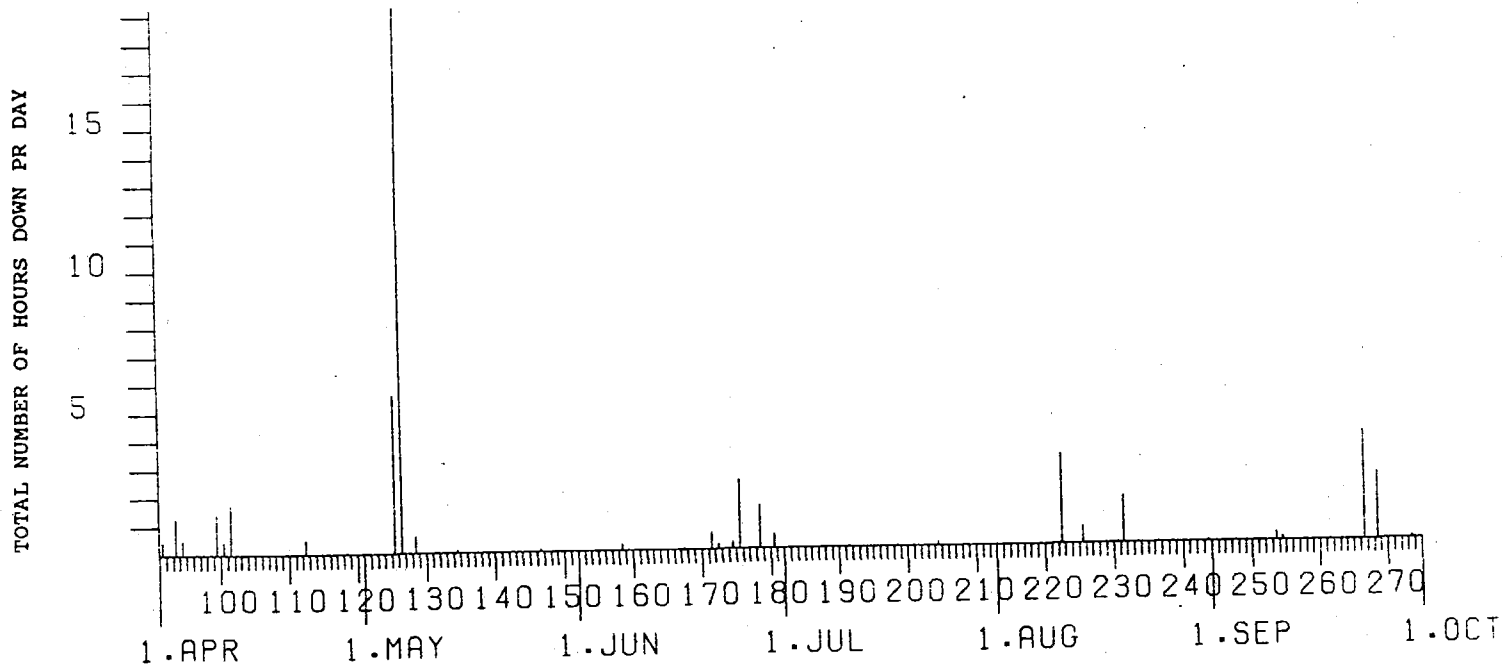Table II.1.2 Online system performance, 1 April - 30 September 1987.

Fig. II.1.1   Detection Processor downtime in the period 1 Apr - 30 Sep 1987.

LIST OF BREAKS IN DP PROCESSING THE LAST   HALF-YEAR

DAY	START		STOP		COMMENTS...........	DAY	START		STOP		COMMENTS...........
91	0	59	1	3	LINE FAILURE	101	9	26	9	57	LINE FAILURE
91	2	3	2	11	LINE FAILURE	101	10	57	11	0	LINE FAILURE
91	3	11	3	14	LINE FAILURE	101	12	7	12	10	LINE FAILURE
91	3	28	3	30	LINE FAILURE	101	12	22	12	30	LINE FAILURE
91	4	31	4	39	LINE FAILURE	111	6	1	6	2	TOD RETARED 6MS
91	5	40	5	42	LINE FAILURE	112	5	32	6	2	POWER BREAK
92	11	5	11	6	LINE FAILURE	118	6	3	6	4	TOD RETARED 10MS
93	20	6	20	26	LINE FAILURE	125	18	24	24	0	MODCOMP FAILURE
93	21	34	21	48	LINE FAILURE	126	0	0	19	17	MODCOMP FAILURE
93	22	28	23	10	LINE FAILURE	127	6	14	6	15	LINE FAILURE
94	0	18	0	35	LINE FAILURE	128	12	6	12	40	POWER BREAK
94	1	38	1	51	LINE FAILURE	134	8	42	8	48	LINE FAILURE
96	7	43	7	44	LINE FAILURE	146	6	1	6	2	LINE FAILURE
97	13	9	13	10	LINE FAILURE	146	6	19	6	20	LINE FAILURE
98	12	20	12	21	LINE FAILURE	146	10	44	10	47	LINE FAILURE
99	6	42	6	43	LINE FAILURE	158	8	27	8	29	LINE FAILURE
99	11	55	12	21	SERVICE NODCOMP	158	12	33	12	35	LINE FAILURE
99	12	27	12	28	LINE FAILURE	158	18	50	18	55	LINE FAILURE
99	21	23	21	40	LINE FAILURE	158	19	10	19	13	LINE FAILURE
99	23	2	23	43	LINE FAILURE	167	6	2	6	3	LINE FAILURE
100	0	18	0	40	LINE FAILURE	171	23	24	24	0	MODCOMP FAILURE
100	6	1	6	2	TOD RETARED 6MS	172	0	0	0	11	MODCOMP FAILURE
100	21	49	21	52	LINE FAILURE	174	7	33	7	48	LINE FAILURE
101	0	10	0	27	LINE FAILURE	175	6	55	9	22	WORK ON POWERLINE
101	1	28	1	35	LINE FAILURE	178	10	46	11	26	LINE FAILURE
101	2	35	2	45	LINE FAILURE	178	13	28	14	20	POWER BREAK
101	4	56	5	9	LINE FAILURE	180	12	44	12	45	LINE FAILURE
101	6	9	6	12	LINE FAILURE	180	14	35	14	39	LINE FAILURE
101	7	12	7	15	LINE FAILURE	180	14	46	15	8	LINE FAILURE
101	8	15	8	21	LINE FAILURE	180	18	34	18	37	LINE FAILURE

Table II.1.1   Daily DP downtime in the period 1 Apr - 30 Sep 1987.

9

```
LIST OF BREAKS IN DP PROCESSING THE LAST     HALF-YEAR
DAY     START       STOP       COMMENTS...........

187      6     2     6     3  LINE FAILURE
188      6    24     6    25  LINE FAILURE
191      9    19     9    21  LINE FAILURE
194      6     3     6     4  LINE FAILURE
194      6     7     6     8  LINE FAILURE
198      6     1     6     2  LINE FAILURE
198      6    12     6    13  LINE FAILURE
204     11    30    11    37  CE SERVICE
222     11     0    11    16  MODCOMP FAILURE
222     11    20    14    14  MODCOMP FAILURE
225      7    44     7    45  TOD RETARED 10MS
225      9     7     9    42  CE MAINTENANCE
230      6    34     6    35  LINE FAILURE
230      6    39     6    40  LINE FAILURE
231     10    50    12    31  CE MAINTENANCE
232      6    47     6    48  LINE FAILURE
233      6     7     6     8  TOD RETARED 12MS
236      8     6     8     7  LINE FAILURE
236      8    21     8    22  LINE FAILURE
243      6    18     6    19  LINE FAILURE
243      6    23     6    25  LINE FAILURE
247      6    32     6    33  LINE FAILURE
250      6     0     6     2  LINE FAILURE
253     13    19    13    33  POWER BREAK
253     15    22    15    25  LINE FAILURE
254      5    56     6     3  LINE FAILURE
261      6     0     6     2  TOD RETARED 14MS
266     11     0    14    53  CE SERVICE MODCOMP
268     11     0    13    22  CE SERVICE MODCOMP
273      5    22     5    26  LINE FAILURE
```

Table II.1.1 (cont.)

II.2   Array communications

Table VII.2.1 reflects the systems performance in the reporting period.

04C and 06C have been the most frequently affected systems due to cable damage (04C) and synchronization problems (06C).

The communication machine (Modcomp) has failed two times, in May and September, a voltage and a "Floating point processor" failure, respectively. The latter failure caused problems during the restarting phase.

Summary

Apr   In April most systems were affected especially in connection with our attempts to localize the noise source common to all communication channels. Systems were switched off one by one, but also in groups of 2 and 3. Later NTA/Hamar and Lillestrøm did observations which revealed noise in the transmission channel equipment between Hamar and Oslo. NTA switched to a spare channel group which for a period gave us improved performance.

May   Apart from 06C which was affected weeks 19, 21 and 22 causing 0.5% outages, the systems were most reliable in May. The high error figures were caused by a Modcomp failure week 19, representing an outage of approx. 15.4% that week. Figures in brackets represent system performance/reliability exclusive Modcomp failure (see Table II.2.1).

Jun   In spite of varying line quality at 06C weeks 25 and 26 and
relatively high error figure (9.5%) this period may be
characterized as satisfactory for the remaining systems,
although a 0.21% error figure at 04C could have been better.

Jul   Defective cable between Berge Central and the 04C CTV was a
problem. Roadwork was going on in the 04C area, affecting the
communication cable which had to be cut/spliced at different
places along the path. NTA, who was responsible for the cable
work, assumed (by the end of the month) that it would take
another 2-3 weeks before the work could be finished.

02C (8.2% outages) was frequently affected, but NTA did not
localize the irregularity.

06C communication system had synchronization problems which
may have been a result of a "stressed" Modcomp, caused by
04C.

High performance by the remaining systems.

Aug   Week 35 NTA finished the cable work at 04C, and the error
figures decreased to 0.06% that week.

NTA was told to check the 06C communication line thoroughly.
Outages occurred frequently, but the station was back in
operation after restarting the Modcomp.

Most satisfactory performance of the other systems.

Sept   After the cable work finished week 34, 04C communication
system functioned most satisfactorily the three following
weeks (35, 36, 37), but 16 September data again disappeared.
After a temporary repair the system was back in operation 23
September. Between 24 and 28 September the performance was bad.

06C pattern did not change compared to July/August. Resynchronization is possible and brings the system up again.

The NMC staff will as soon as they have finished the installation of the new array in Finnmark check relevant equipment (power, modem, Loop Control, Logic, etc.), which may be carried out in conjunction with NTA/Hamar and the NDPC staff.

O.A. Hansen

Sub-array	APR 87 (5) (30.3-4.5)	MAY 87 (4) (4-31.5)	JUN 87 (4) (1-28.6)	JUL 87 (5) (29.6-2.8)	AUG 87 (4) (3.30.8)	SEP 87 (4) (31.8-27.9)	Average ½ yr
01A	1.18	*3.85 (0.004)	0.05	0.01	0.05	0.05	0.86 (0.22)
01B	0.03	*3.85 (0.002)	0.10	0.01	0.04	0.05	0.68 (0.04)
02B	3.29	*3.84 (0.005)	0.05	0.02	0.05	0.05	1.21 (0.57)
02C	*7.90	*3.84 (0.002)	0.05	*8.22	0.04	0.04	3.35 (2.71)
03C	2.55	*3.84 (0.004)	0.04	0.02	0.04	0.03	1.08 (0.44)
04C	*81.08	*3.85 (0.003)	0.21	*51.91	*49.59	*33.50	36.69 (36.05)
06C	*13.98	*4.34 (0.50)	*9.49	*22.99	*30.75	*27.36	18.15 (17.51)
AVER	15.71	3.91	1.48	11.88	11.51	8.72	8.86 (8.22)
Less	04C,06C 2.99 02C,04C,06C	Modcomp failures	04C	02C,04C 06C	04C,06C	04C,06C	04C,06C 04C, 06C
	1.76	0.07	0.08	0.01	0.04	0.04	1.43 (0.80)

* see item II.2 regarding figures preceded by an asterisk.

Table II.2.1   Communications performance. The numbers represent error rates in per cent based on total transmitted frames/week (1 Apr - 30 Sep 1987).

III.   ARRAY PERFORMANCE

Event Processor Operation

In Table III.1 some monthly statistics of the Event Processor operation are given:

	Teleseismic	Core Phases	Sum	Daily
APR 87	264	69	333	11.1
MAY 87	254	62	316	10.2
JUN 87	275	60	335	11.2
JUL 87	332	85	417	13.5
AUG 87	205	57	262	8.5
SEP 87	210	67	277	9.2
	1540	400	1940	10.6

Table III.1 Event Processor Statistics, April - September 1987.

B. Paulsen

IV   IMPROVEMENTS AND MODIFICATIONS

IV.1   NORSAR detection processing

The 'new' NORSAR detection processor was put into routine operation on day 289, after a long period of parallel processing for verification.

The change to the new detection processor was done under a period of bad data conditions. Three subarrays were temporarily out of order, and many communication errors were present. However, these bad data conditions were exploited to gain valuable experience with the data quality control part of the system. We now have a program system that controls all bad data conditions due to communication errors and resynchronizations. Moreover, the data quality control procedure is changed from treating only the special features of the NORSAR array to a more general parameterized control routine. This routine performs data control on the NORSAR, NORESS and new Finnmark arrays using the same program code for all arrays.

The output from the detector system is in the form of accumulated sequential files. One file gives a list of detections, another gives a list of 'events' from the data quality control part. Data quality control reporting includes time and length of data gaps for individual channels and for the array due to communication errors and/or recording gaps. Moreover, spikes are reported if detected, using max. amplitude comparison between one sensor and the average or median value of all sensors. (Other parameterized procedures may also be selected). Using this procedure, spikes of significant amplitudes are effectively removed.

The detector program is executing on the IBM 4341/L01 computer for the NORSAR array. There are no changes in the beam table. Coherent

beams 1 - 180 and incoherent beams 1 - 64 are directed as before
(Beam tables 451 and 271, respectively).

To reduce computer power requirements, the band pass filtering is
done using a 20 Hz sample rate, whereas the array beamforming is done
using 10 Hz sampling. This reduction in sample rate has in practice
shown no degradation of the signal-to-noise ratio within the frequency
bands used. We even get a better performance relative to the 'old'
system where the beamforming was done using two steps: Firstly,
subarray beamforming was done using a small set of beams, and then
array beamforming was done using this set of subarray beams. The new
detector forms array beams using all sensors, with individual delays
for all beams, thus obtaining a better signal-to-noise ratio.

The 4341 computer executes MODCOMP communication, data recording task,
detection processing, event processing and AFTAC telex message
handling for the NORSAR array. For 60 seconds of data, the computer
spends on the average 50 seconds of elapsed time to execute all these
processes. The detection processor runs in a mode where it takes a
3-minute break every time it catches up with real time.

In this mode, close to real time, the program may execute for several
weeks without interruptions. For this reason, the detector system has
a built-in task which may communicate externally, and performs file
management without interrupting the continuity in the data or the exe-
cution of the program. However, the detector program has so far been
stopped every 7 days to do manual maintenance of output files and
backup. (The "old" online disk loop with data and detection lists is
maintained.)

IV.2   MODCOMP subarray communication

From day 320, the MODCOMP processor has been doing data collection only, as subarray beamforming and filtering was removed from the code. The removing of subarray beamforming and filtering has relieved the CPU comsumption on the MODCOMP, leading to a much better perfor-mance on handling the SLEM communication.

IV.3   NORSAR event processing

The new detection process has lead to a significant relief on the event processor, as most of the 'bad data events' are removed.

There are no changes in the event processor code.

An actual improvement in automatic processing results requires a new time delay correction data base.

IV.4   NORESS detection processing

There are no changes in the 'online' RONAPP detection processing, but the new detector package now being used for the NORSAR array pro-cessing has also been applied to NORESS data and gives results inden-tical to those of RONAPP. Potential gain in detection capabilities using extended beam sets for NORESS are discussed elsewhere in this report.

IV.5   Finnmark regional array detection processing

The detector package now being used for the NORSAR array data is now executing regularly on tapes with data from the new Finnmark regional array. Results from this detection processing are given elsewhere in this report.

IV.6   NORESS/Finnmark array event processing

There are no changes in the event processing for NORESS data. The event processing consists of phase identification, phase association and event epicenter determination, and subsequent plotting of relevant data and f-k spectra.

A new program, SEGPRO - Segmented processing, has been developed to do the onset determination as well as phase velocity and azimuth measurements on detections reported from the new detector package, on a routine basis. The SEGPRO package is regularly processing Finnmark array data. The detector and the SEGPRO package together perform all RONAPP functions, and are using the same data interface routines. This means that the programs may use data from disk loops, tape, disk files or any other media or format that is supported.

A new event processor code is under development to process NORESS and Finnmark array data using these routines. The processor will use the SEGPRO output files for detection parameters and f-k matrices, thus preparing for a complete replacement of RONAPP.

The NORSAR and NORESS/Finnmark array event processors differ too much to have a common program, but much individual coding for subprocesses is common to all packages. The main topic for event processor development will be code structuring.

Processes involving file management, plotting and computations will be separated to form smaller entities. This is done both in order to get smaller general purpose routines and to identify and separate codes that may be machine dependent.

IV.7   Hardware to be installed for processing of data from the new
Finnmark, northern Norway, regional array

Fig. IV.7.1 shows how the data processing equipment proposed in conjunction with the newly installed regional array in Finnmark, Norway, will be integrated into and networked with already existing resources at NORSAR's Data Processing Center at Kjeller. The data acquisition systems for the NORSAR and NORESS arrays (not shown in this figure) are integrated into the total system in similar ways.

The data acquisition and real-time processing systems (termed FRS online in the figure) for the new Finnmark array are based on three Sun 3 computers. The bottom Sun 3/260 is interfaced to a CIM (Communication Interface Module) which receives data from the Finnmark field system using a dedicated satellite link. The communication protocol used is SDLC, which is also used for the NORESS installation. The CIM system can buffer up to 20 minutes of data. In normal operation, data are sent on to the Sun system without delays.

Recording of both high frequency (HF) and array data from the new Finnmark site will utilize disk loops that can hold 84 hours of array data and also 84 hours of HF data. One disk drive will be assigned to each of the two data types. The Sun 3/260 computer that handles the data acquisition task will also be running a state-of-health program to verify data quality and generate statistics on uptime, communication errors and calibration results. All data will be permanently archived on tapes, in the NORESS format.

Data contained in the disk loops will be generally accessible using NFS. The data will also be accessible from the IBM system using NORSAR's network software for reading files that are stored on computers in the network.

The other Sun 3/260 system in the "FRS online"-box of Fig. IV.7.1 will be used for real-time processing and subsequent plotting of data. Relevant plots will be produced on the Versatec system. This Sun 3/260 computer is configured in exactly the same way as the acquisition computer, so it can act as a backup for the acquisition task.

The Sun 3/110 will be used for quality checking and array monitoring purposes.

The IBM/PC is the system currently being used for controlling critical tasks in the NORSAR/NORESS system. This system automatically calls the operator on duty in case of system failures. The FRS online system will be integrated into this alarm system. PC/NFS will be used to read current status directly from files stored in the Sun online system.

The third SUN 3/260 system will be used for data exchange, data analysis and program development.

In addition to these four Sun computers, our hardware proposal contains another two Sun 3/60 systems and a Sun 3/50 computer (only one of the Sun 3/60 systems is shown in the figure). These systems will be available in the network as general purpose work stations.

J. Fyen
T. Kværna
B. Paulsen
R. Paulsen
S. Mykkeltveit

ETHERNET 10 Mbit

SUN 3/60

300 Mb

SUN 3/260 C16

X.25

μVAX

X.25

SUN 3/110 LC4

IBM PC

Laser

Cart.

1600/6250

Cart.

71 Mb

Laser

EXA BYTE

IBM 4381 PO2

PRONET RING 10 Mbit

ARPA NET

7.5 Gb

800/1600/ 6250

SUN 3/260 S16

1600/6250

1.3 Gb

700 Mb

1.3 Gb

MUX

11"

24"

VERSATEC

SUN 3/260 S16

1600/6250

1.3 Gb

FRS CIM

64 Kb

1.3 Gb

– 19 –
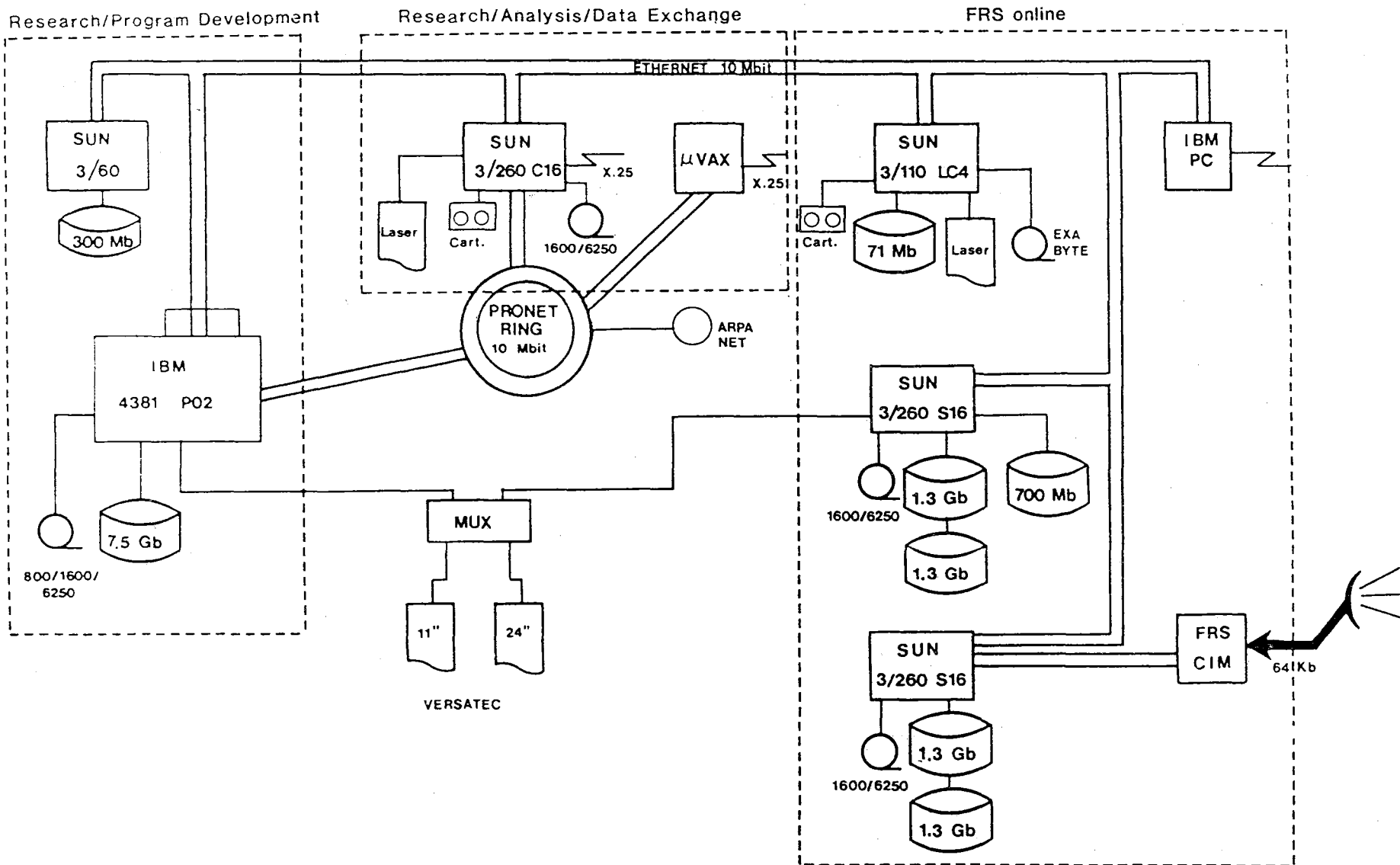
Fig. IV.7.1   The figure shows how the equipment for processing data from the new Finnmark regional array will be integrated into existing equipment at NORSAR's data processing center. Note that the current NORSAR/NORESS data acquisition system (based on IBM 4341 computers) come in addition to this figure.

V.   MAINTENANCE ACTIVITIES

V.1   Activities in the field and at the Maintenance Center

Much time has been spent on preparatory work in connection with the new array in Karasjok, Finnmark, and finally weeks were spent on the installation itself.

In spite of this extensive task, corrective maintenance has, in a few cases, been carried out in the NORSAR array. Otherwise, visits have been limited to occurrences of more acute character, such as power failure, localization of cables which otherwise most certainly would have been damaged by excavators.

NORESS has been visited and corrective actions carried out.

A cable connection between the HF-equipment and the multiplexer (Megamux) has been replaced by a fiber optic link.

Blåsjø has been visited and corrective maintenance carried out.

At the NDPC, NORSAR communication circuits have been regularly checked.

The NORSAR subarray electronics have been checked and monitored regularly.

A summary of the activities performed during the period is given in Table V.1. For completeness we list activities carried out for all systems, i.e., NORSAR, NORESS, Blåsjø and the new array in Karasjok.

O.A. Hansen

Subarray/ area	Task	Date
NORSAR	P.W. Larsen attended a project meeting with Sandia in connection with the new Finnmark array.	14 Apr
Karasjok	P.W. Larsen participated in a survey in Karasjok together with representatives from Sandia.	15,16 Apr
NORSAR	P.W. Larsen attended a meeting at NORSAR together with the project manager and Barlindhaug A/S, the consultants	28 Apr
Oslo	NMC staff participated in a fiber optic course.	27-30 Apr
NORESS	Repaired a DHL 70 card for site AO	21 Apr
NDPC	Daily routine check of SP/LP data. Weekly calibration of SP/LP seismometers. Daily check of communication systems.	April
04C	P.W. Larsen met representatives from NTA/ Hamar and road administration 2 May in the 04C area to clarify responsibilities in connection with 04C communication cable rerouting.	2 May
06C	Replacement of the vertical long period centering device (RCD), incl. adjustments	19,20,21 May
NORESS	NMC staff assisted representatives from Sandia Nat. Lab. (Dick Kromer) in connection with replacing the cable between HF-equipment and the Megamux with a fiber optic link connection.	19,20,21
NMC	Continued planning and preparation in connection with the Finnmark array.	May
NDPC	Daily check of SP/LP data. Weekly calibration of SP/LP seismometers. Daily checks of communication systems.	May

Subarray/ area	Task	Date
01B (05)	Cable localized in connection with excavation damage.	16 June
01B (03)	In connection with trenching, cable pointed out.	24 June
02B (04)	Cable pointed out.	17 June
04C (02)	Cable pointed out.	19 June
06C (03)	Cable work.	17,18,22 June
Karasjok	Survey in connection with the new array.	11-15 June
Blåsjø	Various repair and maintenance work carried out.	16-20 June
NORESS	A fiber connector repaired at site C2	27 June
NDPC	SP/LP daily checks. Calibration of SP/LP seismometers weekly. Daily control of communication systems.	June
02B (tel.)	Corrective maintenance performed.	21,23 July
04C (03)	Cable localized.	29 July
06C (04)	Found damaged cable.	30 July
Karasjok	P.W. Larsen attended a meeting in Alta regarding contractual relations.	6 July
Karasjok	P.W. Larsen visited Karasjok in connection with start of the construction work (main building and cable trenching).	14-17 July
FINESA	Visited and expanded the array with 5 new C-points.	29 July
NDPC	Daily check of SP/LP data. Weekly calibration of SP/LP seismometers. Daily control of the communication systems.	July

Subarray/ area	Task	Date
06C	Visit in connection with damaged cable.	7 Aug
01B	Visit in connection with damaged cable.	12 Aug
NDPC	Daily check of SP/LP data. LP seismometers continuously checked with regard to mass position (MP), and free period (FP). Adjustment carried out when outside specifications. Communication systems checked daily.	Aug
Karasjok	NMC staff engaged in the new Finnmark array throughout the period.	Sept
NDPC	In addition to ordinary daily/weekly checks/ tests, the A/D converters of all the data acquisition equipment (SLEMs) have been checked with respect to their ability to reproduce correct numbers.	Sept

Table V.1 Activities in the field and at the NORSAR Maintenance
Center, including NDPC activities related to the NORSAR
array, 1 Apr - 30 Sep 1987.

V.2   Improvements and modifications (NORSAR array)

No changes since last reporting period.

V.3   Array status

As of 30 Sept. 87 the following channels deviated from tolerances:

        01A 01   8 Hz filter
            02   -"-
            04   30 dB attenuation

```
01B    05
       08

04C    01
       08

06C    04
       05    Broadband filter installed.
       08
```

O.A. Hansen

VI.   DOCUMENTATION DEVELOPED

Bache, T.C., S.R. Bratt and H. Bungum (1986): High-frequency
     attenuation along 5 teleseismic paths from Central Asia,
     Geophys. J.R. astr. Soc., 85, 505-522.

Loughran, L.B. (ed.): Semiannual Technical Summary, 1 October 1986 -
     31 March 1987, NORSAR Sci. Rep. No. 2-86/87, Kjeller, Norway.

                                  L.B. Loughran

VII SUMMARY OF TECHNICAL REPORTS / PAPERS PREPARED

VII.1 A scattering model of regional P_n wave propagation

The P_n phase is crucial for the detection and location of regional
events. It is therefore important to determine its characteristic
properties. The properties of P_n are well understood in one-
dimensional crust-mantle models: P_n is an ordinary head wave asso-
ciated with the Moho in models of uniform plane layers and P_n can be
interpreted as a sum of whispering gallery waves forming a so-called
interference head wave in models of spherical layers and/or models
having a positive velocity gradient below the Moho (Menke and
Richards, 1980). The phenomenon of the whispering gallery can explain
the relatively long duration and high frequencies of P_n at teleseismic
distances. However, it cannot explain the often observed relatively
large amplitudes in the later part of the signal. Similar charac-
teristics are observed at regional distances. To determine the cause
of these characteristics we have analyzed in some detail the NORESS
records of P_n from a suite of 6 mining explosions in the Blåsjø area.
The explosion site is about 300 km from NORESS in an azimuth direction
of 240°. A typical record section of P_n from these explosions is shown
in Fig. VII.1.1.

It can be seen that the first arrival is relatively weak. In fact,
this arrival is easily missed for small events, whence P_n is often
associated with the dominant part of the wave train. We have applied
wide-band f-k analysis (Kværna and Doornbos, 1986) to the P_n wave
trains from all 6 events. Slowness solutions as a function of fre-
quency are summarized in the velocity-azimuth spectrum of Fig.
VII.1.2. The solutions show a pronounced and consistent anomaly within
the range 2-4 Hz; this is also the range where the signal has its
maximum energy (Fig. VII.1.3). From an analysis of slowness as a func-
tion of time (Fig. VII.1.4 displays the results for one of the events)

we infer that the first arrival has a slowness and azimuth consistent with P_n in a one-dimensional crust-mantle model, and the anomaly is related to wave energy being delayed by about 0.5-0.6 seconds. The anomaly cannot be generated locally near the surface since this would significantly perturb the wave front; the wavenumber solution shows that the wave front is in fact very nearly plane. The observational results suggest that these "P_n" waves are actually the result of scattering at depth. Ray tracing backward in the direction given by the measured slowness leads to the result that the 0.5-0.6 s time delay is explained by a scattering source within the depth range 30-40 km. The Moho here is usually taken to be at about 35 km depth. Hence the observational results are consistent with scattering by topographic relief of the Moho. An interesting geological aspect is that the inferred location of the proposed topographic feature, 70 km from NORESS in the southwest direction, coincides with the border of the Oslo Graben.

Scattering will of course affect all waves interacting with a rough Moho discontinuity. However, the scattered waves usually arrive in the coda of a relatively strong primary wave. In contrast, the first arriving P_n is relatively weak due to the small coefficient of refraction through the Moho, and scattering due to topography of the boundary may dominate the wave train.

To illustrate these concepts, we can apply a recently developed method for modelling scattering by topographic relief (Doornbos, 1988). The first applications of this method concerned the relatively complicated case of a solid-liquid boundary. We have done some numerical experiments with a liquid layer over a solid half space, letting velocities and densities correspond to values in the crust and mantle. One of the results is given in Fig. VII.1.5. Here we have assumed a boundary

topography characterized by a correlation length of 6 km and an average height of 1 km, and the wave field is taken monochromatic at 2 Hz. The figure shows energy flux of P transmitted upward through the boundary, as a function of slowness of incident P. Two modes of scattering are shown: (1) The specular flux E^O in the direction defined by the plane wave-plane interface concept. The specular flux through a rough interface is reduced with respect to the flux through a plane. (2) The diffuse flux E^{SC} due to multiple scattering in all (upward) directions. E^{SC} does not exist for a plane interface. The figure illustrates well the sharp increase of the ratio E^{SC}/E^O as the slowness approaches the critical value corresponding to P_n, thus supporting in a qualitative way the scattering model for propagation of this wave.

It should be noted that E^O and E^{SC} are not observable parameters. What can be inferred is the flux at a receiver location on the surface. To model this we need to know the areal extent of topography, and the decay factor accounting for attenuation of P_n along the Moho. Clearly these parameters as well as those describing the topography needed to compute E^{SC} and E^O are presently not or only poorly constrained, and further experiments are needed to establish useful constraints. Our preliminary results nevertheless suggest that the scattering model of P_n wave propagation is viable, and consequently that a careful calibration is needed before using this phase for event location and velocity determination purposes.

D.J. Doornbos, Univ. of Oslo
T. Kværna

References

Doornbos, D.J. (1988): Multiple scattering by topographic relief with application to the core-mantle boundary. Geophys. J., in press.

Kværna, T. and D.J. Doornbos (1986): An integrated approach to slowness analysis with arrays and three-component stations. Semi-annual Technical Summary, 1 Oct 1985 - 31 Mar 1986, NORSAR Sci. Rep. No. 2-85/86, Kjeller, Norway.

Menke, W.H. and P.G. Richards (1980): Crust-mantle whispering gallery phases: A deterministic model of teleseismic P_n wave propagation. J. Geophys. Res. 85, 5416-5422.

3213

AOZ

2829

Beam

0.0   2.0   4.0

SECONDS

1985-210/13:55:53.865

11/06/87 08:47:44 NORSAR
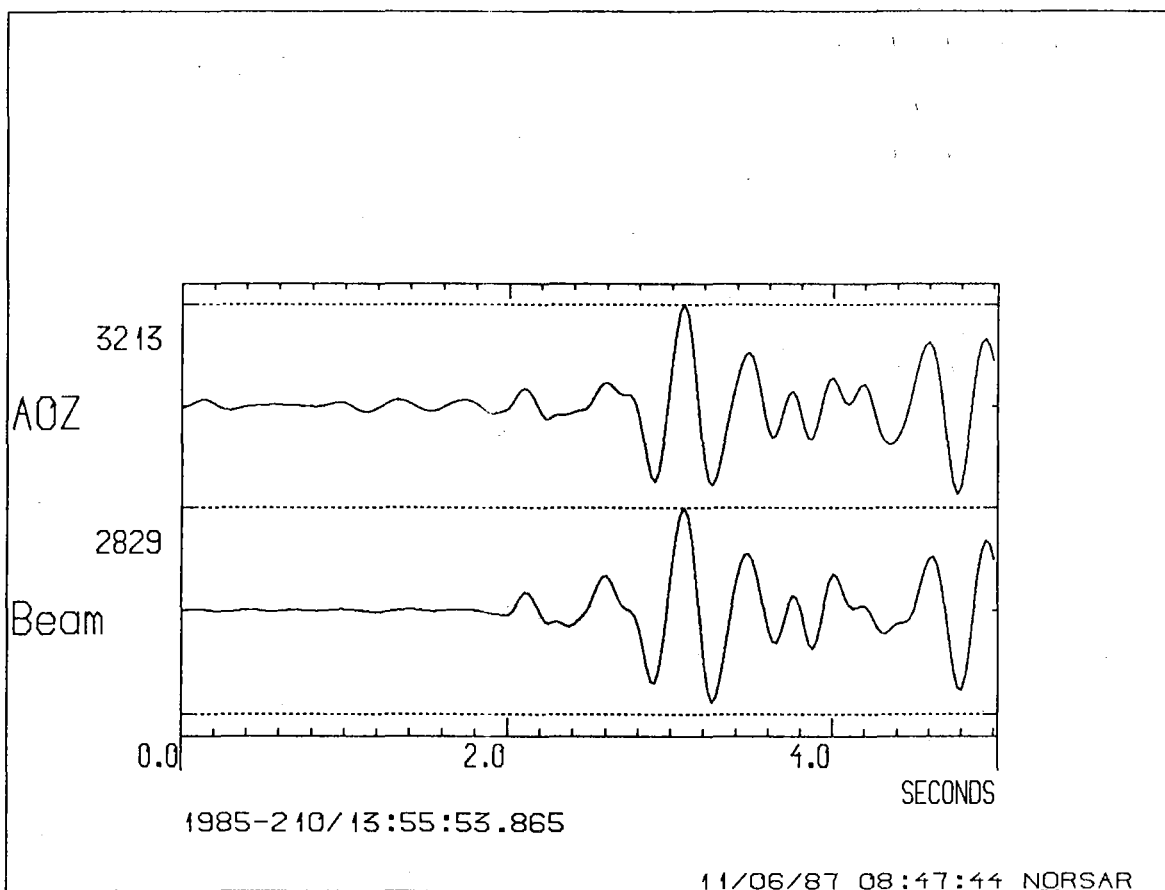
Fig. VII.1.1   Noress record of the P_n phase from an explosion in the
Blåsjø area. The top trace is the single channel obser-
vation, and the lower trace is the steered beam, both
bandpass filtered between 2.0 Hz and 4.0 Hz. Note the
relatively weak first arrival at about 2.0 seconds com-
pared to the stronger signal arriving 0.5-0.6 seconds
later.

SLOWNESS ANALYSIS — BLÅSJØ EVENTS

MOVING FREQUENCY BANDS — PN PHASE

BAND: 0.8 HZ   STEP: 0.4 HZ
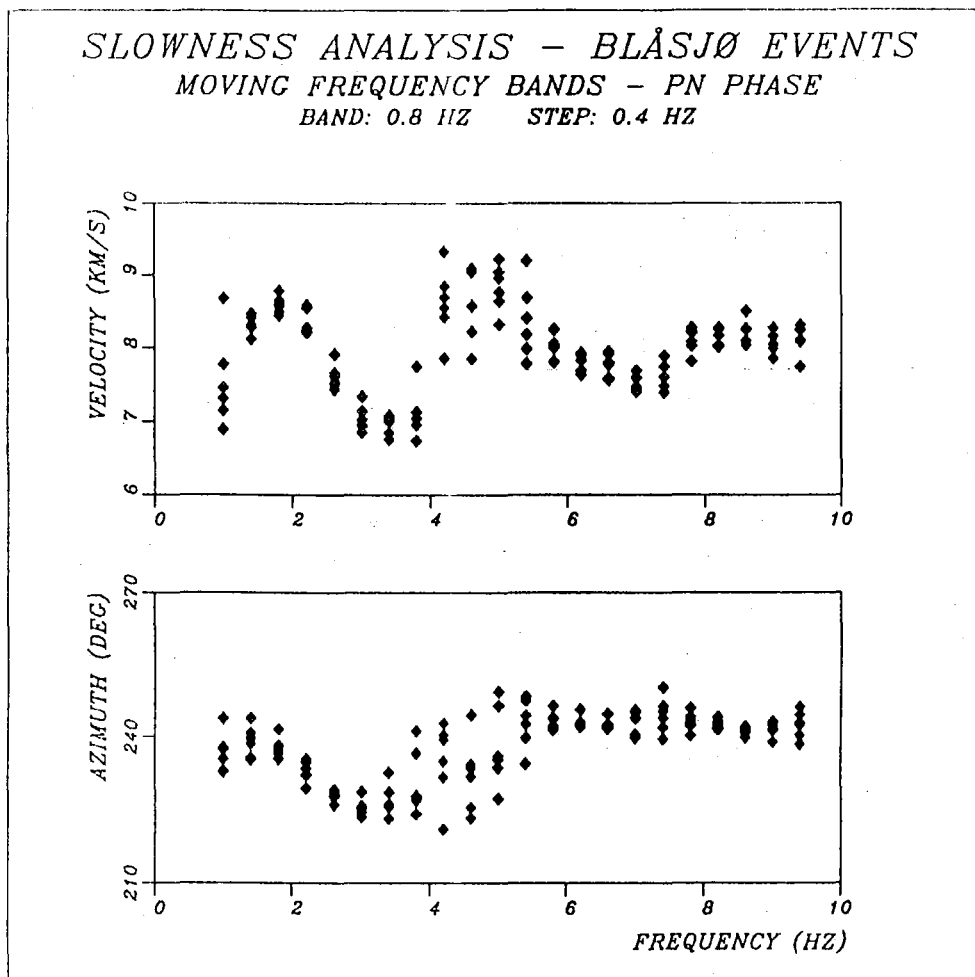
Fig. VII.1.2   Velocity and azimuth estimates for the P_n phases as a
function of frequency. The six events were processed by
the wide-band method in 0.8 Hz wide frequency windows
with 0.4 Hz steps. Between 2 and 4 Hz the deviation from
theoretical azimuth is between 10 and 15 degrees, and
the apparent velocity is significantly lower than
expected for the P_n phase.

BLAASJOE
MEAN UNCORRECTED SPECTRA
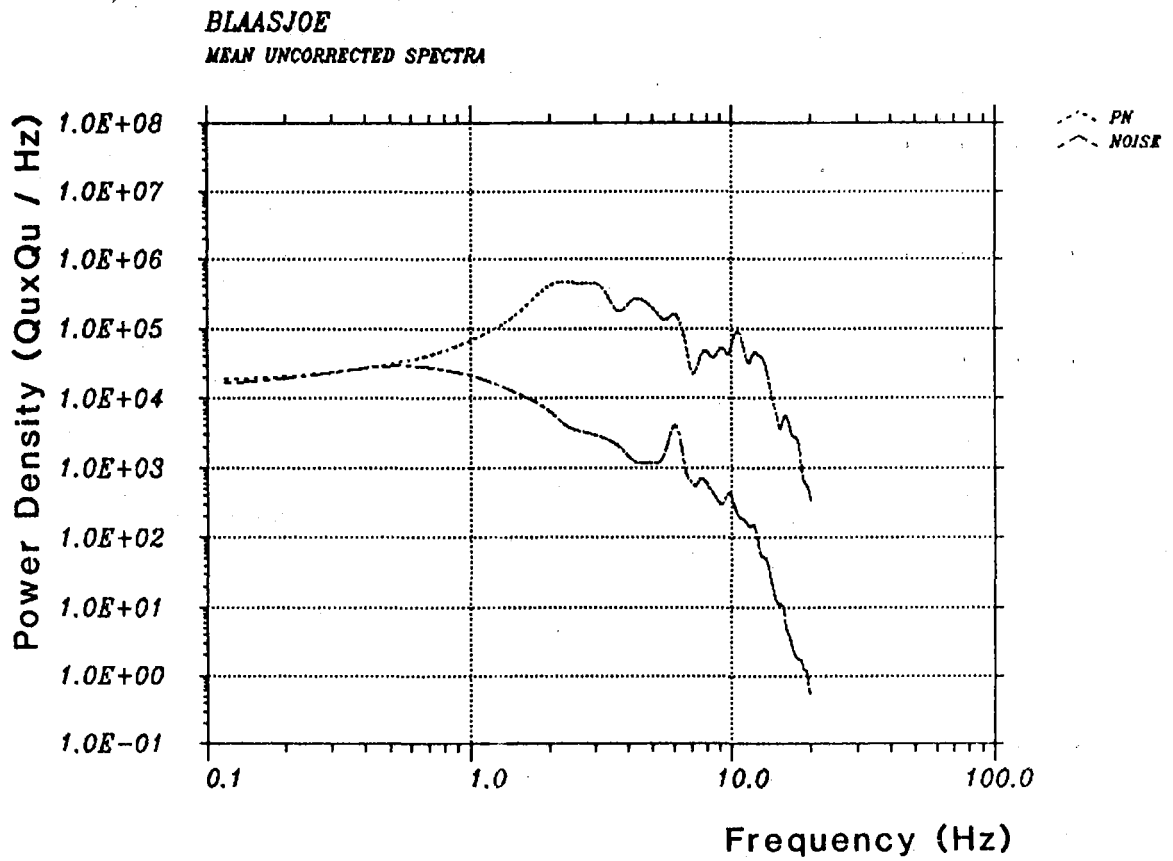
Fig. VII.1.3 This figures shows the uncorrected power density spectra
of both the P_n phase and the preceding noise for a typi-
cal Blåsjø event.
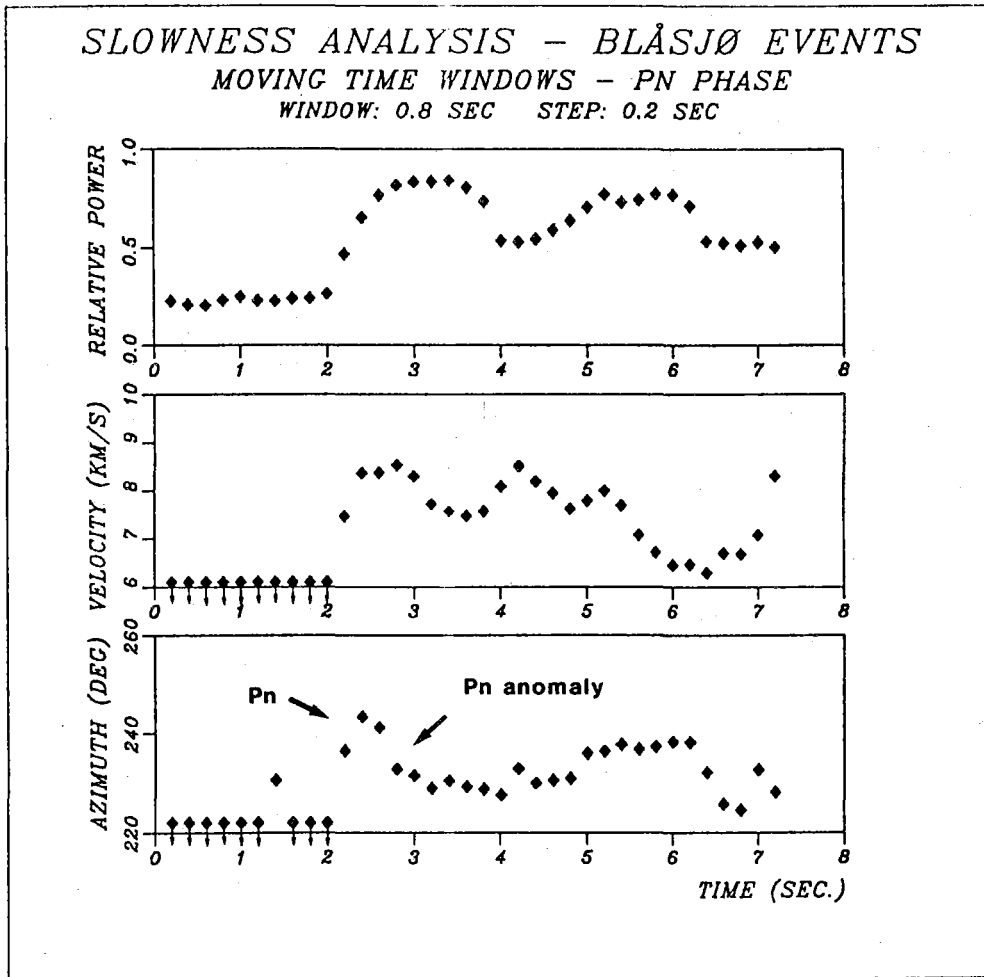
Fig. VII.1.4 Slowness estimates for one of the Blåsjø events as a
function of time. The data were processed by the wide-
band method in the frequency range 2.0-4.0 Hz. The
traced data were prealigned to compensate for offset
across the array.
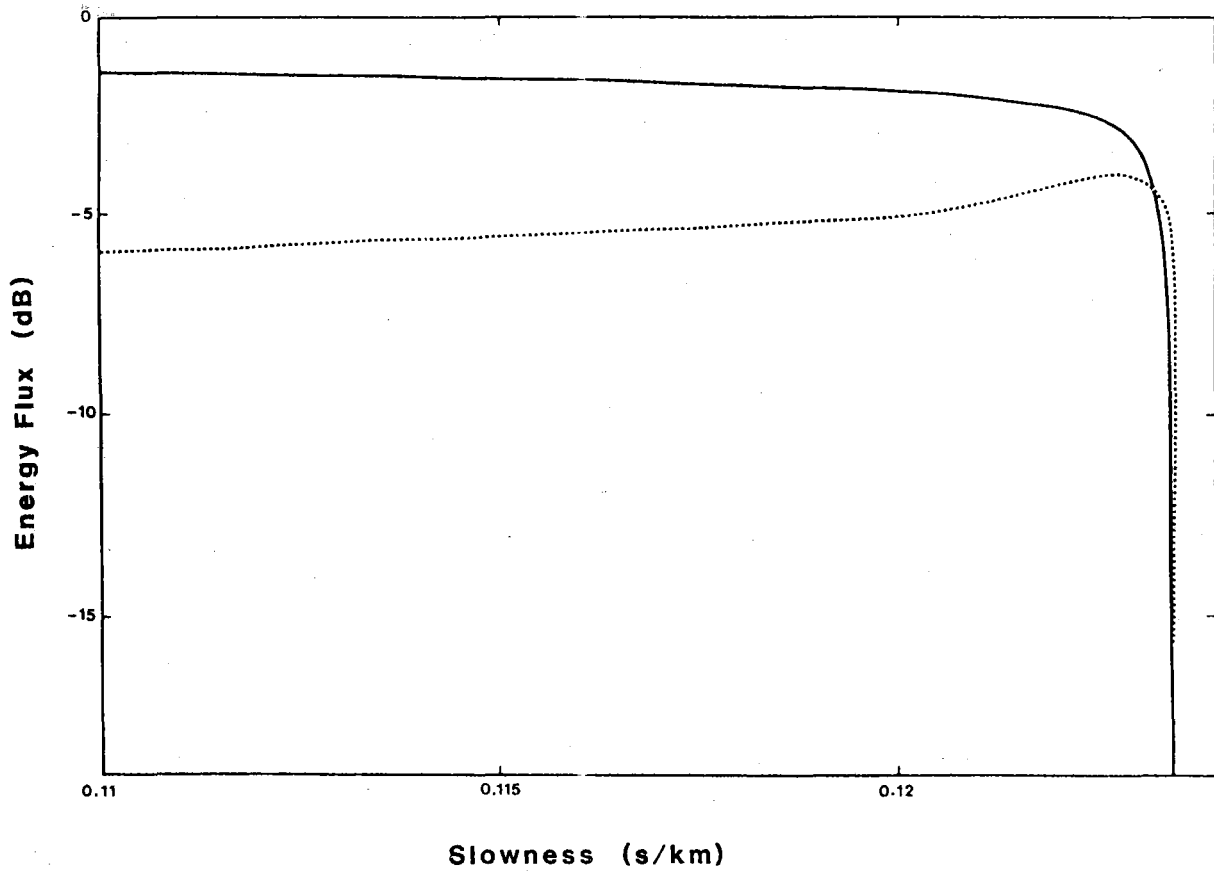
Fig. VII.1.5 Energy flux at 2 Hz through rough solid-liquid interface with the velocity-density structure $v_p^{+/-} = 6.8/8.1$ km/s, $v_s^{+/-} = 4.5/0$ km/s, $\rho^{+/-} = 2.9/3.4$ g/cm^3. The boundary roughness is characterized by an average height of 1 km and a correlation length of 6 km. The scattered flux is upward through the boundary. ————— : specular direction; ·············· : integrated diffuse flux.

VII.2   Preliminary tests for surface waves in 2-D structures

Introduction

Surface waves at short periods (T ⩽ 20 s), and especially the Lg
crustal surface waves, usually exhibit complex wavetrains. For
example, relative amplitudes of the Lg to body-wave phases observed at
the NORSAR array were shown to be strongly path-dependent (Kennett et
al, 1985), and large transversal motion was observed on Lg-phases pro-
duced by explosive sources in the North Sea (Kennett and Mykkeltveit,
1984).

Lateral heterogeneities are thought to be responsible for this
complexity, but due to the lack of methods which are available to
model surface wave propagation in laterally heterogeneous structures,
little of the complex wavetrains has yet been explained. In order to
get some further insight into these surface wavetrains, we have ini-
tiated a research effort aiming at comparing surface wave recordings
at the NORSAR and NORESS arrays with results of numerical modelling,
using a coupled mode scheme. The preliminary results presented here do
not intend to model a realistic situation, but to check the applicabi-
lity of the method, and especially to analyze the influence of its two
main parameters.

Method

We give here an outline of a coupled local mode method, the details of
which can be found in Maupin (1987). It is appropriate for propagation
across 2-D structures, the angle of incidence of the waves upon the
structure being possibly nonperpendicular to the symmetry direction y
of the structure. The wavefield is decomposed into a laterally varying
sum of the local modes:

$$\vec{u}(x,y,z,t) = \int\limits_{-\infty}^{+\infty} \int\limits_{-\infty}^{+\infty} (\sum_r c_r(x)\vec{u}_r(x,z;\omega,p)$$

$$\exp(-i \int\limits_{0}^{x} k^r(\zeta)d\zeta))\ e^{-ipy}\ e^{i\omega t}\ dp\ d\omega \tag{1}$$

where $\vec{u}$ is a displacement-stress vector of the elastic wavefield, $\vec{u}_r$ are displacement-stress vectors of the local modes, and $(k^r,p,0)$ is the local wave vector of the mode r in the cartesian coordinate system (x,y,z), at the frequency ω.

The lateral heterogeneity introduces a lateral variation of the wavenumbers k^r, as well as energy transfers between modes expressed by lateral variations of the amplitude coefficients c_r. The lateral variations of these two quantities satisfy the equations:

$$\frac{dk^r}{dx} = F_{rr}$$

$$\frac{dc_r}{dx} = \sum_{q \neq r} F_{qr} \frac{1}{(k^q-k^r)} \cdot \exp(i \int\limits_{0}^{x} (k^q-k^r)\ d\zeta)\ c_q \tag{2}$$

where F_{qr} is an expression involving the local mode displacements and tensions, combined with the elastic coefficients and density in interface terms, and with their lateral derivatives in an integral over depth.

The system (2) is transformed to yield a first-order equation in x for reflection and transmission matrices, which is solved numerically in x using a fourth-order Runge-Kutta scheme.

The method is tested on the continental margin model designed by
Badal and Serón (1987) (Fig. VII.2.1) to calculate Love wave
transmission by finite element method. We use an integration step in
x of 5 km and a variable integration step in z of the form $a^{(n-1)}$ dz_0
for the n-th step, with $dz_0 = 0.5$ km and $a = 1.02$. In the following
two paragraphs, we investigate the influence on the coupling matrices
of the precision with which the local modes are calculated, and of the
number of modes used in the representation of the wavefield.

Influence of the number of zones

The local modes $\vec{u}^r$ appear free of lateral differentiation in the
expression F_{qr} of equation (2). In order to facilitate their com-
putation, it is thus possible not to calculate them at each integra-
tion step in x, but to take them as constant inside zones where the
total lateral variation of the structure is small enough for their
shape not to vary significantly. The coarser a zoning we define across
the laterally heterogeneous structure, the less accurate local dis-
placement functions we use in the calculation of the expression F_{qr},
which in turn result in less accurate coupling matrices and local
wavenumbers.

In order to determine how fine the zoning must be, we divide the con-
tinental margin of Fig. VII.2.1 into 2, 5 and 10 zones. The coupling
equation is integrated with the three different zonings, using the
local modes at a period of 20 s, calculated at the center of each zone
by a classical Haskell-Dunkin method. The resulting local phase velo-
cities of the Rayleigh wave fundamental mode are shown on Fig.
VII.2.2a as a function of x. The phase velocities calculated at the
center of each zone by the Haskell-Dunkin method, as well as the local
phase velocities calculated in each of the smaller zones using the
variational method, are shown on Fig. VII.2.2b for comparison.

The variational method is designed to calculate first-order variations of the phase velocity associated with velocity and density variations as a function of depth, preferably for flat layer boundaries. Equation (2) treats separately the effect on phase velocities of sloping layer boundaries and velocity variations inside the layers. It gives obviously more accurate results than the variational method in this continental margin model, where the slope of the layer boundaries is important.

The accuracy of the phase velocity improves significantly when using 5 zones instead of 2, but remains stable between 5 and 10 zones. The number of zones required to fit a given velocity curve can be foreseen from the linear trend of the integrated phase velocity inside a zone. The proper zoning for a given model and frequency depends on the curvatures of the different mode phase velocity variations. The discrepancy observed between the integrated phase velocity and the zonal phase velocities around $x = 30$ km may be related to a systematic discrepancy between the vertically varying velocity profile and the set of homogeneous layers required by the Haskell-Dunkin method to calculate the zonal phase velocities.

The zoning must be designed to calculate accurately not only the phase velocities, but also the transmission and reflection matrices. Fig. VII.2.3 shows the transmission matrices for the 6 first modes of Rayleigh and Love waves at right angle to the continental margin when the modes are calculated at 20 s period for 2, 5 and 10 zones. The zoning has a negligible influence on the transmission matrices. The reflection matrices are zero whatever the zoning for this model.

When the propagation is not at right angle to the structure, Love and Rayleigh waves are coupled. As the dispersion curves of Love and Rayleigh modes of the same harmonic rank are usually very close and may even cross each other, small relative errors in k produce large errors in (k^q-k^r), leading to a loss of accuracy in the Rayleigh-Love

coupling terms. The accuracy of the phase velocity has therefore a stronger influence on the coupling matrices in that case.

Influence of the mode cut-off

To be complete, the wavefield representation (1) should include all the surface wave modes and body-wave terms, or the infinite set of modes of a structure equivalent to the spherical Earth. For practical reasons, we need to restrict the set of modes to those which have somewhere along the structure a significant energy in the frequency range we are studying. Except in particular cases of well-defined waveguides, the coupling between modes usually decreases gradually with harmonic rank difference and the mode cut-off is often chosen somewhat arbitrarily. Therefore, it is important to know which elements in the coupling matrices are influenced by the drop-off of the higher modes.

Transmission matrices for Love waves crossing the continental margin at right angle were calculated for the 6, 8 and 10 first modes at a period of 10 s (Fig. VII.2.4). The influence of the mode cut-off can essentially be inferred from on the last row and column of the matrices. It is clear for example that the addition of modes 9 and 10 has no significant influence on the transmission matrix of the first 7 modes, including the 6th mode which is very strongly coupled to neighboring modes.

The important point to note here is that the energy of the higher modes not accounted for is mainly fed into the coupling terms of the higher modes of the representation, and not systematically into the diagonal terms. Therefore the cut-off does not produce an upper bias of the self-transmission terms.

Conclusion

We have shown that the coupled-local modes method can be applied to model wave propagation in realistic structures, needing a reasonable amount of lateral zones and local modes to achieve a satisfactory precision in transmission and reflection coefficients. The method has acceptable computing times (typically 10 minutes of CPU time on the IBM 4381/P02 of NORSAR for the examples displayed in Figs. VII.2.3 and VII.2.4). Next, we intend to apply this method across laterally heterogeneous structures around Scandinavia, like the North Sea Graben and the Tornquist-Teisseyre lineament, and compare the results of the modelling with surface wave data recorded at the NORSAR and NORESS arrays.

<div align="right">V. Maupin, Postdoctorate Fellow</div>

References

Badal, J. and F.J. Serón (1987): Love wave normally incident at the Atlantic margin of the Iberian Peninsula. Annales Geophysicae, 5B, 273-280.

Kennett, B.L.N., S. Gregersen, S. Mykkeltveit and R. Newmark (1985): Mapping of crustal heterogeneity in the North Sea basin via the propagation of Lg-phases. Geophys. J.R. astr. Soc., 83, 299-306.

Kennett, B.L.N. and S. Mykkeltveit (1984): Guided wave propagation in laterally varying media. II: Lg waves in north-western Europe. Geophys. J.R. astr. Soc., 79, 257-267.

Maupin, V. (1987): Surface waves across 2-D structures: a method based on coupled local modes. Submitted to the Geophys. J.R. astr. Soc.

Fig. VII.2.1 Continental margin model after Badal & Serón (1987).

Fig. VII.2.2a

□   zonal phase velocity

+——+   integrated phase velocity using 10 zones

x——x   integrated phase velocity using 5 zones

•– – –•   integrated phase velocity using 2 zones
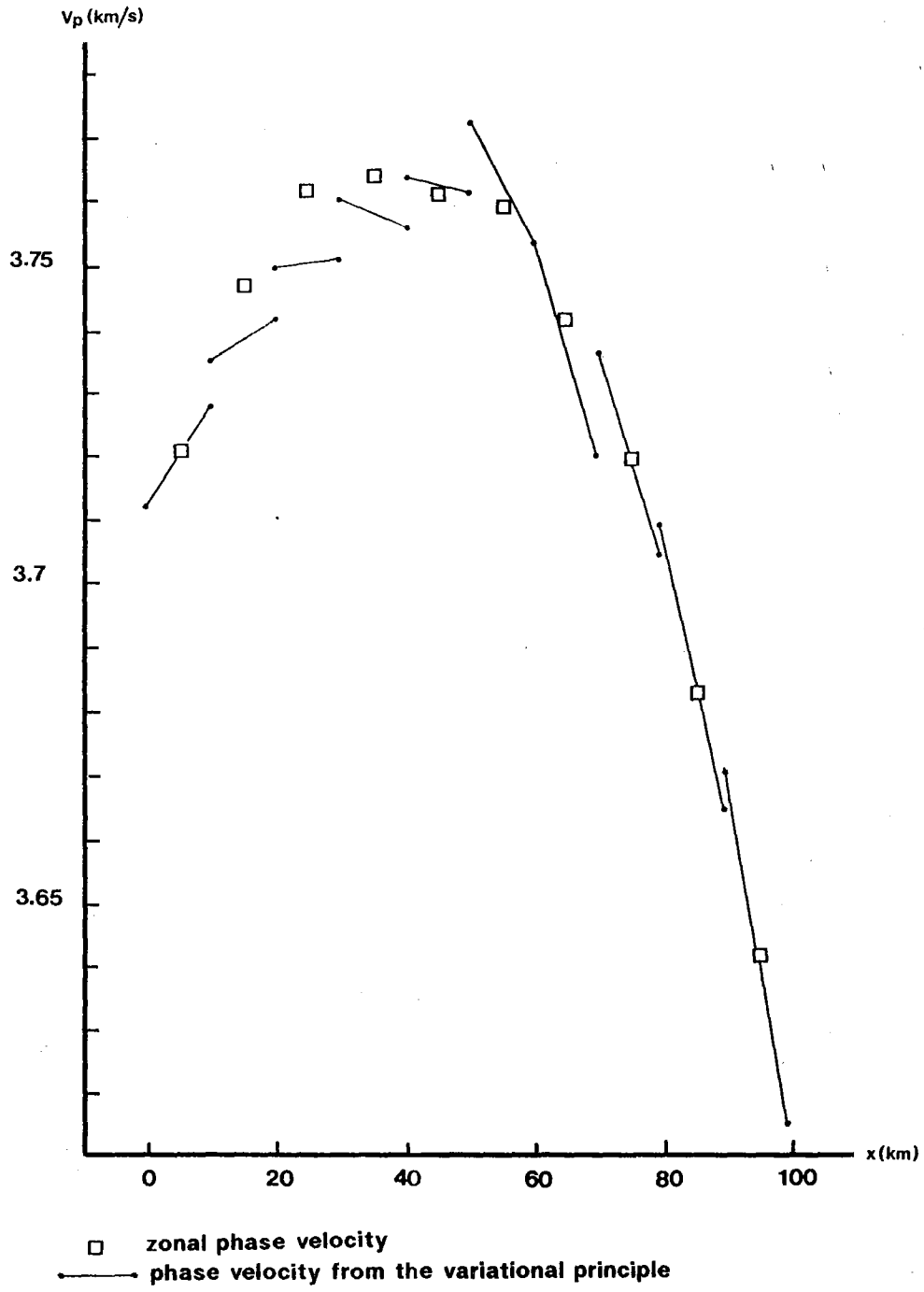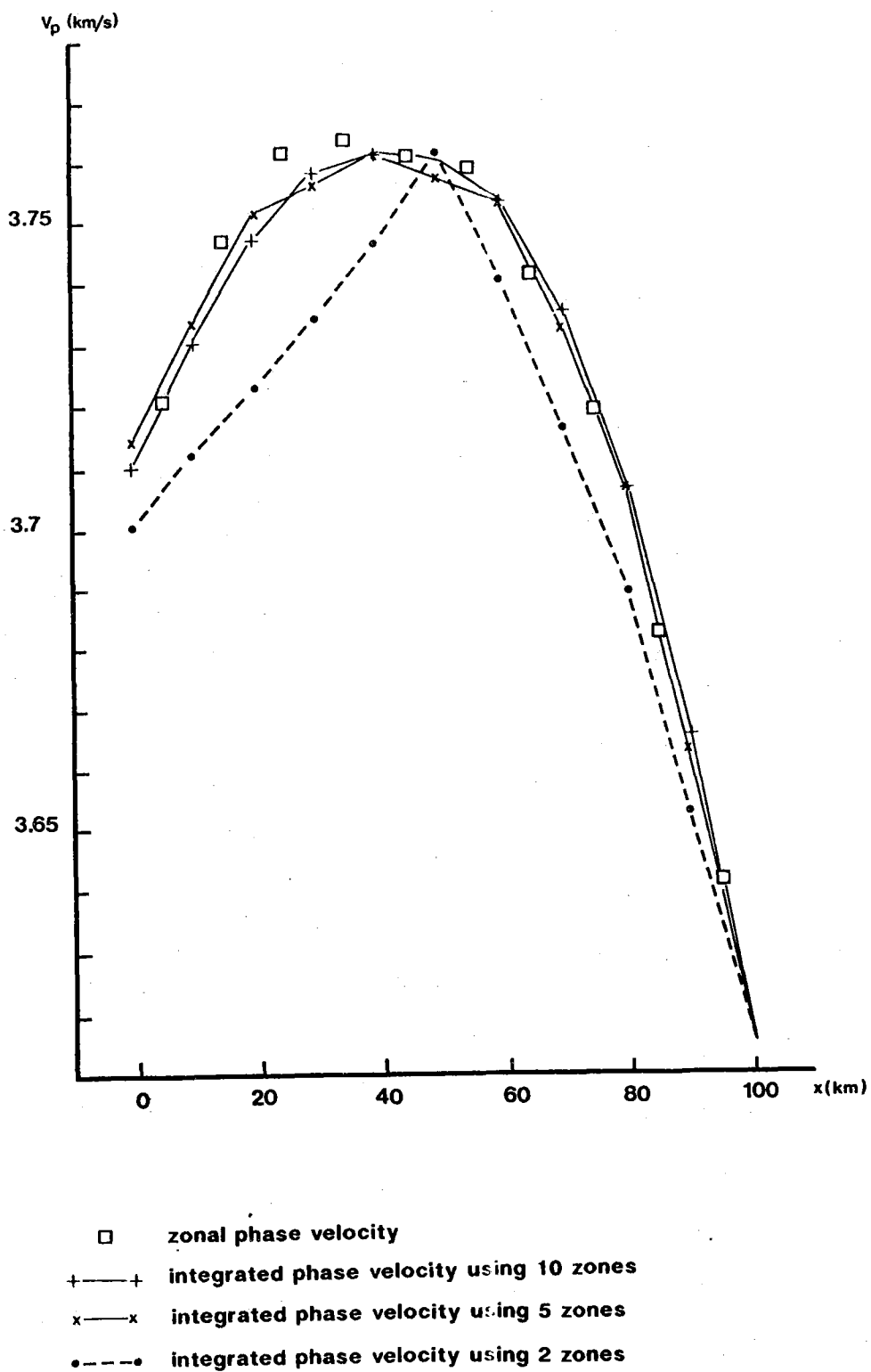
Fig. VII.2.2b

2 zones :

	1	2	3	4	5	6		1	2	3	4	5	6
1	99	3	6	3	5	4		86	39	27	7	9	6
2	6	94	29	9	9	6		46	85	21	3	1	1
3	4	28	93	20	5	6		9	26	79	53	4	4
4	2	13	18	95	17	0		10	14	48	76	38	2
5	3	8	2	15	93	31		11	8	14	31	89	25
6	5	7	8	6	29	94		9	2	2	11	22	96

5 zones :

	1	2	3	4	5	6		1	2	3	4	5	6
1	99	4	7	3	5	4		83	43	28	6	9	7
2	6	94	28	8	8	6		50	84	19	5	1	2
3	5	27	93	22	3	5		8	26	78	55	4	4
4	3	13	19	94	20	0		10	13	49	75	38	2
5	4	7	0	17	91	33		11	8	14	31	88	26
6	5	7	7	7	31	93		11	2	2	12	22	95

10 zones :

	1	2	3	4	5	6		1	2	3	4	5	6
1	99	3	7	3	5	4		84	42	28	6	9	7
2	6	94	28	8	8	6		49	84	20	4	0	2
3	5	27	93	23	3	5		8	27	77	55	4	4
4	3	13	20	94	20	0		10	13	50	75	38	2
5	4	7	0	17	91	33		11	8	14	31	89	26
6	5	7	7	7	32	93		10	2	2	12	22	96

Rayleigh modes   Love modes

Fig. VII.2.3   Transmission matrices in % for the 6 first Rayleigh and Love modes across a continental margin model, at 20 s of period, using 2, 5 and 10 zones. The matrix elements are amplitude transmission coefficients for modes which carry a unit energy flux.

	1	2	3	4	5	6
1	96	13	14	14	6	4
2	21	73	59	21	4	2
3	8	52	35	67	21	27
4	6	34	65	62	23	7
5	5	17	17	24	40	84
6	6	10	18	14	85	44

	1	2	3	4	5	6	7	8
1	96	12	14	14	7	5	6	3
2	20	73	59	21	5	1	1	2
3	7	52	34	68	24	23	5	3
4	5	34	65	60	21	7	10	8
5	5	17	18	21	45	72	38	1
6	3	6	9	6	58	4	73	30
7	5	6	12	13	55	52	27	54
8	8	4	8	12	13	35	48	77

	1	2	3	4	5	6	7	8	9	10
1	96	12	14	13	7	5	6	4	3	2
2	20	73	59	21	5	0	2	4	3	2
3	6	52	34	68	24	23	6	6	3	2
4	4	33	65	58	21	7	10	15	13	9
5	5	17	18	22	45	72	39	2	2	1
6	3	6	9	7	58	5	71	34	7	1
7	6	6	12	13	55	53	28	52	10	5
8	5	3	5	9	13	31	38	59	60	6
9	5	5	6	9	0	16	28	39	61	58
10	7	7	9	15	3	5	14	25	47	80

Fig. VII.2.4 Transmission matrices in % for the 6, 8 and 10 first Love modes across a continental margin model, at 10 s of period. The matrix elements are amplitude transmission coefficients for modes which carry a unit energy flux.

VII.3   False alarm statistics and threshold determination

for regional event detection

In order to improve the event detection performance during automatic processing of regional array data, the detection thresholds for the different beams need to be closely examined. In this context, several factors should be considered:

i)   We wish to make the detection process as sensitive as possible with emphasis on small events, i.e., we want to operate on a low threshold.

ii)   We need to specify how many false alarms per time unit can be accepted; e.g., operation of the NORSAR array has shown that false alarm rates of up to 50 % are acceptable.

iii) Too many false alarms will cause the phase association algorithm to produce fictitious events.

iv)   The number of false alarms increases with the number of beams. In an extended beam set, we should only include the beams that improve the detectability without significantly increasing the number of false alarms.

In this study we have attempted to determine the thresholds for a large beam set from false alarm considerations. The procedure has been as follows:

1)   Based on previous studies (Kværna and Mykkeltveit, 1986) and the NORSAR staff's experience with processing of regional array data (RONAPP), define the filter bands that appear most appropriate for regional event detection. The resulting twelve filters are given in Table VII.3.1.

2)   For each filter band, find the best array sub-geometry and the
        corresponding steering delays for coherent beamforming. For
        detection of P-waves we have attempted to have maximum 3 deci-
        bels signal loss due to missteering. For coherent beam detec-
        tion of S-waves, we have also applied the 3 dB criterion. The
        resulting P-wave beam deployment spanned the velocity space
        from 6.0 km/s to infinity, whereas the velocity space from
        about 3.8 km/s to 5.3 km/s was spanned by the S-beams. This
        resulted in 72 P-beams and 132 S-beams.

3)   For each filter band, find the best array sub-geometry for
        incoherent beamforming of the vertical channels. The sub-
        geometries were chosen from the criterion that the noise should
        be uncorrelated between channels. Due to the wide response pat-
        tern of the incoherent beams (Ringdal et al, 1975), only one
        incoherent beam (with infinite velocity) was formed for each
        filter band.

4)   For each filter band, form an incoherent beam from the
        eight horizontal channels.

5)   Under the assumption that the SNR is lognormally distributed
        during noise conditions, it can be shown that the cumulative
        distribution of number of detections versus detection threshold,
        approximately follows a straight line when both are plotted
        with logarithmic axes (see Appendix 1). In this study, we have
        selected a time interval (1987/:072.04.30.0 -
        1987/072:16.00.00.0), and run all beams with a low threshold.
        From the cumulative distributions we have extrapolated the
        noise slopes down to a common level, in this case 10 detec-
        tions, and found the corresponding detection thresholds.

In addition to the obtained threshold values, a description of the
beam deployment is given in Table VII.3.2a and Table VII.3.2b.

Fig. VII.3.1 (a-1) show the cumulative distributions for the coherent
P-beams and the incoherent beams made from the vertical channels.
The dashed tangent lines are the inferred noise slopes extrapolated
down to the 10 detections level. At this threshold we thus expect to
have 10 false alarms ("noise detections") in each filter band during
the examined time interval.

From Fig. VII.3.1 we can see that the threshold differences between
the coherent and incoherent beams vary between 4.5 and 7 decibels.
From this observation we can infer that for detection of phases where
we consistently can achieve coherent beam gain exceeding these
threshold differences, coherent beam detection is superior to inco-
herent detection. From NORESS experience (Kværna and Mykkeltveit,
1986), coherent beamforming of Pn phases will typically result in a
SNR gains between 8 and 15 dB, thus coherent beams are clearly
superior for P-phase detection. For secondary phases like Lg where we
may not achieve coherent beam gain exceeding the threshold differen-
ces, incoherent beamforming may outperform the coherent procedure.

Another interesting feature seen from Fig. VII.3.1i) and Fig.
VII.3.1j), is the large number of detections exceeding the obtained
thresholds for the two filters 8.0-16.0 Hz and 10.0-16.0 Hz. These
filter bands have been subjected to additional detection analysis
of a 24 hours time interval, where we found that the majority of
the detections exceeding the obtained thresholds occurred during
working hours. A viable hypothesis is therefore that most of these
detections are due to nearby man-made activity.

Fig. VII.3.2 (a-d) show the cumulative distributions for the inco-
herent beams from both the vertical and horizontal channels. An
interesting feature is that the inferred thresholds from the inco-
herent beams based on 8 horizontal channels, is not higher than the
thresholds inferred from the incoherent beams based on 22 vertical
channels. This observation suggests that incoherent beamforming on
a mixture of horizontal channels more effectively reduces the
noise variance than using vertical channels alone.

The number of noise detections (10) chosen as a common limit for each
filter band in this study is of course rather arbitrary, and has been
made mainly for the purpose of achieving a common basis for com-
parison. In practical operation, it may be desirable to operate at
different false alarm rates, and the corresponding thresholds may
easily be inferred, e.g., to reduce the number of detections in the
8.0-16.0 Hz filter band by a factor of two (Fig. VII.3.1i), the
thresholds have to be raised by about 3 decibels.

It should be emphasized that the false alarms discussed in this
paper are due to the stochastic nature of the noise, and
that intervals with different noise characteristics (Fyen, 1986)
may give deviations from these curves. Noise bursts and close
events which may be considered as false alarms do not follow
the lognormal distribution. To avoid detection of these signals,
the thresholds would have to be raised above the levels obtained
in this study. Fig. VII.3.3 shows a histogram of RONAPP detections
with apparent velocities less than 3.0 km/s for a period of 86 days.
These signals are mostly generated by local activity in the
northeastern direction from NORESS. These detections can easily be
separated from the 'interesting' local and regional events on the
basis of their apparent velocities. The incoherent beams that mostly

detect these local events, are also our best tool for detecting regional Lg phases. So raising the threshold to avoid the low velocity signals, would also imply missing a number of regional Lg detections. This illustrates some of the conflicting interests that has to be taken into account when determining thresholds and detection beams.

In conclusion, the thresholds obtained from the extrapolated noise slopes, indicate the lowest operational level. If in the detection process we want to exclude signals generated by nearby activity or local noise bursts, the thresholds should be raised. But as outlined earlier, many other factors have to be considered for a final beam deployment and the corresponding thresholds.

T. Kværna
S. Kibsgaard
F. Ringdal

References

Fyen, J. (1986): NORESS noise spectral studies – noise level characteristics. Semiannual Technical Summary, 1 April – 30 September 1986, NORSAR Sci. Rep. No. 1-86/87, Kjeller, Norway.

Kværna, T. and S. Mykkeltveit (1986) Optimum beam deployment for NORESS P-wave detection. Semiannual Technical Summary, 1 April – 30 September 1986, NORSAR Sci. Rep. No. 1-86/87, Kjeller, Norway.

Ringdal. F., E.S. Husebye and A. Dahle (1975): P-wave envelope representation in event detection using array data, in Exploitation of Seismograph Networks, K. G. Beauchamp, Editor,

Appendix 1

We assume that the quantity STA/LTA (short-term to long-term average) computed at regular intervals on a seismic trace (beam or single channel) follows a lognormal distribution during noise conditions (Ringdal et al, 1975).

Setting U = log (STA/LTA) we thus get the following probability density of this variable

$$f(u) = \frac{1}{\sqrt{2\pi} \cdot \sigma} \cdot e^{-\frac{(u-\mu)^2}{2\sigma^2}} = \frac{1}{\sigma} \cdot \phi \left(\frac{u-\mu}{\sigma} \right) \tag{1}$$

where $\phi(z)$ denotes the standard Gaussian density.

The probability of U exceeding a given threshold value becomes

$$F(u) = P(U > u) = \int_u^\infty f(t) \, dt = 1 - \Phi \left(\frac{u-\mu}{\sigma} \right) \tag{2}$$

where $\Phi(z)$ denotes the standard Gaussian distribution function.

With a logarithmic frequency axis, we obtain from (2) the following slope S(u) of the distribution function at a given threshold u

$$S(u) = \frac{d(\log F(u))}{du} = \frac{F'(u)}{F(u)} = \frac{-\frac{1}{\sigma} \cdot \phi\left(\frac{u-\mu}{\sigma}\right)}{1 - \Phi\left(\frac{u-\mu}{\sigma}\right)} \tag{3}$$

For values of $t \geqslant 3$, we may use the following approximation, with a relative error of less than 10 per cent:

$$1 - \Phi(t) \approx \frac{1}{t} \cdot \phi(t) \tag{4}$$

Applying this approximation to (3), and also noting that $\mu \approx 0$, since STA/LTA fluctuates around 1 during noise conditions, we obtain

$$S(u) \approx -\frac{u}{\sigma^2} \qquad \text{for } \frac{u}{\sigma} \geqslant 3 \tag{5}$$

In practical detector operation, we are only interested in thresholds corresponding to large values of $\frac{u}{\sigma}$, thus the approximation (5) is applicable. For example, a threshold value of $u = 3.5 \cdot \sigma$ corresponds to 1 false alarm in 4000 independent STA/LTA computations, whereas $u = 4\sigma$ gives 1 false alarm per 30,000 such computations. A practical operating threshold is likely to be somewhere between these values; thus the slope (5) will be approximately constant around the threshold value, for a given σ.

Nr.	Prototype	Type	Low	High	Order
BP01	BU	BP	1.0	3.0	3
BP02	BU	BP	1.5	3.5	3
BP03	BU	BP	2.0	4.0	3
BP04	BU	BP	2.5	4.5	3
BP05	BU	BP	3.0	5.0	3
BP06	BU	BP	3.5	5.5	3
BP07	BU	BP	5.0	7.0	3
BP08	BU	BP	6.5	8.5	3
BP09	BU	BP	8.0	16.0	3
BP10	BU	BP	10.0	16.0	3
BP11	BU	BP	1.0	2.0	2
BP12	BU	BP	2.0	3.0	2

Table VII.3.1 This table show the filters applied in the experiment. All were recursive Butterworth bandpass filters of order 2 or order 3.

Coherent P-Beams

Filter	Configuration	# beams	Test(dB)	Threshold(dB)	# Detections
1.0- 3.0 Hz	AO CD	1	6.0	12.0	28
1.5- 3.5 Hz	AO CD	1	6.0	11.0	40
2.0- 4.0 Hz	AO CD	10	6.0	12.7	51
2.5- 4.5 Hz	AO BCD	10	6.0	12.4	50
3.0- 5.0 Hz	AO BC	7	6.0	11.4	58
3.5- 5.5 Hz	AO BC	9	6.0	10.9	64
5.0- 7.0 Hz	AO BC	9	6.0	11.7	64
6.5- 8.5 Hz	AO BC	9	6.0	11.5	70
8.0-16.0 Hz	AOAB	8	4.0	8.4	100
10.0-16.0 Hz	AOAB	8	4.0	8.5	114
1.0- 2.0 Hz	AO CD	1	6.0	12.7	29
2.0- 3.0 Hz	AO CD	1	6.0	12.7	28

Coherent S-Beams

Filter	Configuration	# beams	Test(dB)	Threshold(dB)	# Detections
1.0- 3.0 Hz	AO CD	6	6.0	12.7	40
1.5- 3.5 Hz	AO CD	12	6.0	12.9	49
2.0- 4.0 Hz	AO CD	12	6.0	12.9	58
2.5- 4.5 Hz	AO BCD	12	6.0	12.5	66
3.0- 5.0 Hz	AO BC	12	6.0	12.3	58
3.5- 5.5 Hz	AO BC	12	6.0	12.0	61
5.0- 7.0 Hz	AO BC	12	6.0	12.7	45
6.5- 8.5 Hz	AOABC	12	6.0	11.8	72
8.0-16.0 Hz	AOAB	12	6.0	9.0	93
10.0-16.0 Hz	AOAB	12	6.0	9.0	114
1.0- 2.0 Hz	AO CD	6	6.0	13.2	33
2.0- 3.0 Hz	AO CD	12	6.0	13.7	49

Table VII.3.2a In addition to the inferred thresholds and the number
of detections exceeding these thresholds, a description
of the coherent beam deployment for detection of P and
S-phases is shown in this table. The respective coloums
describe the following parameters:

Filter : The investigated filter band.
Configuration: The array sub-geomery applied in the
beamforming. AO means AOZ, A means A-
ring, etc.
beams : Number of coherent beams within the
filter band.
Test : The experimental threshold in dB.
Threshold : The threshold in dB inferred form the
slope of the cumulative distributions.
Detections : Number of detections exceeding the
deduced thresholds.

Incoherent beams on vertical channels
_____

Filter	Configuration	# beams	Test(dB)	Threshold(dB)	# Detections
1.0- 3.0 Hz	AO CD	1	1.9	6.4	48
1.5- 3.5 Hz	AO CD	1	1.9	6.6	61
2.0- 4.0 Hz	AO CD	1	1.9	6.9	44
2.5- 4.5 Hz	AO BCD	1	1.9	6.9	42
3.0- 5.0 Hz	AO BCD	1	1.9	7.2	33
3.5- 5.5 Hz	AO BCD	1	1.9	6.8	36
5.0- 7.0 Hz	AO BCD	1	1.2	4.7	72
6.5- 8.5 Hz	AO BCD	1	1.2	4.5	95
8.0-16.0 Hz	AO BCD	1	1.2	4.0	77
10.0-16.0 Hz	AO BCD	1	1.2	4.0	80
1.0- 2.0 Hz	AO CD	1	1.9	6.8	36
2.0- 3.0 Hz	AO CD	1	1.9	7.9	45

Incoherent beams on horizontal channels
_____

Filter	Configuration	# beams	Test(dB)	Threshold(dB)	# Detections
1.0- 3.0 Hz	E-W N-S	1	1.9	6.8	35
1.5- 3.5 Hz	E-W N-S	1	1.9	7.0	50
2.0- 4.0 Hz	E-W N-S	1	1.9	7.4	40
2.5- 4.5 Hz	E-W N-S	1	1.9	6.8	48
3.0- 5.0 Hz	E-W N-S	1	1.9	6.1	54
3.5- 5.5 Hz	E-W N-S	1	1.9	5.3	52
5.0- 7.0 Hz	E-W N-S	1	1.2	5.1	44
6.5- 8.5 Hz	E-W N-S	1	1.2	4.8	81
8.0-16.0 Hz	E-W N-S	1	1.2	3.7	81
10.0-16.0 Hz	E-W N-S	1	1.2	3.7	92
1.0- 2.0 Hz	E-W N-S	1	1.9	7.3	23
2.0- 3.0 Hz	E-W N-S	1	1.9	8.6	29

Table VII.3.2b In this table we have shown the same parameters as in
Table VII.3.2a, but now for the incoherent beams.
E-W means the channels AOE, C2E, C4E and C7E.
N-S means the channels AON, C2N, C4N and C7N.
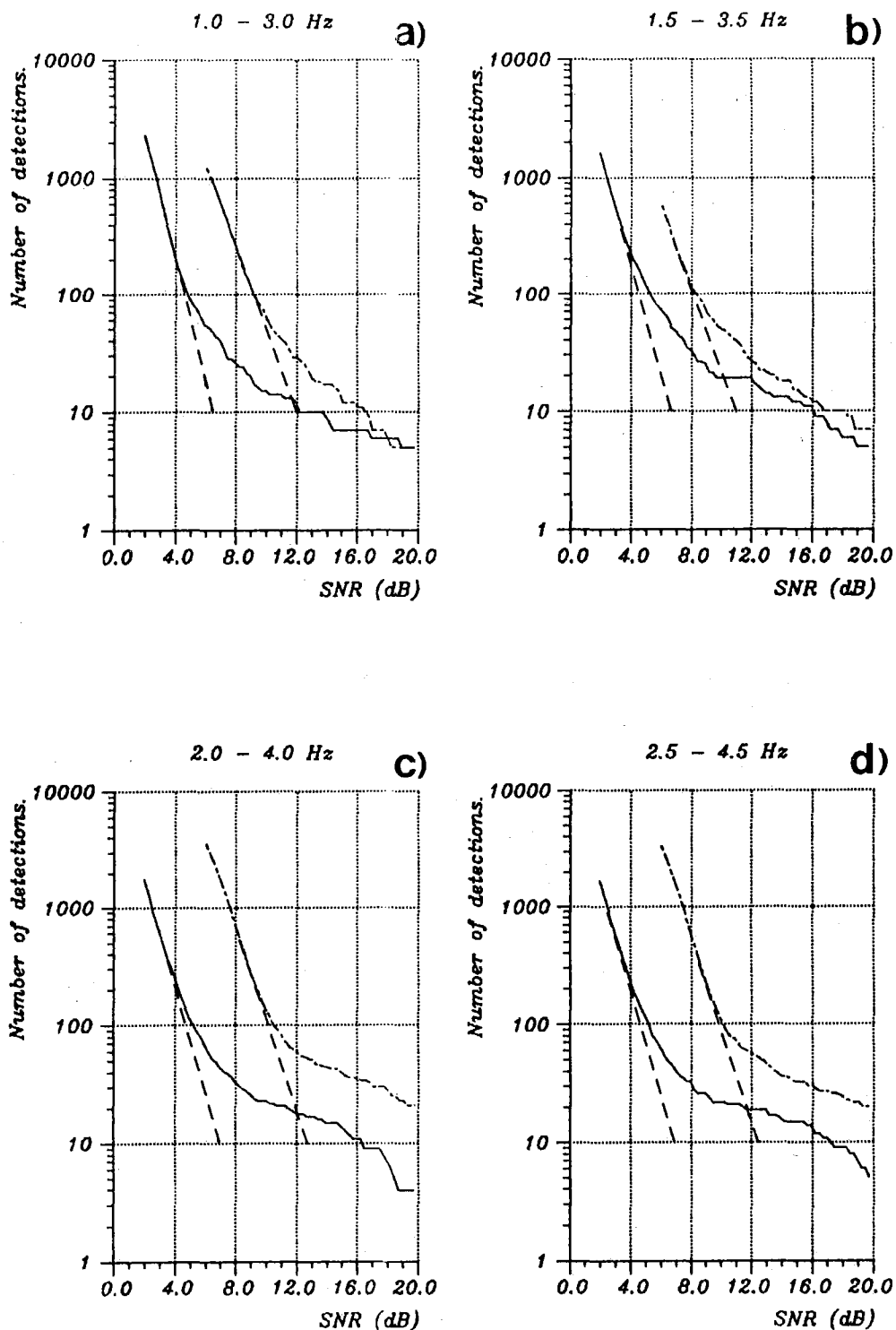
Fig. VII.3.1 These figures (a-l) show the cumulative distributions for the coherent P-beams (dashed-dotted curves) and for the incoherent beams made from the vertical channels (solid lines) in all filter bands investigated. The dashed lines indicate the slopes of the distribution of 'noise' detections.
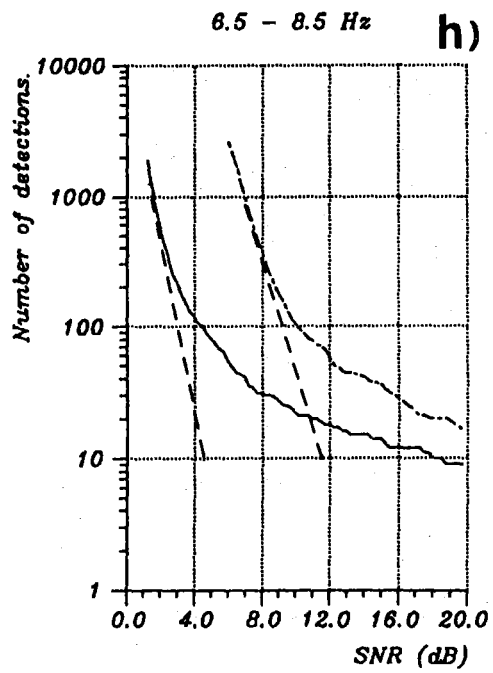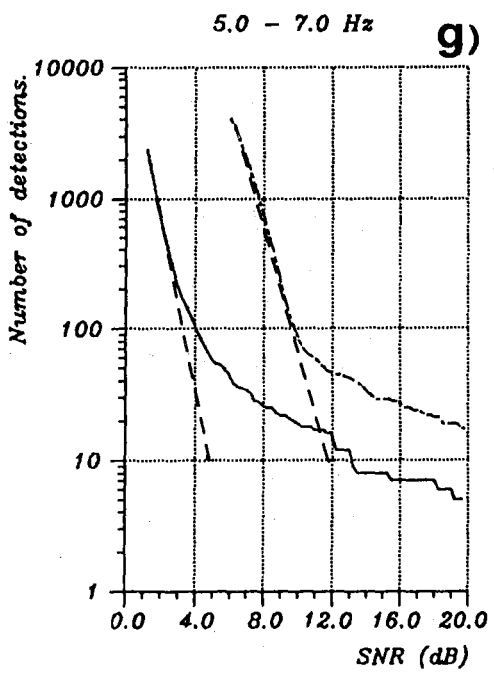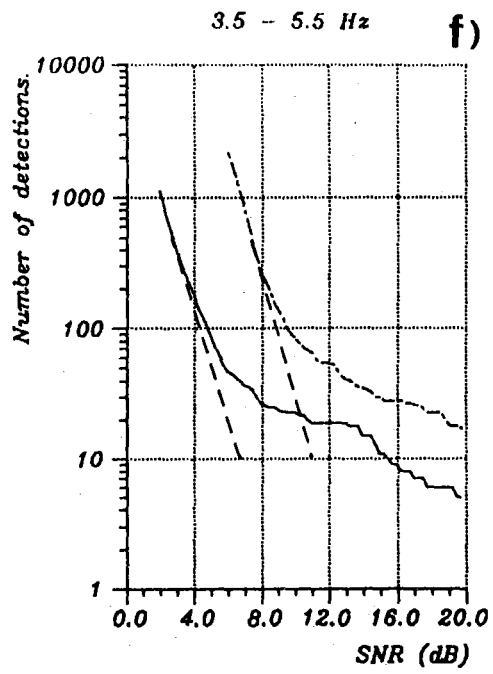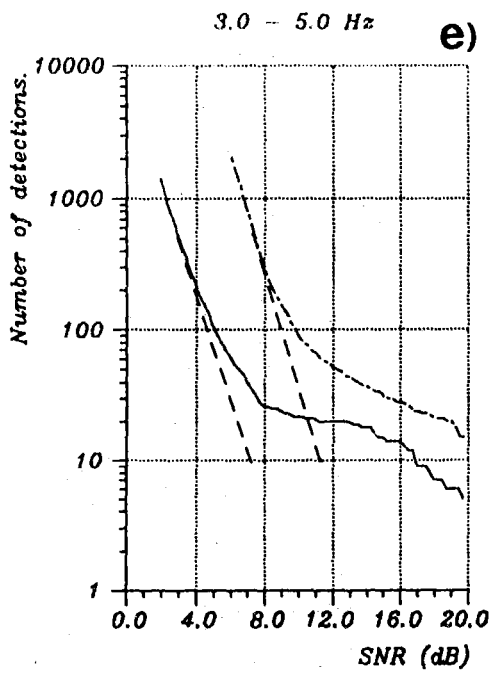
Fig. VII.3.1 (cont.)
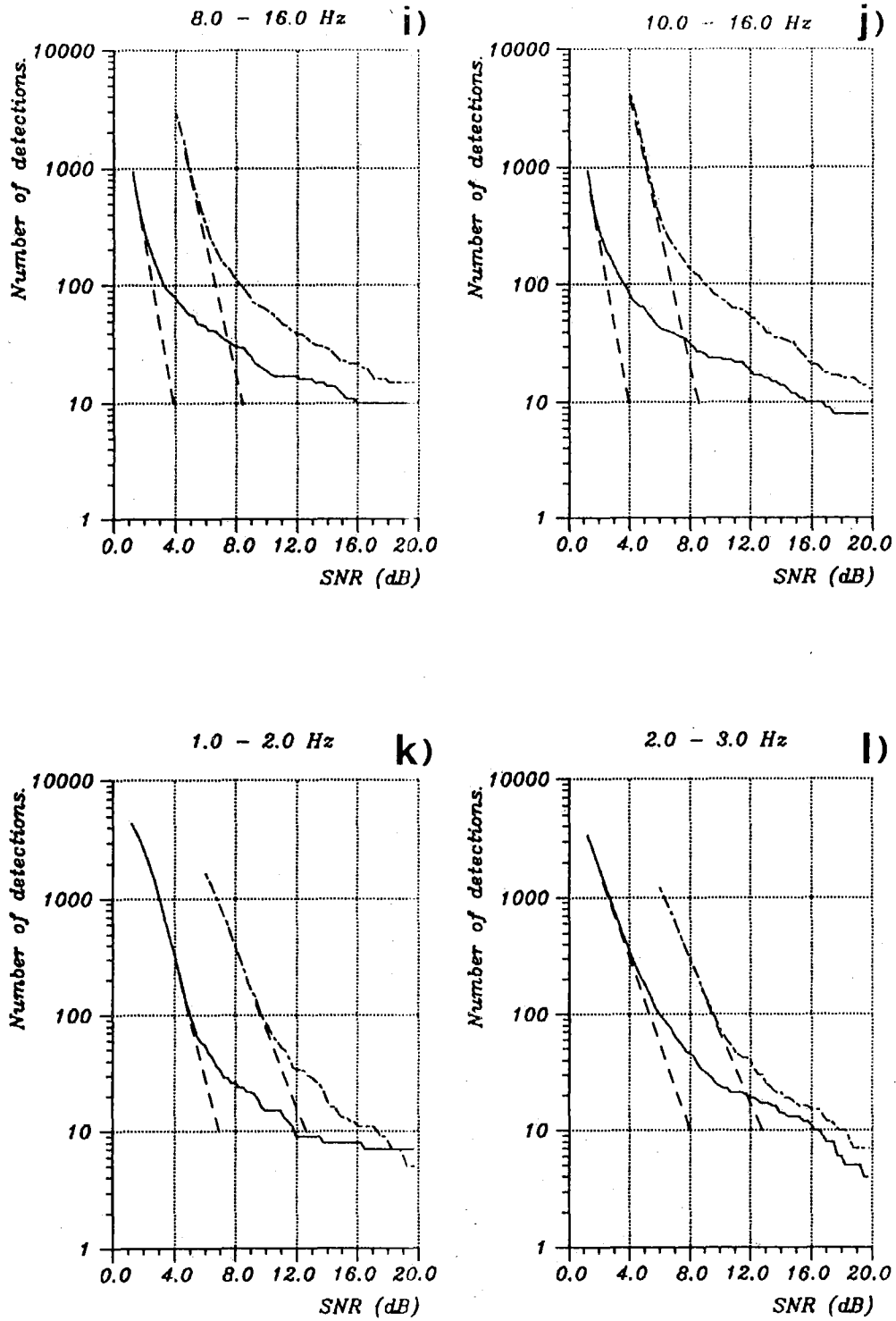
Fig. VII.3.1 (cont.)
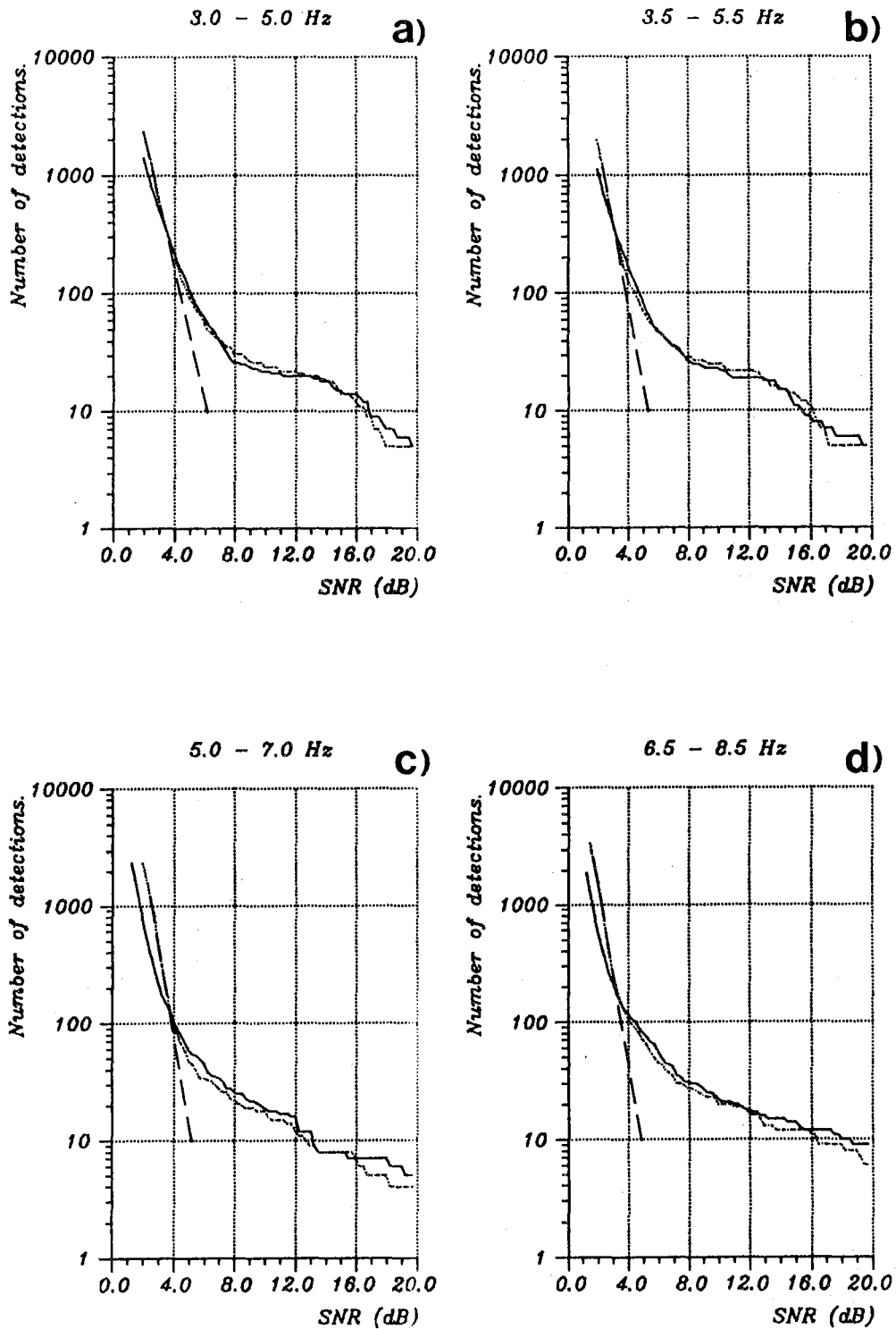
Fig. VII.3.2 This figure (a-d) show the cumulative distributions for the incoherent beams from the vertical channels (solid lines) and from the horizontal channels (dotted lines) for four different filter bands. The dashed lines indicate the noise slopes inferred from the 'noise' distributions of the 'horizontal' beams.
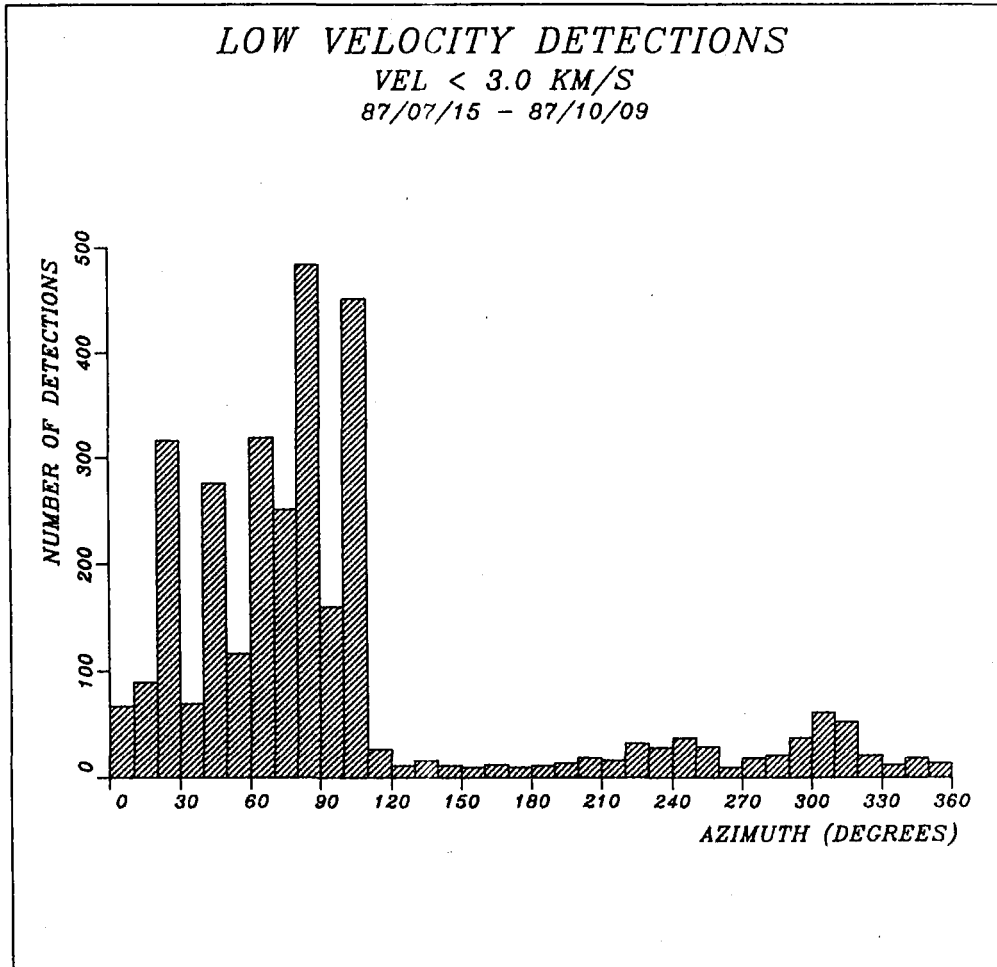
Fig. VII.3.3   This histogram displays the azimuthal distribution of
               RONAPP detections during the 86-day period indicated,
               with apparent velocities less than 3.0 km/s. Within the
               investigated time interval there were totally 10000
               detections. 3140 of these detections had an apparent
               velocity less than 3.0 km/s.

VII.4 Initial results from analysis of data recorded at the new regional array in Finnmark, Norway

During the summer and fall of 1987, a regional array was installed near the town of Karasjok in the county of Finnmark in northern Norway. The new Finnmark array was designed to be as closely as possible a copy of the NORESS regional array, which was established in southern Norway in 1984. The geometries of the two arrays are therefore practically identical (deviations between corresponding sensor positions are of the order of a few tens of meters, due to local terrain conditions), and the data outputs are the same for the two arrays. Fig. VII.4.1 shows the location of the two regional arrays in Norway, and also the location of the FINESA regional array in Finland, which was described by Korhonen et al (1987). The geometry of NORESS (and for most practical purposes, also the geometry of the Finnmark array) is shown in Fig. VII.4.2.

Data from the new Finnmark array have been transmitted continuously via satellite to the NORSAR data processing center at Kjeller since November 1, 1987. The data are subjected to automatic detection processing, with a beam deployment identical to the one used for NORESS.

In the following, we report on some findings resulting from analysis of data from the new Finnmark array. It should be emphasized at the outset that the available data cover no more than a two-week period, and that a comprehensive assessment of the capabilities of the new array must await the collection of data covering a longer time span.

Noise spectra

Fig. VII.4.3a shows corrected noise spectra for altogether 17 elements of the new Finnmark array (the vertical sensors at A0 and the C- and

D-rings, see Fig. VII.4.2), taken it 00.00 GMT on day 315. For comparison, NORESS noise spectra for the same number of channels and taken at the same time, are shown in Fig. VII.4.3b. From these figures, it is seen that below 2.0 Hz, the Finnmark array experiences a higher noise level than NORESS, whereas above 2.0 Hz the Finnmark site is clearly the quieter.

The high noise level at low frequencies at the Finnmark site has been confirmed by other data and is typically even higher than shown in Fig. VII.4.3a. At the time of these spectra, the nearby coast of Finnmark experienced a wind force 4, which is moderate. The noise level at these low frequencies is generally believed to be governed by the passage of major weather fronts over the open ocean. Therefore, it should not be unexpected to find the higher microseismic noise levels at the Finnmark array, since this array is located closer to the coast than the NORESS array.

For the frequency range above 2 Hz, the noise level at the Finnmark site appears to be 3-5 dB below that of NORESS. A possible explanation here is that the noise in this band is lower at the northern site because of a lower population density and also lower level of traffic and industrial activities, compared to the NORESS site. These noise levels must also be rated as low relative to year-round averages for NORESS, as investigated by Fyen (1987).

Figs. VII.4.4a and 4b each show ten uncorrected spectra, taken hourly between 00.00 GMT and 10.00 GMT of day 315, for the Finnmark and NORESS arrays, respectively. Each single spectrum represents an average of 17 spectra for the vertical sensors of AO, the C- and D-rings. The NORESS spectra show the well-established (Fyen, 1986a,b; 1987) difference between night-time and day-time noise characteristics

(particularly around 6 Hz). The Finnmark data are generally below those of the NORESS site for frequencies above 2 Hz. The two or three curves with the higher noise power in Fig. VII.4.4a represent cases of high frequency noise bursts at the Finnmark site during daytime. These bursts are visually confirmed by careful inspection of the seismograms. A more comprehensive study is needed to clarify the origin of this noise. There is so far, however, no indication of constant noise sources like power plants and sawmills.

It should be emphasized again that in order to establish reliable estimates of ambient noise levels at the new array site, studies like those undertaken by Fyen (1986a,b; 1987) for NORESS are needed. The material analyzed so far, however, indicates that in the range of primary interest to regional seismic verification (i.e., above 2 Hz), the noise level at the new Finnmark array site is generally somewhat lower than the NORESS noise level.

Noise suppression by beamforming

The NORESS array has proved very proficient in the enhancement by beamforming of the SNR, yielding gains that are often of the order of or even in excess of $\sqrt{N}$ (N being the number of sensors used in the beamforming). It has been shown that this success is largely due to the highly effective noise suppression that can be obtained by selecting appropriate sub-geometries for the various signal frequencies. As a first check on the new array's capabilities in this regard, noise suppression curves were computed and compared with corresponding results from NORESS.

In Fig. VII.4.5a, the noise suppression in the frequency range 0-20 Hz
for vertical beamforming (no shifts introduced) is shown for three
one-minute intervals taken hourly at 00.00, 01.00 and 02.00 GMT on day
315. The sub-geometry used is that of AO, the B- and C-ring instru-
ments (13 sensors). The dots in this figure represent average values
for NORESS that are taken from Fyen (1986c). The $\sqrt{N}$ level is at about
-11 dB, and the general impression left from this figure is that the
new array is as effective in suppressing noise as NORESS, for this
sub-geometry. For another sub-geometry, comprising the sensors of AO,
the C- and D-rings, corresponding results are given in Fig. VII.4.5b.
Again, we see that the noise suppression capability is comparable to
or maybe even better than the average performance of NORESS. This
strongly suggests that the spatial characteristics (e.g., correlation
lengths vs. frequency) of the noise field are very similar to those
found at NORESS. It has previously been established (Korhonen et al,
1987) that the NORESS and FINESA arrays exhibit strong similarities in
this regard.

**Analysis of data from two regional events located at the Finnmark
array**

As examples of regional events recorded on the Finnmark array, we pre-
sent the records for two presumed mining explosions in the Kola penin-
sula of the USSR.

The C-ring seismograms for the first event are shown in Fig. VII.4.6.
The event occurred at 67.6°N, 34.0°E (according to the University of
Helsinki bulletin), at an epicentral distance of 408 km and an azimuth
of 117.9°. The phases Pn, Pg, Sn and Lg can be clearly identified by
visual inspection. These phases were subjected to wide-band slowness

analysis, with results given in Figs. VII.4.7 and VII.4.8. We see that the phase velocities derived are in the expected range for these phases and that deviations from the "true" azimuth are within 6-7˚.

Data for the second event are shown in Fig. VII.4.9. This event is located at 68.1˚N, 33.2˚E, at an epicentral distance of 349 km and an azimuth of 113.7˚. Besides the phases identified for the first event, we now also see a clearly developed Rg phase. It is of particular interest to note the difference between the two events in this regard, particularly since they are separated by not more than about 60 km. The occurrence of Rg waves in the records for events of epicentral distances of the order of 350 km also sharply contrasts what we have found at NORESS, where Rg waves are never observed beyond 100 km distance. The results of the wide-band slowness analysis of the phases Pn, Pg, Lg and Rg for this event are shown in Figs. VII.4.10 and VII.4.11. Again we see that the phase velocities are reasonable, and the azimuths deviate by not more than 5˚ from the "true" value.

Regional event detection

An initial study has been made comparing the regional event detection performance of the two arrays in Norway. A two-week period (Oct 31 - Nov 18, 1987) was selected for this purpose, and analysis of RONAPP processing results for the two arrays was conducted. For both arrays, the beam deployments and thresholds were identical, and the same as those used for the past two years in regular NORESS operation.

Fig. VII.4.12 shows a map displaying all regional events located by NORESS during this time period, whereas Fig. VII.4.13 gives a similar map for the Finnmark array. We recall that in order for one array to

locate a regional event, at least two phases (P and Lg) from that
array must be detected and associated.

Comparing these two figures is quite instructive, and probably gives a
reliable impression of what can be expected during long-term
operation. The actual number of located events is similar for the two
arrays (NORESS 152, Finnmark 117). However, there is almost no overlap
of the two populations; in fact only 8 events were located by both
arrays. The large majority of located events are within 500 km of the
respective arrays, and represent in most cases presumed local explo-
sions of low magnitude (M_L < 1.5). Sites where such explosions are
clustered can be easily identified on the plots. It is noteworthy in
particular that the Finnmark array detects and locates a large number
of mining explosions in the Kola peninsula.

Fig. VII.4.14 shows a map of all events of estimated M_L > 2.0 located
by at least one array. In those cases when both arrays located the
same event, the location by the closest array was chosen. Events with
at least one confirming phase (P or Lg) from the other array are
encircled. Details pertaining to the figure are given in Table
VII.4.1.

Compared to the previous figures, it is clear that relaxing the cri-
terion for "common" events to requiring only one confirming phase from
the other array significantly increases the overlap of the
populations. The majority of events in Fig. VII.4.14 are thus detected
by both arrays. It is particularly interesting to observe the good
performance for the event cluster near 65°N 40°E, which is at a con-
siderable distance from both arrays (700 and 1500 km, respectively).
These events were in the magnitude range 2.5-2.7 and the locations
have been independently confirmed by the Finnish network.

In almost all cases of confirming detections by one phase only, this corresponded to a P phase (Table VII.4.1). This result is somewhat surprising in view of earlier P and Lg detection studies for NORESS and may not be representative. Further assessment of the joint detection and location potential of the two arrays will require a more extensive data base, and will be the subject of further study.

S. Mykkeltveit
F. Ringdal
J. Fyen
T. Kværna

References

Fyen, J. (1986a): NORESS noise spectral studies, preliminary report. Semiannual Technical Summary, 1 Oct 1985 - 31 Mar 1986, NORSAR Sci. Rep. No. 2-85/86, Kjeller, Norway.

Fyen, J. (1986b): NORESS noise spectral studies - noise level characteristics. Semiannual Technical Summary, 1 Apr 1986 - 30 Sept 1986, NORSAR Sci. Rep. No. 1-86/87, Kjeller, Norway.

Fyen, J. (1986c): NORESS noise spectral studies - beam suppression. Semiannual Technical Summary, 1 Apr 1986 - 30 Sept 1986, NORSAR Sci. Rep. No. 1-86/87, Kjeller, Norway.

Fyen, J. (1987): NORESS noise spectral studies. Noise level characteristics. Semiannual Technical Summary, 1 Oct 1986 - 31 Mar 1987, NORSAR Sci. Rep. No. 2-86/87, Kjeller, Norway.

Korhonen, H., S. Pirhonen, F. Ringdal, S. Mykkeltveit, T. Kværna, P.W. Larsen and R. Paulsen (1987): The Finesa array and preliminary results of data analysis. Univ. of Helsinki, Inst. of Seismology, Report S-16.

Reference Array		NORESS	Finnmark
Total no. of events located by reference array		152	117
No. of events $M_L \geqslant 2.0$		31	42
No. of events $M_L \geqslant 2.0$ located by the reference array, detected or not detected by the other array.	Both P and Lg	8	8
	P only	14	12
	Lg only	1	1
	Not detected	8	21

Table VII.4.1 Statistics of detected and located regional events for the two arrays in Norway during a two-week test period.

REGIONAL ARRAYS IN FENNOSCANDIA

LONGITUDE (DEG E)
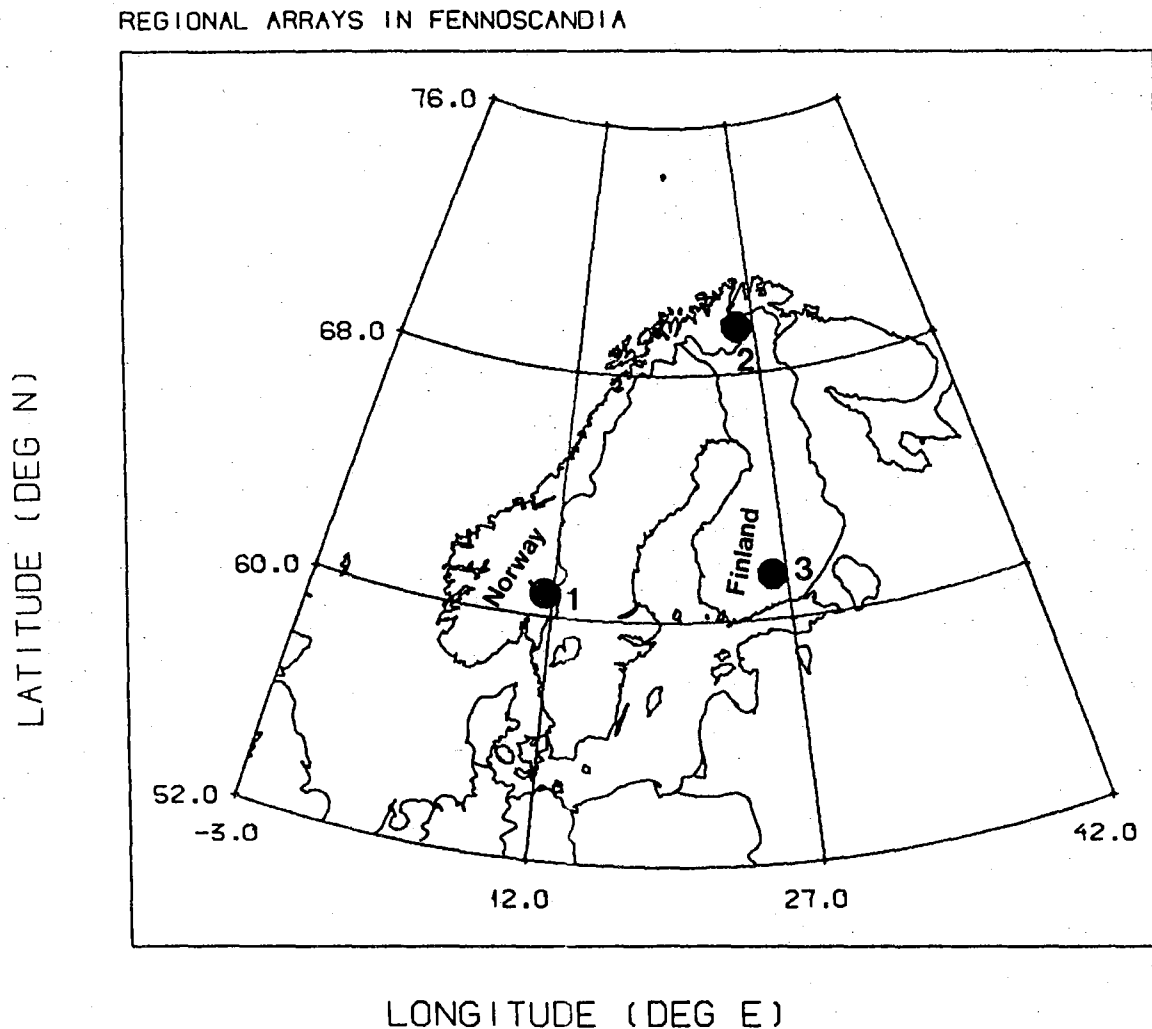
87/11/25 11.42 NORSAR

Fig. VII.4.1 The figure shows the network of three regional arrays in
Fennoscandia. 1: The NORESS array in southern Norway;
2: The new array in Finnmark, northern Norway; and
3: The FINESA array in Finland.
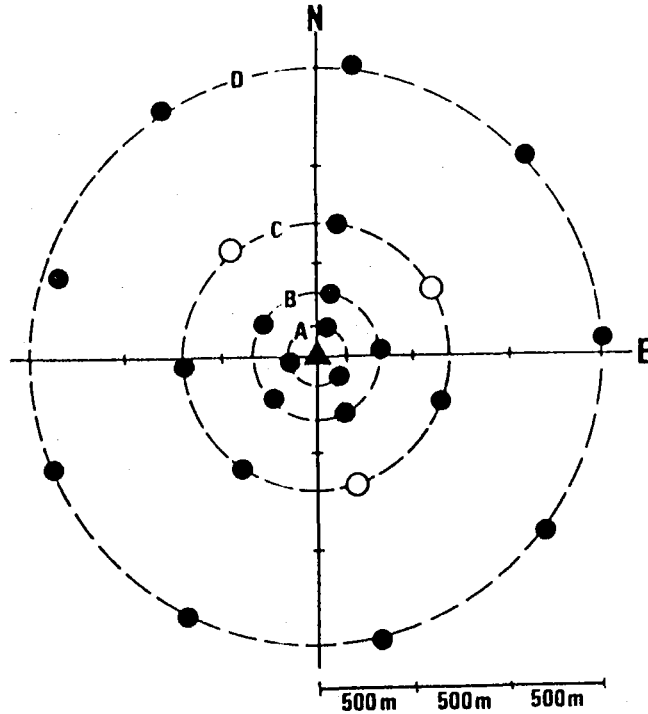
LEGEND:

● VERTICAL SHORT PERIOD

○ 3-COMPONENT SHORT PERIOD

▲ 3-COMPONENT BROAD BAND
   AND 3-COMPONENT SHORT PERIOD

Fig. VII.4.2   The geometry of the NORESS array. The geometry of the
new Finnmark array comes very close to being identical
to that of NORESS; deviations between corresponding ele-
ment positions are of the order of some tens of meters.
The channel assignments (vertical only vs. three-
component, short period vs. broadband) are identical for
the two arrays. The short period instrument at the
center of the array is denoted AO.

FINMARK NOISE

11/20/87 10:24:49
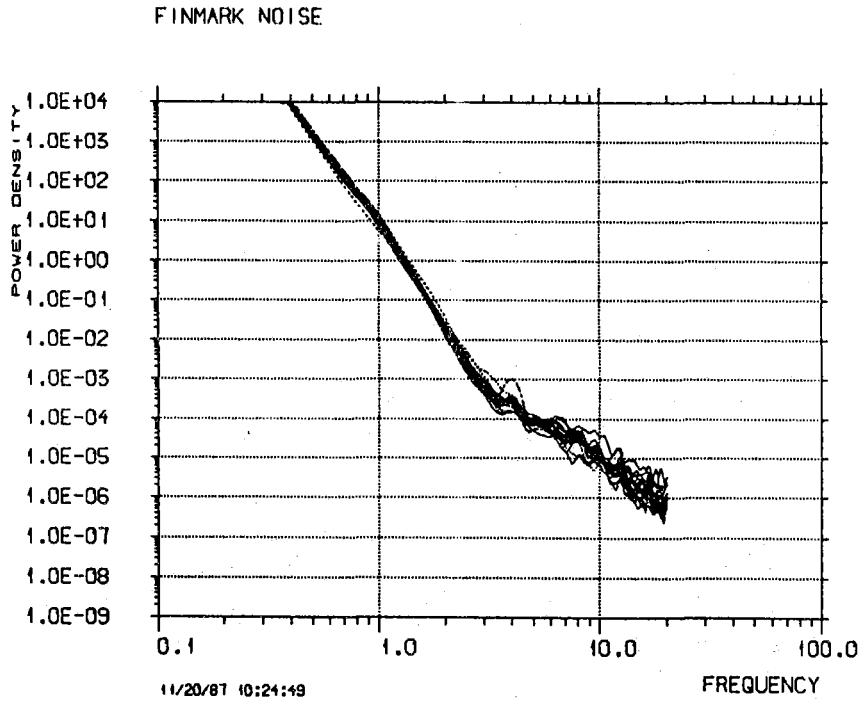
Fig. VII.4.3a Noise spectra corrected for system response for the
Finnmark array for 17 vertical channels at AO, the C-
and D-rings. The spectra are base don one minute of data
at 00.00 GMT on day 315. The power density is in nm^2/Hz.

NORESS NOISE

11/24/87 09:31:56
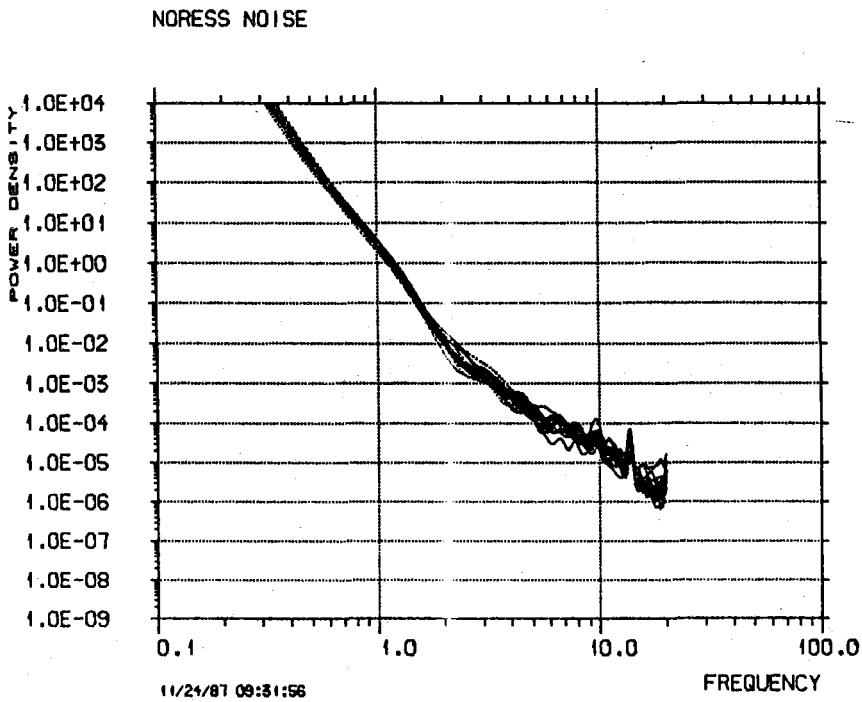
Fig. VII.4.3b Same as Fig. VII.4.3a, but for NORESS data taken at
00.15 GMT on day 315.

FINNMARK AVERAGE NOISE 00-10
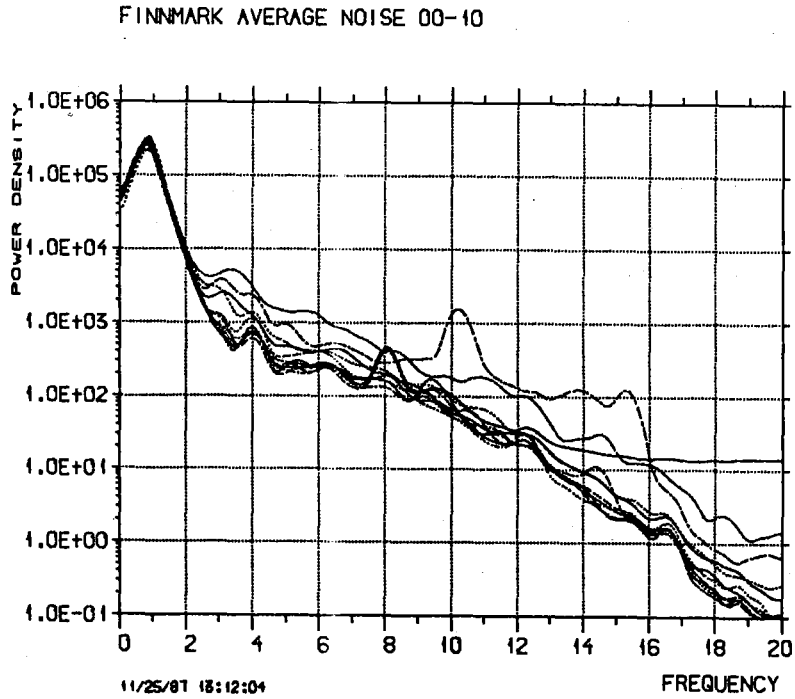
Fig. VII.4.4a Uncorrected noise spectra for the Finnmark array for ten one-minute intervals taken hourly between 00.00 and 10.00 GMT on day 315. Each spectrum represents an average of the 17 vertical sensors of AO, the C- and D-rings.

NORESS AVERAGE NOISE 00-10
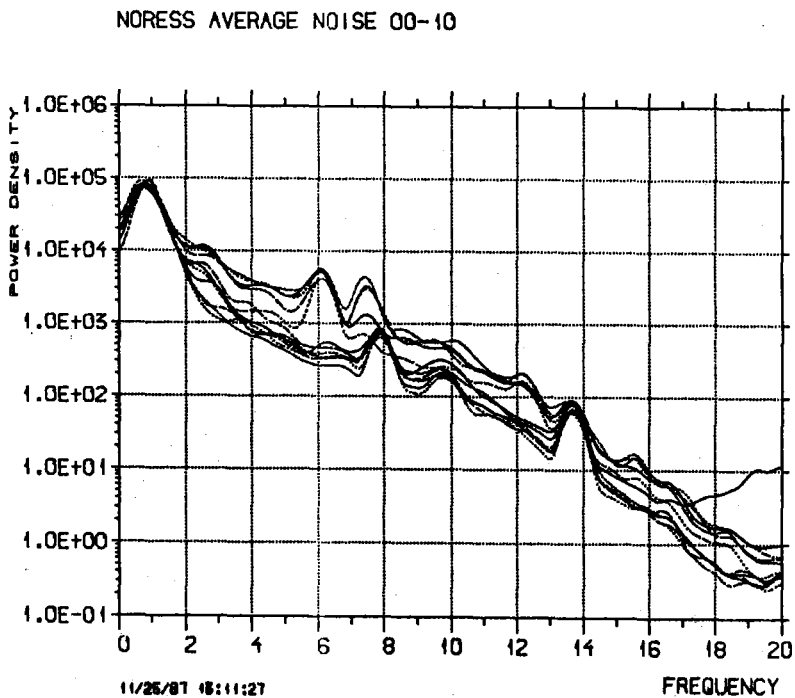
Fig. VII.4.4b Same as Fig. VII.4.4a, but for NORESS data taken hourly between 00.00 and 10.00 GMT on day 315.

FINNMARK CRING BEAM SUPPRESSION
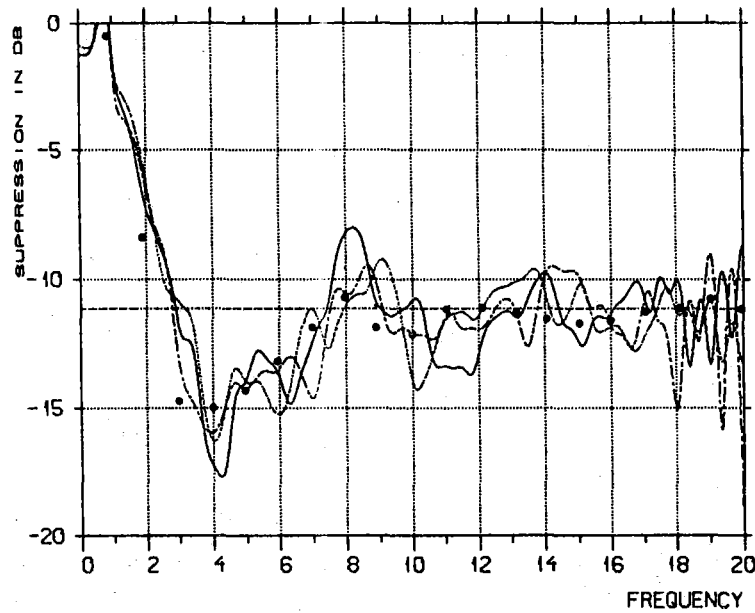
Fig. VII.4.5a Finnmark array noise suppression by beamforming for the sub-
geometry comprising the AO, B- and C-ring sensors. To produce
these curves, a vertical beam is formed and the spectrum for
this beam is divided by the average of the single sensor
spectra. The three curves result from one minute of data
taken hourly at 00.00, 01.00 and 02.00 GMT on day 315. The
dots represent typical NORESS noise suppression values for
this sub-geometry. The horizontal line at -11.1 dB represents
√N suppression for 13 sensors.

FINNMARK TELEV BEAM SUPPRESSION
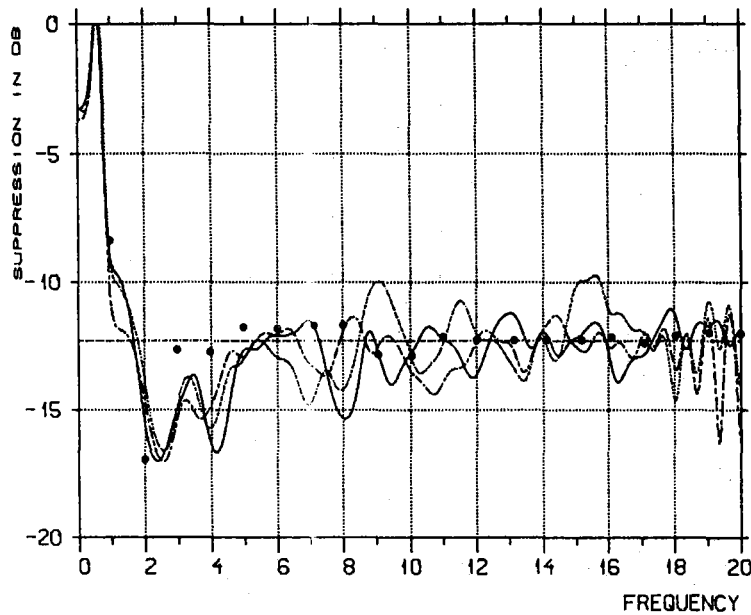
Fig. VII.4.5b Same as Fig. VII.4.5a, but for the sub-geometry comprising
the sensors of AO, the C- and D-rings. The horizontal line at
-12.3 dB represents √N suppression for 17 sensors.
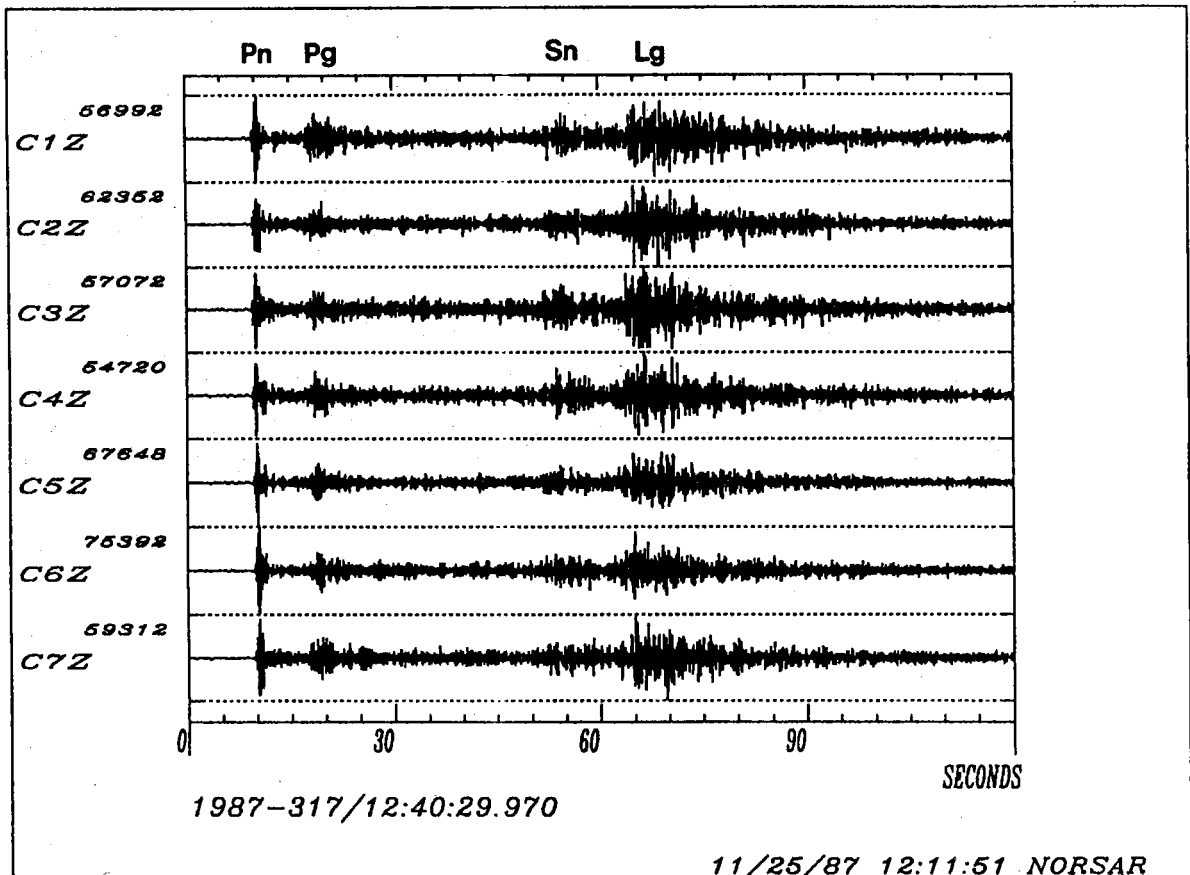
Fig. VII.4.6   Finnmark array data for a presumed mining explosion at
67.6°N, 34.0°E. The plot shows data for the vertical
instruments of the C-ring.

Wide-band slowness analysis

Contours in decibels below maximum peak

Pn

Time 1987/317:12 40 39.170
Interval   3.0 sec

Channels:

A0Z	C4Z
A1Z	C5Z
A2Z	C6Z
A3Z	C7Z
B1Z	D1Z
B2Z	D2Z
B3Z	D3Z
B4Z	D4Z
B5Z	D5Z
C1Z	D6Z
C2Z	D7Z
C3Z	D8Z
	D9Z

BAND   6.0– 8.0 Hz

VEL: 7.38 km/s   AZ: 123.07 deg.   REL.PWR: 0.66   PWR: 73.7 dB

11/26/87 14:05:16

Wide-band slowness analysis

Contours in decibels below maximum peak

Pg

Time 1987/317:12 40 46.970
Interval   3.0 sec

Channels:

A0Z	C4Z
A1Z	C5Z
A2Z	C6Z
A3Z	C7Z
B1Z	D1Z
B2Z	D2Z
B3Z	D3Z
B4Z	D4Z
B5Z	D5Z
C1Z	D6Z
C2Z	D7Z
C3Z	D8Z
	D9Z

BAND   2.0– 4.0 Hz

VEL: 7.22 km/s   AZ: 117.33 deg.   REL.PWR: 0.71   PWR: 66.1 dB

11/26/87 14:29:54

Fig. VII.4.7   Wide-band slowness spectra for the Pn phase (top) and Pg
phase (bottom) for the event in Fig. VII.4.6.

Wide-band slowness analysis

Contours in decibels below maximum peak

Sn

Horizontal slowness Sx (sec/km)

Horizontal slowness Sy (sec/km)

Time 1987/317:12 41 20.970

Interval   3.0 sec

Channels:

AOZ	C4Z
A1Z	C5Z
A2Z	C6Z
A3Z	C7Z
B1Z	D1Z
B2Z	D2Z
B3Z	D3Z
B4Z	D4Z
B5Z	D5Z
C1Z	D6Z
C2Z	D7Z
C3Z	D8Z
	D9Z

BAND   3.5- 5.5 Hz

VEL: 4.02 km/s AZ: 124.62 deg. REL.PWR: 0.31 PWR: 63.3 dB

11/26/87 16:43:47

Wide-band slowness analysis

Contours in decibels below maximum peak

Lg

Horizontal slowness Sx (sec/km)

Horizontal slowness Sy (sec/km)

Time 1987/317:12 41 33.970

Interval   3.0 sec

Channels:

AOZ	C4Z
A1Z	C5Z
A2Z	C6Z
A3Z	C7Z
B1Z	D1Z
B2Z	D2Z
B3Z	D3Z
B4Z	D4Z
B5Z	D5Z
C1Z	D6Z
C2Z	D7Z
C3Z	D8Z
	D9Z

BAND   3.0- 5.0 Hz

VEL: 4.22 km/s AZ: 119.10 deg. REL.PWR: 0.37 PWR: 73.9 dB

11/26/87 14:34:55

Fig. VII.4.8   Wide-band slowness spectra for the Sn phase (top) and Lg phase (bottom) for the event in Fig. VII.4.6.
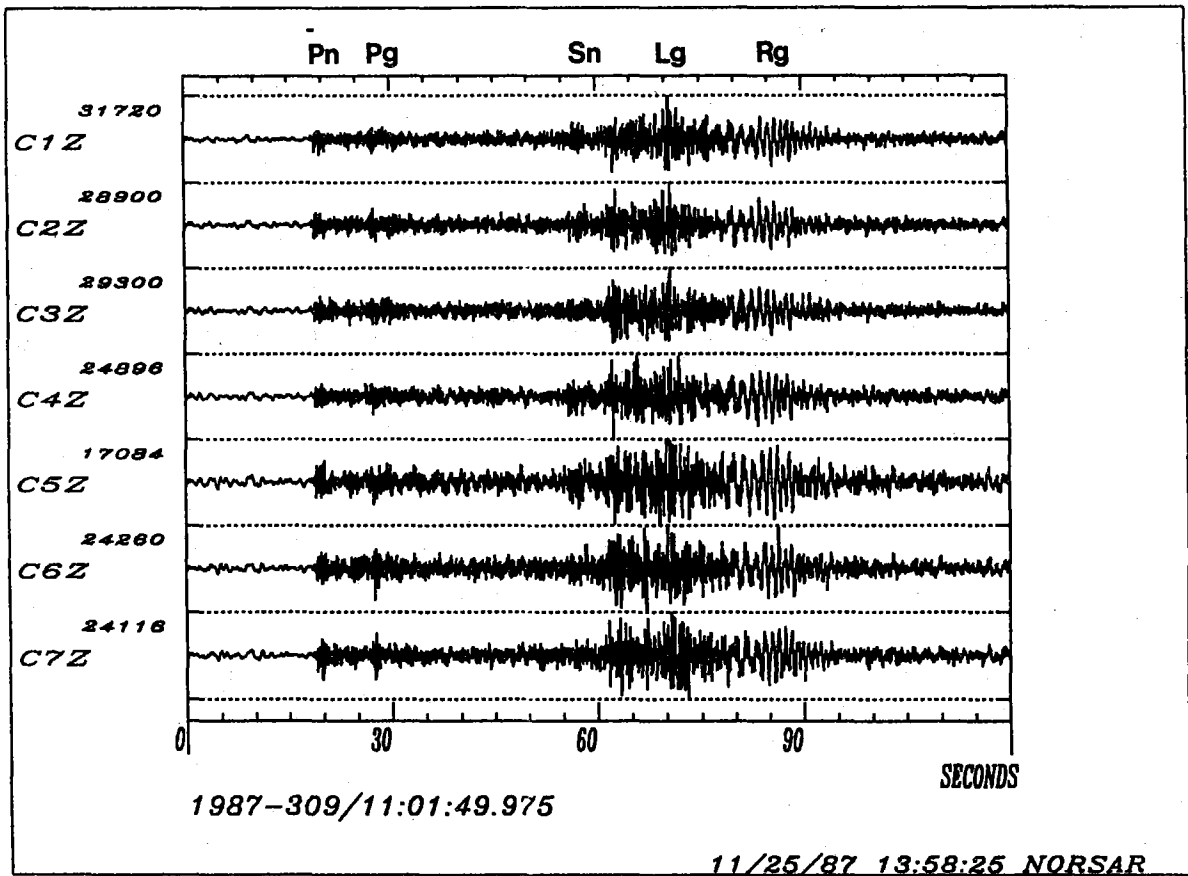
Fig. VII.4.9 Finnmark array data for a presumed mining explosion at
68.1°N, 33.2°E. The plot shows data for the vertical
instruments of the C-ring.

Wide-band slowness analysis

Contours in decibels below maximum peak

Pn

Time 1987/309:11 02 07.975
Interval   3.0 sec

Channels:

AOZ	C4Z
A1Z	C5Z
A2Z	C6Z
A3Z	C7Z
B1Z	D1Z
B2Z	D2Z
B3Z	D3Z
B4Z	D4Z
B5Z	D5Z
C1Z	D6Z
C2Z	D7Z
C3Z	D8Z
	D9Z

BAND   5.0- 7.0 Hz
VEL: 8.17 km/s   AZ: 118.64 deg.   REL.PWR: 0.71   PWR: 57.5 dB

11/26/87 16:05:28

Wide-band slowness analysis

Contours in decibels below maximum peak

Pg

Time 1987/309:11 02 15.975
Interval   3.0 sec

Channels:

AOZ	C4Z
A1Z	C5Z
A2Z	C6Z
A3Z	C7Z
B1Z	D1Z
B2Z	D2Z
B3Z	D3Z
B4Z	D4Z
B5Z	D5Z
C1Z	D6Z
C2Z	D7Z
C3Z	D8Z
	D9Z

BAND   4.0- 6.0 Hz
VEL: 7.69 km/s   AZ: 118.70 deg.   REL.PWR: 0.63   PWR: 58.4 dB

11/26/87 16:12:46

Fig. VII.4.10 Wide-band slowness spectra for the Pn phase (top) and Pg phase (bottom) for the event in Fig. VII.4.9.

Wide-band slowness analysis

Contours in decibels below maximum peak

Lg

Time 1987/309:11 02 58.475
Interval   4.0 sec

Channels:

AOZ	C4Z
A1Z	C5Z
A2Z	C6Z
A3Z	C7Z
B1Z	D1Z
B2Z	D2Z
B3Z	D3Z
B4Z	D4Z
B5Z	D5Z
C1Z	D6Z
C2Z	D7Z
C3Z	D8Z
	D9Z

Horizontal slowness Sx (sec/km)

BAND   2.0- 4.0 Hz
VEL: 4.03 km/s AZ: 115.03 deg. REL.PWR: 0.68 PWR: 68.6 dB

11/26/87 16:57:50

Wide-band slowness analysis

Contours in decibels below maximum peak

Rg

Time 1987/309:11 03 08.975
Interval 10.0 sec

Channels:

AOZ	C4Z
A1Z	C5Z
A2Z	C6Z
A3Z	C7Z
B1Z	D1Z
B2Z	D2Z
B3Z	D3Z
B4Z	D4Z
B5Z	D5Z
C1Z	D6Z
C2Z	D7Z
C3Z	D8Z
	D9Z

Horizontal slowness Sx (sec/km)

BAND   0.9- 1.0 Hz
VEL: 3.18 km/s AZ: 115.70 deg. REL.PWR: 0.97 PWR: 74.6 dB

11/26/87 16:32:34

Fig. VII.4.11 Wide-band slowness spectra for the Lg phase (top) and Rg
phase (bottom) for the event in Fig. VII.4.9.
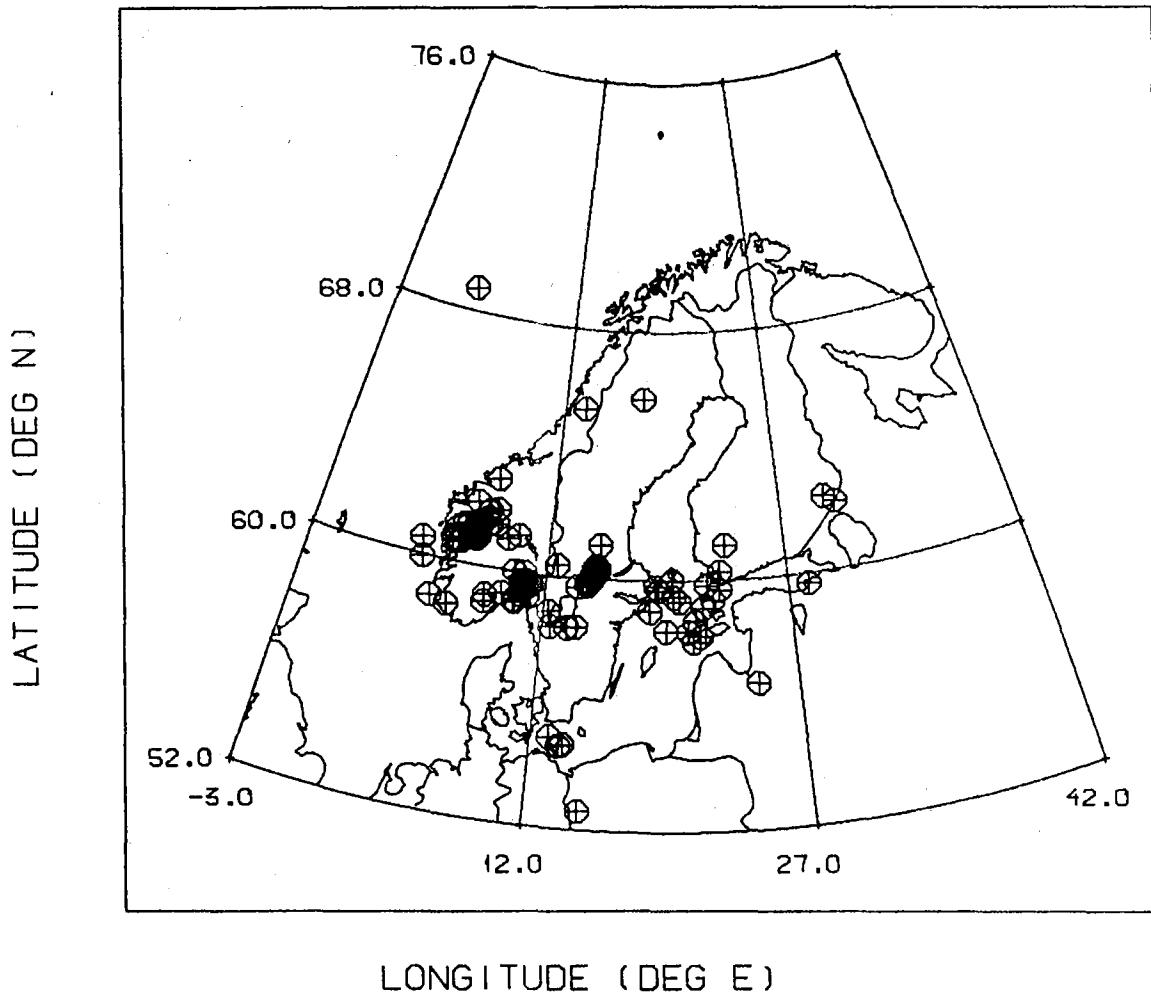
87/11/24 14.07   NORSAR

Fig. VII.4.12 Regional events located by the NORESS array during a
two-week test period.
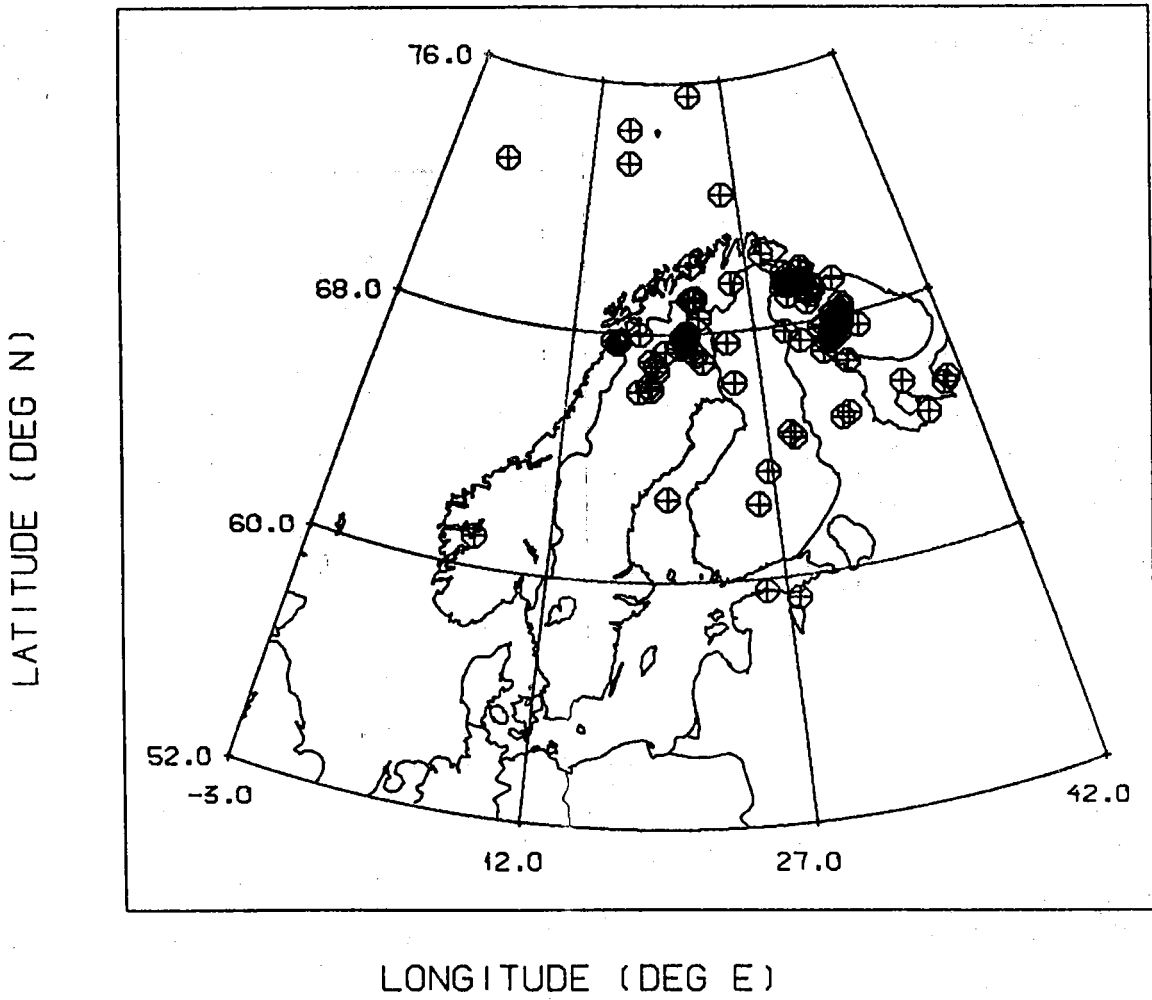
87/11/24 14.15 NORSAR

Fig. VII.4.13 Regional events located by the Finnmark array during a
two-week test period.
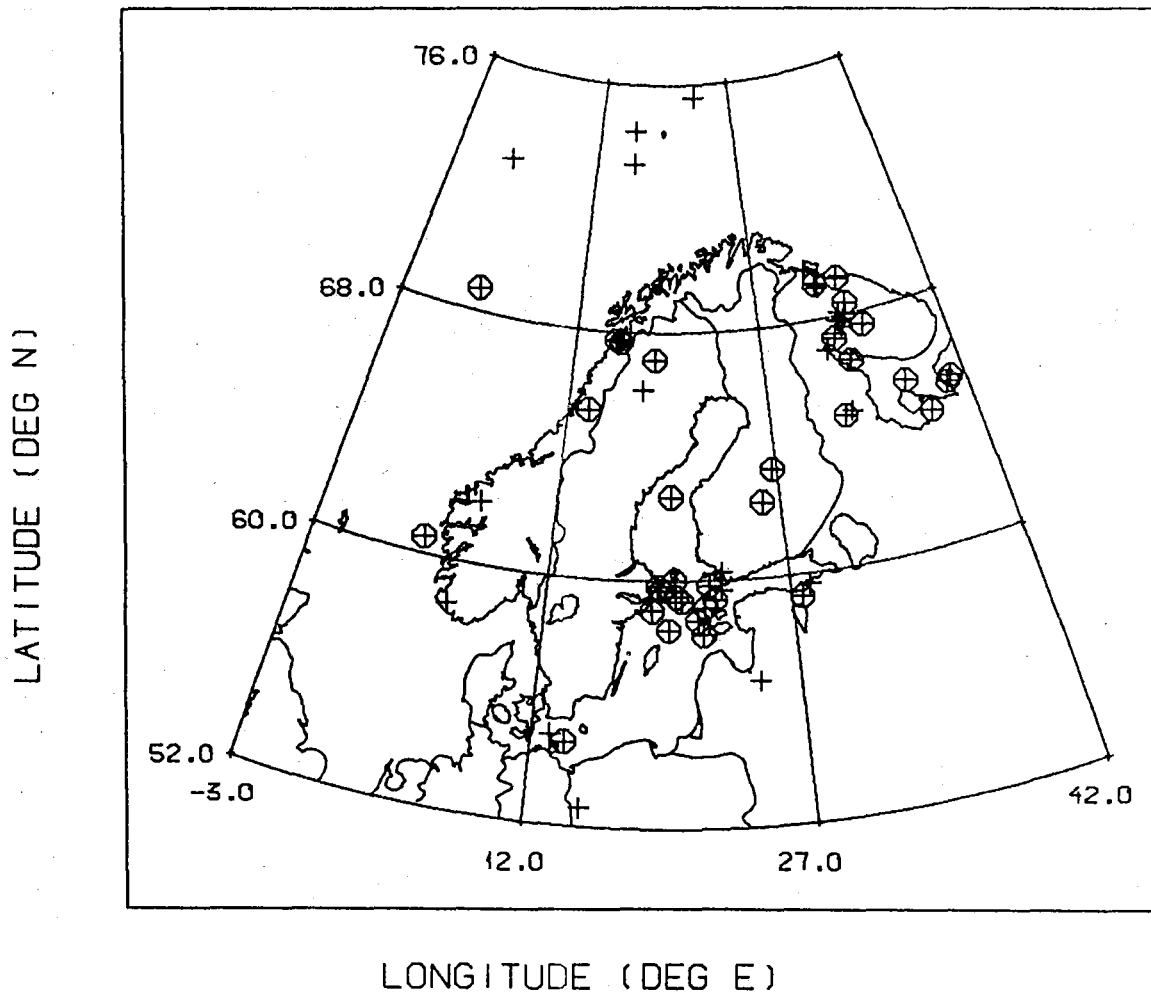
87/11/25 12.43   NORSAR

Fig. VII.4.14 Regional events of $M_L > 2.0$ located by at least one of
the two arrays in Norway during a two-week test period.
Events with at least one confirming phase from the other
array are encircled.

VII.5   Magnitudes of Large Semipalatinsk Explosions using P Coda and
         Lg Measurements at NORSAR

The objective of this study is to investigate the potential of using
NORSAR recorded P coda and Lg waves to obtain stable magnitude
estimates of large underground explosions, thereby improving the
possibility of obtaining reliable yield estimates from teleseismic
recordings.

The NORSAR array (Bungum et al, 1971) has been in operation since
1970. Originally comprising 22 subarrays, with a total of 132 short
period vertical seismometers, the array was reduced to 7 subarrays (42
SPZ seismometers) in 1976. In order to obtain consistency over time,
this analysis has been restricted to data from these 7 subarrays. With
the exception of occasional subarray or instrument outages, this pro-
vides for a stable, high quality recording system, making possible
reliable comparison of seismic events recorded during the entire time
period.

The general characteristics of NORSAR recorded P coda and Lg waves for
Semipalatinsk explosions have earlier been studied by Ringdal (1983)
and Baumgardt (1985). Ringdal (1983) found by comparing with ISC
reported m_b that the use of Lg based magnitudes effectively eliminated
the systematic P-wave magnitude differences observed at NORSAR for
explosions from the two main test sites within the Semipalatinsk area
(Shagan River and Degelen Mountains). Gupta et al (1985) studied
NORSAR P and P coda recordings from NTS explosions, and found that P
coda measurements provided significantly more precise yields than
those based on the initial P. They also obtained promising results in
applying P coda measurements to NORSAR recordings from Semipalatinsk
explosions.

The propagation path from Semipalatinsk to NORSAR is indicated in Fig. VII.5.1, where also a map of the NORSAR array is shown. In spite of the large epicentral distance (4200 km), the Lg phase can be identified for most explosions of $m_b > 5.0$. However, as shown in the example of Fig. VII.5.2, the Lg amplitude is usually only slightly higher than that of the preceding P coda, and this feature is largely independent of event size.

The data base for this study consists of 72 presumed explosions from the Shagan River area, USSR, covering the time period 1972 to 1987. All such events of ISC $m_b > 5.0$ were included, except for a few cases of NORSAR system outages. The event set is listed in Table VII.5.1, together with ISC or PDE magnitude estimates (m_b) as well as parameters estimated in this study. For most of the events, very accurate location estimates have been computed by Marshall et al (1985), and additional such data have been provided by P. Marshall (personal communication). Otherwise, NEIS or NORSAR location estimates are used. In addition, this study has also made use of maximum likelihood m_b magnitudes estimated at Blacknest from ISC data (P. Marshall, personal communication) and m_b (Lg) estimates published by Nuttli (1986).

Parameter estimation methods

Lg and P coda magnitudes were estimated from NORSAR data for each event using three different methods (for illustration, see Fig. VII.5.2). All three methods were applied to filtered NORSAR SP channels, using a 0.6-3.0 Hz Butterworth bandpass filter. In earlier studies (Ringdal, 1983), this frequency band has been found to retain the main P and Lg energy while suppressing microseismic noise.

The first method pertains to the Lg phase and comprises direct measurement on individual traces of the largest cycle with a period close to 1 Hz, within a group velocity window of 3.25-3.70 km/s. (The

average Lg group velocity is close to 3.5 km/s.) The amplitude (zero to peak) and the corresponding period were measured and converted to ground motion A_{ij} (i'th event, j'th channel). The amplitudes were then corrected for dispersion, geometrical spreading and anelastic attenuation as described by Nuttli (1986), using parameter values (Q_0 = 700, ξ = 0.4) derived by Nuttli for the nearby station KON. This resulted in an Lg magnitude estimate MLA_{ij} for each analyzed trace.

Repeating this process for all center instruments of the 7 operational NORSAR subarrays (deleting faulty channels) the NORSAR Lg magnitude MLA was then estimated as:

$$MLA_i = \frac{1}{N} \cdot \sum_{j=1}^{N} MLA_{ij} \tag{1}$$

where N (N < 7) is the number of channels.

The second and third methods both comprise automatic RMS measurements of individual channels and pertain to P coda and Lg magnitudes, respectively. For the P coda measurement, a time window of 30 seconds is selected, starting 20 seconds after P onset. The LG window is 2 minutes long, covering the group velocity interval of 3.67 to 3.33 km/s. In addition, a 30 second noise window immediately before P onset was selected for each processed channel. The estimation procedure described in the following was applied for each event to all 42 currently operational NORSAR SP channels, except that faulty channels were deleted.

We denote by s_{ijk} the k'th sample of the filtered trace of event i, instrument j. We define the log mean square L_{ij} by

$$L_{ij} = \log \left[\frac{1}{K} \cdot \sum_{k=1}^{K} s^2_{ijk} \right] \qquad (2)$$

where K is the number of samples in the selected time window. The quantity L_i is defined as

$$L_i = \frac{1}{M} \cdot \sum_{j=1}^{M} L_{ij} \qquad (3)$$

where M(≤ 42) is the number of operative channels.

We denote L_i^N, L_i^C and L_i^L the values of L_i when computed over the noise window (30 seconds, K = 600), P coda window (30 seconds, K = 600) and Lg window (120 seconds, K = 2400), respectively.

The NORSAR P coda RMS magnitudes (MCR_i) and Lg RMS magnitudes (MLR_i) are then estimated by correcting for noise and adjusting to standard scales as follows:

$$MCR_i = 0.5 \cdot \log\left[\exp(L_i^C) - \exp(L_i^N)\right] + B_C \qquad (4)$$

$$MLR_i = 0.5 \cdot \log\left[\exp(L_i^L) - \exp(L_i^N)\right] + B_L \qquad (5)$$

The constants B_C and B_L are determined by the constraints:

$$\sum (MCR_i - MBMLE_i) = 0 \tag{6}$$

$$\sum (MLR_i - MBLG_i) = 0 \tag{7}$$

where $MBLG_i$ is the Lg magnitude given by Nuttli (1986) of the i'th event, $MBMLE_i$ is the maximum likelihood m_b estimate discussed earlier and the sums are taken over all common events.

We also computed <u>uncorrected</u> P coda and Lg magnitudes for purpose of comparison. These were obtained by deleting the noise term in (4) and (5).

Data analysis

The three estimation methods described above were applied to the events in the data set of Table VII.5.1. The procedure to compensate for background noise level had negligible effect on the RMS P coda magnitudes, since the SNR in these cases was consistently high. However, for some of the smaller events ($m_b(ISC) < 5.6$), the effect on RMS Lg was significant, and the resulting estimates must be considered more uncertain than for the large explosions. This is illustrated in Figs. VII.5.3 and VII.5.4, which show, respectively, the uncorrected and corrected RMS Lg estimates plotted against the NORSAR amplitude based Lg magnitudes.

Table VII.5.2 gives a list of standard deviation of magnitude differences for all combinations of sources. We note that the NORSAR P coda magnitude correlate well with ISC maximum likelihood m_b ($\sigma = 0.06$), as is also seen from the plot in Fig. VII.5.5. In fact, the

correlation is about as good as between the two ISC-based measurements.

It has earlier been noted by many authors that P coda provides much more stable m_b estimates than the initial P phase, which is subject to strong focussing or defocussing along its ray path. Such effects are to a large extent averaged out in the P coda by various scattering mechanisms. Nevertheless, our analysis has shown that P coda amplitudes across NORSAR are positively correlated with initial P amplitude patterns. Thus, not all of the P focussing/defocussing effects are eliminated, and, by reciprocity, focussing at the source would be expected to significantly affect P coda magnitudes, especially over a larger epicentral area than considered in this paper.

From Table VII.5.2 we also note that the various Lg based measures show surprisingly little correlation with each other, although the RMS noise correction explains much of the scatter between the two Lg estimates based on NORSAR data. Fig. VII.5.6 shows NORSAR RMS Lg versus Nuttli (1986) m_b (Lg) for common events. Even at high magnitudes, where NORSAR noise corrections are insignificant, there is a large scatter. The reasons for this lack of consistency need to be further investigated, but it must be noted that the NORSAR measurements have the advantage of being based on a system stable over time, and with high quality digital recording.

Comparing the Lg based measurements to the ISC maximum likelihood m_b, it appears that the NORSAR RMS Lg shows best correlation ($\sigma = 0.092$). Fig. VII.5.7 compares these two magnitude measures, whereas Fig. VII.5.8 shows NORSAR P coda versus NORSAR RMS Lg magnitudes. Comparing these two figures, it is evident that Fig. VII.5.8 has a slightly larger scatter ($\sigma = 0.101$) and, moreover, apparently could be split into two subpopulations with parallel trends.

Figs. VII.5.9 and VII.5.10 show that this is no coincidence. On Fig.
VII.5.9, the NORSAR P coda - RMS Lg magnitude differences are plotted
as a function of event location (Marshall et al (1985) and NEIS data).
The P coda - Lg statistics are clearly region dependent within the
Shagan River area; in particular the northeast part show consistently
low P coda magnitudes, whereas the southwest part shows P coda magni-
tudes consistently higher than those based on Lg. Fig. VII.5.10 shows
that the same trend is apparent when comparing ISC maximum likelihood
m_b to NORSAR RMS Lg magnitudes. It is clear that application of
regional corrections would improve the mutual consistency of these
magnitudes.

Marshall et al (1985) found that explosions in the northeast and
southwest portions of the Shagan River area produce distinctly dif-
ferent P waveforms when recorded at the UK seismological array sta-
tions, suggesting that the Shagan River site can be subdivided into
two test areas characterized by different geophysical properties. Our
results support this suggestion. Our data show an average bias $m_b(P)$ -
$m_b(Lg)$ of -0.059 ± 0.014 for NE Shagan, and 0.112 ± 0.009 for SW
Shagan. Thus, if we attempt to explain this anomaly as resulting from
the systematic differences in P recordings only, we obtain a relative
$m_b(P)$ bias of about 0.17 m_b units between the two areas. On the other
hand, the possibility of an $m_b(Lg)$ bias cannot be ruled out either.

Fig. VII.5.11 illustrates the relative occurrence of large Semipala-
tinsk explosions after 1976 as a function of NORSAR RMS Lg magnitudes.
The plot, which has a nominal vertical scaling, has been obtained by
adding Gaussian density functions with standard deviations of 0.015
magnitude units centered at each observed magnitude value. The three
clear peaks on this plot might indicate different yield categories. It
is interesting to note that the highest magnitude group includes
explosions from both the southwest and the northeast areas of Shagan
River, whereas similar plots based on P-wave magnitudes would place
all of the largest events in the southwest area. The rightmost peak of

the diagram (magnitude 6.06) would correspond to a yield between 150 and 200 kilotons TNT if Nuttli's (1986) formulae are used. With the inherent uncertainty in the absolute calibration level, this is clearly not inconsistent with the 150 kiloton upper limit of the Threshold Test Ban Treaty.

In conclusion, NORSAR based P coda and Lg magnitudes appear to provide magnitude estimates of large Semipalatinsk explosions comparable in stability to those of a world-wide network. There are indications that the Lg based measurements avoid some of the bias inherent in P-based magnitudes. It would furthermore be reasonable to expect that such measurements based on network averaging would provide even better stability. In conjunction with calibration data to obtain accurate absolute reference to yield, such data would appear to provide for very reliable monitoring of a threshold treaty.

F. Ringdal
B.K. Hokland

References

Baumgardt, D.R. (1985): Comparative analysis of teleseismic P coda and Lg waves from underground explosions in Eurasia. Bull. Seism. Soc. Am. 75, 1413-1433.

Gupta, I.N., R.R. Blandford, R.A. Wagner, J.A. Burnetti and T.W. McElfresh (1985): Use of P coda for determination of yield of nuclear explosions. Geophys. J.R. astr. Soc., 83, 2, 541-554.

Marshall, P.D., T.C. Bache and R.C. Lilwall (1985): Body wave magnitudes and locations of Soviet underground explosions at the Semipalatinsk Test Site. AWRE Report No. 0 16/84, AWRE, MOD(PE), Aldermaston, Berksh., UK.

Nuttli, O.W. (1986): Lg magnitudes of selected East Kazakhstan under-
    ground explosions. Bull. Seism. Soc. Am. 76, 1241-1251.

Ringdal, F. (1983): Magnitudes from P coda and Lg using NORSAR data,
    in NORSAR Semiannual Technical Summary 1 Oct 82 - 31 Mar 83,
    NORSAR Sci. Rep. No. 2-82/83, NTNF/NORSAR, Kjeller, Norway.

ORIGIN DATE	ORIGIN TIME	MB	*** LG(AMP) ***			*** LG(RMS) ***			*** PCODA ****		
			MLA	N	STD	MLR	N	STD	MCR	N	STD
11/02/72	01.26.57.7	6.1	6.132	7	0.040	6.121	42	0.069	6.207	42	0.058
12/10/72	04.27.07.7	6.0	6.157	7	0.066	6.120	42	0.068	6.013	42	0.079
07/23/73	01.22.57.8	6.1	6.185	7	0.082	6.199	41	0.078	6.286	41	0.060
12/14/73	07.46.57.0	5.8	5.951	7	0.087	5.876	42	0.063	5.826	39	0.074
10/16/74	06.32.57.5	5.5	5.455	7	0.086	5.413	42	0.062	5.596	42	0.065
12/27/74	05.46.56.8	5.6	5.849	7	0.054	5.711	42	0.060	5.512	42	0.093
04/27/75	05.36.57.3	5.6	5.677	7	0.060	5.550	42	0.054	5.732	42	0.072
10/29/75	04.46.57.5	5.8	5.755	7	0.100	5.632	42	0.062	5.733	42	0.057
12/25/75	05.16.57.0	5.7	5.817	7	0.053	5.804	42	0.067	0.000	0	0.000
04/21/76	05.02.57.4	5.3	0.000	0	0.000	0.000	0	0.000	5.226	42	0.062
06/09/76	03.02.57.6	5.3	5.462	7	0.091	5.203	42	0.056	5.126	42	0.093
07/04/76	02.56.57.7	5.8	5.831	7	0.036	5.813	42	0.063	5.909	42	0.075
08/28/76	02.56.57.5	5.8	5.762	7	0.085	5.737	41	0.069	5.761	41	0.063
05/29/77	02.56.57.8	5.8	5.788	7	0.066	5.669	39	0.061	5.796	41	0.057
06/29/77	03.06.58.0	5.3	5.274	7	0.021	5.070	39	0.054	5.279	40	0.072
09/05/77	03.02.57.8	5.8	5.953	7	0.075	5.891	39	0.067	5.789	40	0.072
10/29/77	03.07.02.9	5.6	5.889	7	0.083	5.784	39	0.061	5.768	41	0.070
06/11/78	02.56.57.7	5.9	5.824	7	0.066	5.752	39	0.059	5.918	39	0.072
07/05/78	02.46.57.3	5.8	5.823	7	0.086	5.789	39	0.057	5.877	39	0.066
08/29/78	02.37.06.5	5.9	6.005	7	0.060	6.006	39	0.057	5.914	39	0.090
09/15/78	02.36.57.3	6.0	5.948	7	0.093	5.906	38	0.059	5.979	41	0.077
11/04/78	05.05.57.5	5.6	5.906	7	0.039	5.691	39	0.061	5.631	41	0.069
11/29/78	04.33.02.9	6.0	5.982	7	0.086	5.969	39	0.067	6.004	41	0.070
06/23/79	02.56.57.6	6.2	6.088	4	0.084	6.065	21	0.070	6.174	23	0.057
07/07/79	03.46.57.4	5.8	5.996	7	0.091	5.967	39	0.074	5.850	41	0.071
08/04/79	03.56.57.2	6.1	6.105	7	0.032	6.098	39	0.062	6.170	41	0.076
10/28/79	03.16.56.9	6.0	6.060	6	0.056	6.033	39	0.063	5.936	41	0.085
12/02/79	04.36.57.5	6.0	5.962	5	0.046	5.903	33	0.067	6.074	35	0.050
06/29/80	02.32.57.7	5.7	5.722	4	0.073	5.676	28	0.094	5.794	25	0.049
09/14/80	02.42.39.3	6.2	0.000	0	0.000	0.000	0	0.000	6.222	36	0.049
10/12/80	03.34.14.1	5.9	5.946	6	0.043	5.912	39	0.061	5.840	41	0.089
12/14/80	03.47.06.6	5.9	5.887	5	0.075	5.911	39	0.045	5.965	41	0.070
12/27/80	04.09.08.2	5.9	5.948	5	0.040	5.908	39	0.076	5.949	41	0.069
03/29/81	04.03.50.0	5.6	5.719	5	0.052	5.521	39	0.053	5.519	41	0.070
04/22/81	01.17.11.4	6.0	5.945	5	0.060	5.888	33	0.046	5.991	35	0.065
05/27/81	03.58.12.1	5.5	5.576	4	0.020	5.442	27	0.061	5.320	29	0.098
09/13/81	02.17.18.2	6.1	6.115	6	0.081	6.092	34	0.076	6.129	35	0.071
10/18/81	03.57.02.6	6.1	5.951	7	0.072	5.976	39	0.057	6.069	35	0.065
11/29/81	03.35.08.7	5.7	5.789	5	0.078	5.566	33	0.062	5.693	35	0.071
12/27/81	03.43.14.1	6.2	6.046	6	0.040	6.056	39	0.074	6.183	41	0.065
04/25/82	03.23.05.4	6.1	6.074	6	0.072	6.056	39	0.077	6.111	39	0.071
07/04/82	01.17.14.4	6.1	0.000	0	0.000	0.000	0	0.000	6.078	32	0.089
08/31/82	01.31.00.5	5.3	0.000	0	0.000	0.000	0	0.000	5.356	39	0.065
12/05/82	03.37.12.6	6.1	5.989	6	0.088	5.968	37	0.078	6.076	36	0.060
12/26/82	03.35.14.1	5.7	5.834	5	0.065	5.653	39	0.061	5.731	29	0.061
06/12/83	02.36.43.5	6.1	6.051	5	0.077	6.070	24	0.071	6.132	24	0.072
10/06/83	01.47.06.5	6.0	5.917	4	0.021	5.876	18	0.054	6.034	18	0.068
10/26/83	01.55.04.8	6.1	5.996	6	0.076	5.993	32	0.055	6.097	32	0.065
11/20/83	03.27.04.4	5.5	0.000	0	0.000	0.000	0	0.000	5.481	32	0.071

Table VII.5.1   List of events used in this study. The table includes
date, origin time, m_b(ISC/PDE) as well as NORSAR based
measurements discussed in the text and standard
deviations across NORSAR. Zero entries indicate either
no NORSAR data available or SNR too low for reliable
measurement.

ORIGIN DATE	ORIGIN TIME	MB	*** LG(AMP) ***			*** LG(RMS) ***			*** PCODA ****		
			MLA	N	STD	MLR	N	STD	MCR	N	STD
02/19/84	03.57.03.4	5.9	5.764	5	0.053	5.724	27	0.051	5.889	27	0.057
03/07/84	02.39.06.4	5.7	5.775	5	0.075	5.696	27	0.058	5.632	27	0.073
03/29/84	05.19.08.2	5.9	5.905	5	0.035	5.897	27	0.057	5.889	27	0.071
04/25/84	01.09.03.5	6.0	5.905	6	0.072	5.862	33	0.066	5.972	33	0.071
05/26/84	03.13.12.4	6.0	6.075	6	0.063	6.064	33	0.064	5.965	33	0.115
07/14/84	01.09.10.5	6.2	6.089	6	0.073	6.043	33	0.074	6.148	31	0.088
10/27/84	01.50.10.6	6.2	6.101	6	0.077	6.075	32	0.067	6.254	32	0.073
12/02/84	03.19.06.3	5.8	5.973	5	0.141	5.864	27	0.076	5.747	25	0.081
12/16/84	03.55.02.7	6.1	6.055	5	0.093	6.030	27	0.066	6.113	27	0.068
12/28/84	03.50.10.7	6.0	6.009	6	0.057	5.978	33	0.073	6.147	33	0.073
02/10/85	03.27.07.6	5.9	5.898	7	0.070	5.791	38	0.069	5.947	39	0.068
04/25/85	00.57.06.5	5.9	5.979	5	0.078	5.850	27	0.065	5.936	29	0.069
06/15/85	00.57.00.7	6.0	6.024	5	0.075	5.966	28	0.062	6.099	28	0.069
06/30/85	02.39.02.7	6.0	5.983	4	0.068	5.917	28	0.059	6.058	28	0.065
07/20/85	00.53.14.5	5.9	5.884	7	0.076	5.855	36	0.071	5.912	36	0.068
03/12/87	01.57.17.0	5.4	5.385	6	0.081	5.223	31	0.059	5.437	33	0.068
04/03/87	01.17.08.0	6.2	6.062	6	0.079	6.048	31	0.070	6.245	32	0.052
04/17/87	01.03.04.0	6.0	5.928	6	0.072	5.895	31	0.069	6.077	32	0.060
06/20/87	00.53.04.0	6.1	5.992	7	0.117	5.962	34	0.070	6.124	37	0.092
08/02/87	00.58.08.0	5.9	5.945	6	0.103	5.866	30	0.074	5.885	30	0.074
11/15/87	03.31.08.0	6.0	6.024	7	0.088	5.959	34	0.063	6.098	36	0.058
12/13/87	03.21.08.0	6.0	6.094	6	0.088	6.066	29	0.080	6.081	30	0.066
12/27/87	03.05.08.0	6.0	6.109	6	0.106	6.032	30	0.083	6.211	30	0.052

```
AVERAGE STANDARD DEVIATIONS:            0.070          0.064          0.069
STANDARD DEVIATION OF MEAN VALUES:      0.028          0.011          0.012
```

Table VII.5.1 (cont.)

	ISC/PDE	ISC(M-L)	MB(LG)	PCODA	LG(RMS)	LG(AMP)
ISC/PDE	0.000	0.066	0.119	0.068	0.093	0.109
ISC(M-L)	0.066	0.000	0.120	0.060	0.092	0.136
MB(LG)	0.119	0.120	0.000	0.127	0.116	0.135
PCODA	0.068	0.060	0.127	0.000	0.101	0.130
LG(RMS)	0.093	0.092	0.116	0.101	0.000	0.065
LG(AMP)	0.109	0.136	0.135	0.130	0.065	0.000

Table VII.5.2   Standard deviations of differences between various
magnitude estimates discussed in the text.
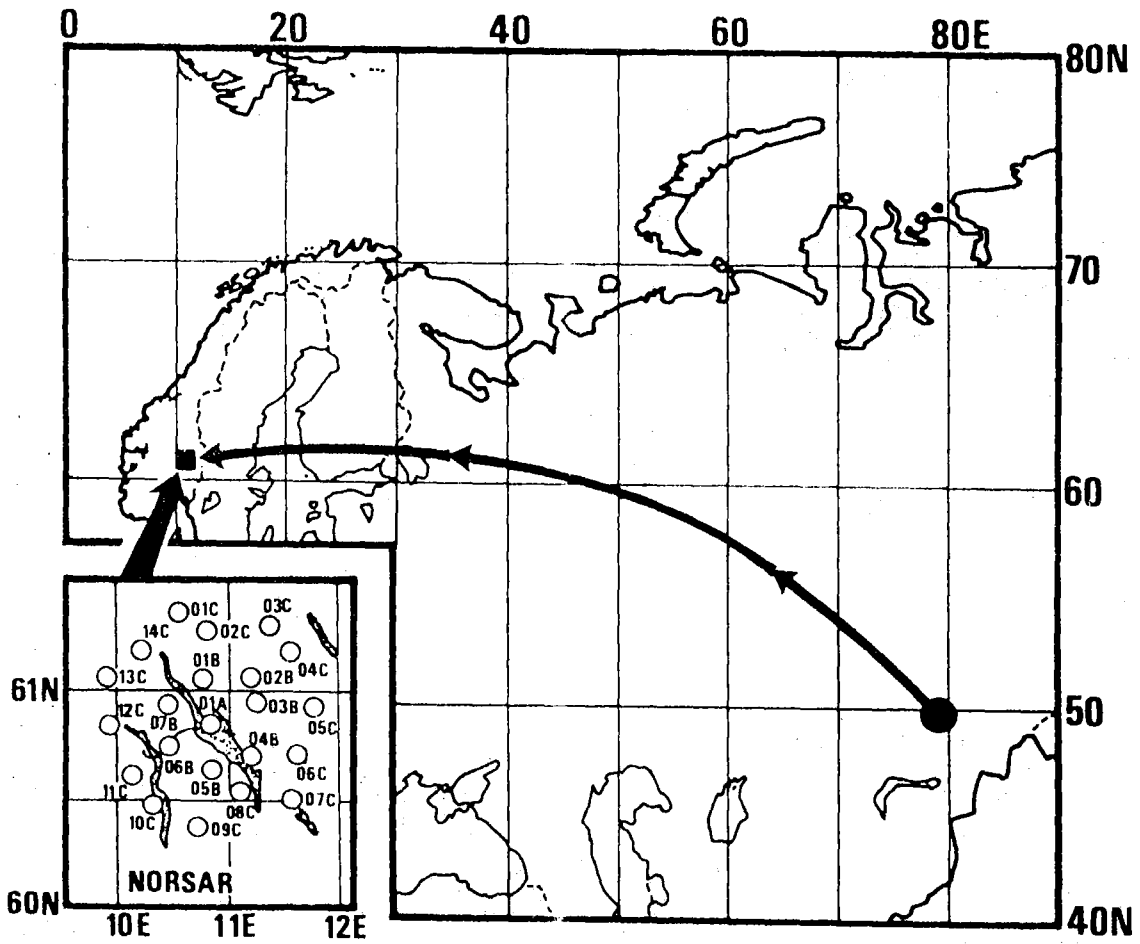
Fig. VII.5.1 Map showing the propagation path from Semipalatinsk to
NORSAR (distance approximately 4200 km). The original
NORSAR array configuration is also displayed.
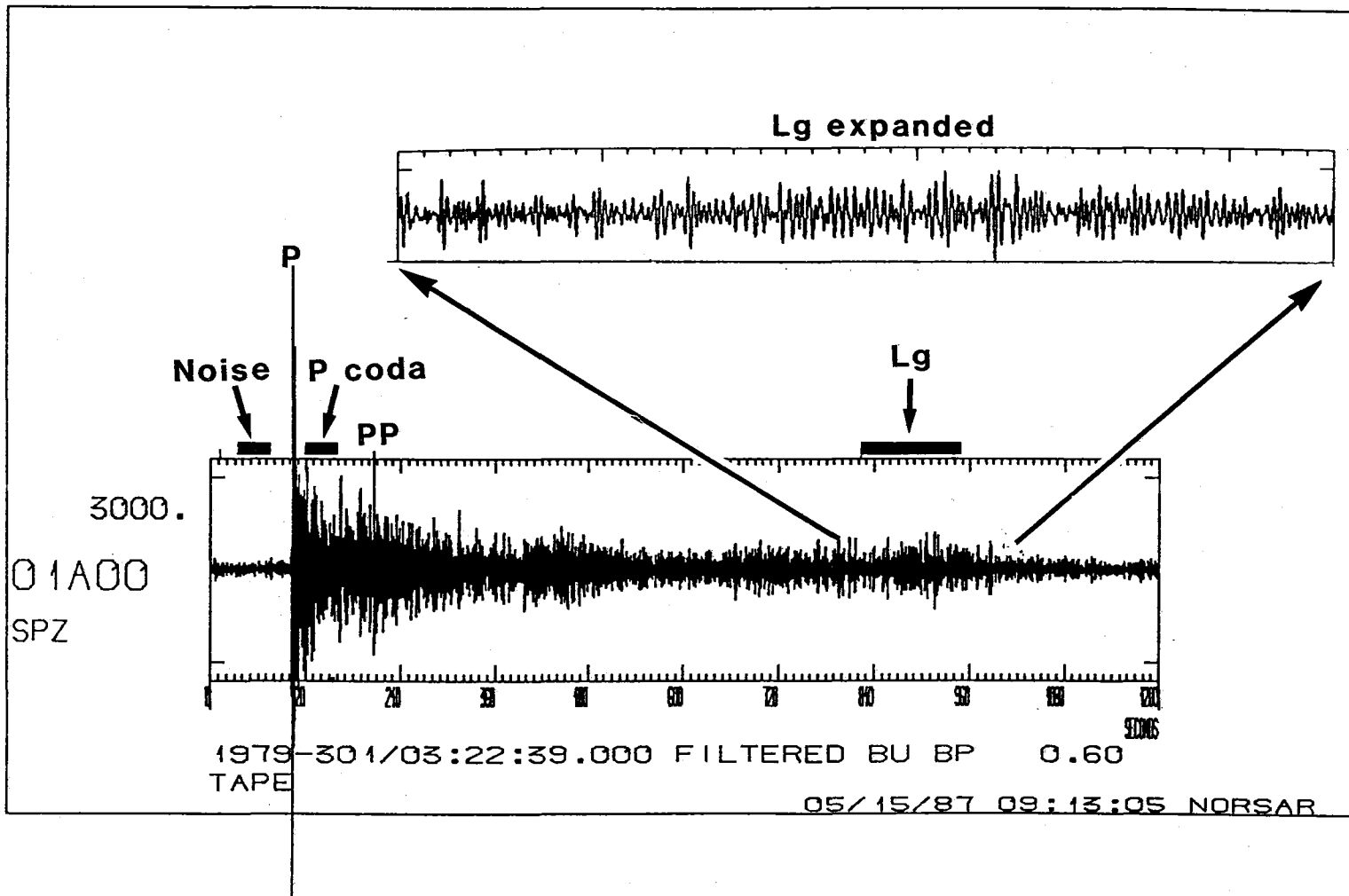
Fig. VII.5.2 Example of a typical NORSAR-recording of a Semipalatinsk explosion (instrument 01A00). The plot covers 20 minutes of data filtered in the passband 0.6-3.0 Hz. The time windows used for RMS Lg, RMS P coda and RMS noise measurements as described in the text are indicated. An expanded plot is shown of the portion of the trace used for NORSAR Lg amplitude.

MAGNITUDE COMPARISON
Shagan River events
SLOPE= 1.00   INTERC= 0.01   STD= 0.031
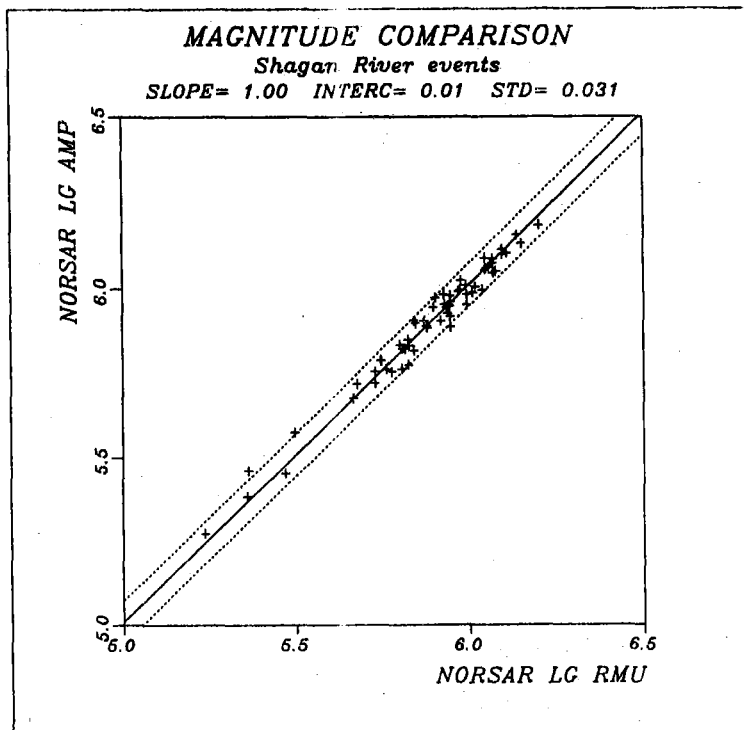
Fig. VII.5.3   Plot of amplitude based NORSAR Lg magnitudes versus
NORSAR RMS Lg magnitudes. In this plot no noise correc-
tion has been applied. The slope has been restricted to
1.00, and the dotted lines correspond to plus/minus two
standard deviations.

MAGNITUDE COMPARISON
Shagan River events
SLOPE= 1.00   INTERC= 0.06   STD= 0.065
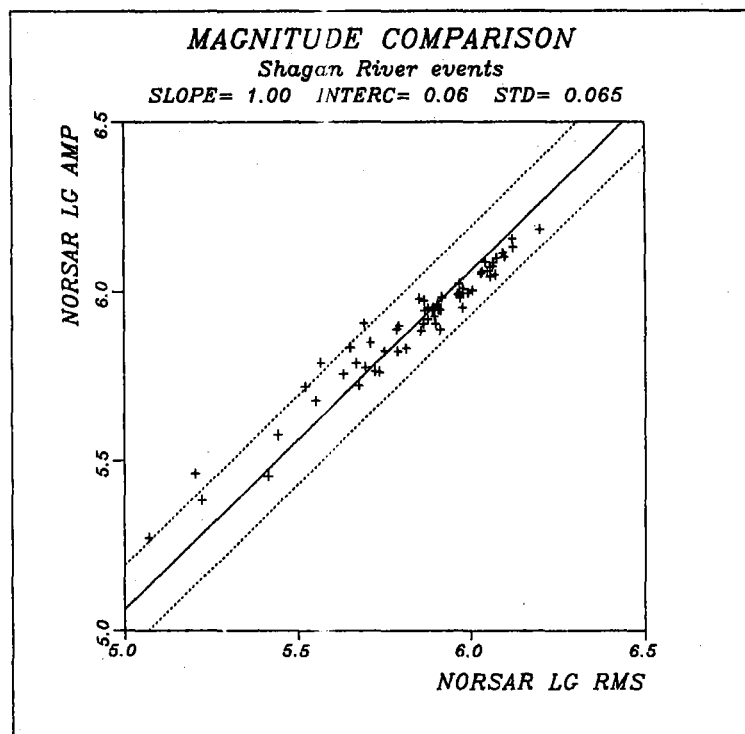
Fig. VII.5.4   Same as Fig. VII.5.3, except that the NORSAR RMS Lg
magnitudes have been corrected for noise as discussed
in the text. Note the effect of this at low magnitudes.
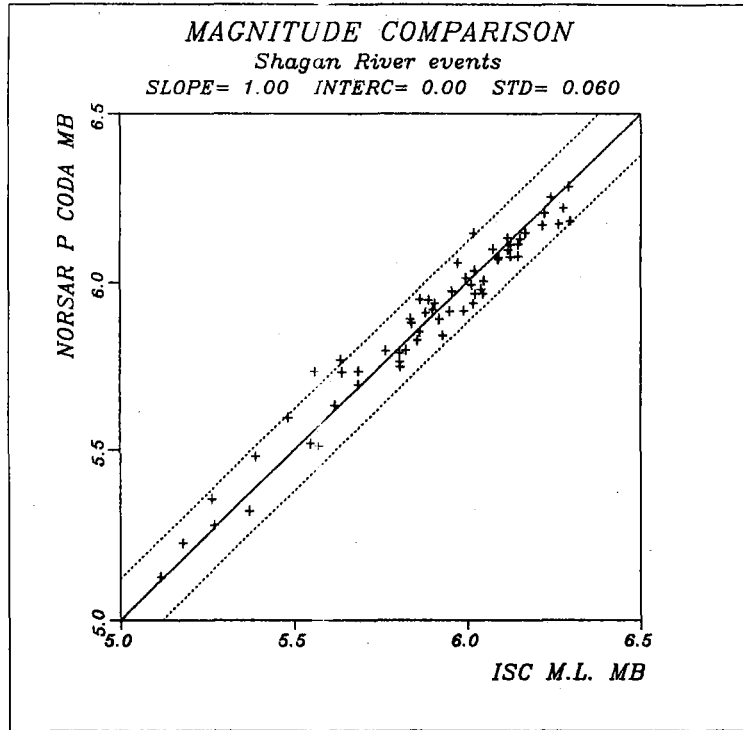
Fig. VII.5.5 Plot of NORSAR P coda magnitudes versus ISC maximum likelihood m_b. (Slope restricted to 1.00; dotted lines correspond to plus/minus two standard deviations.)
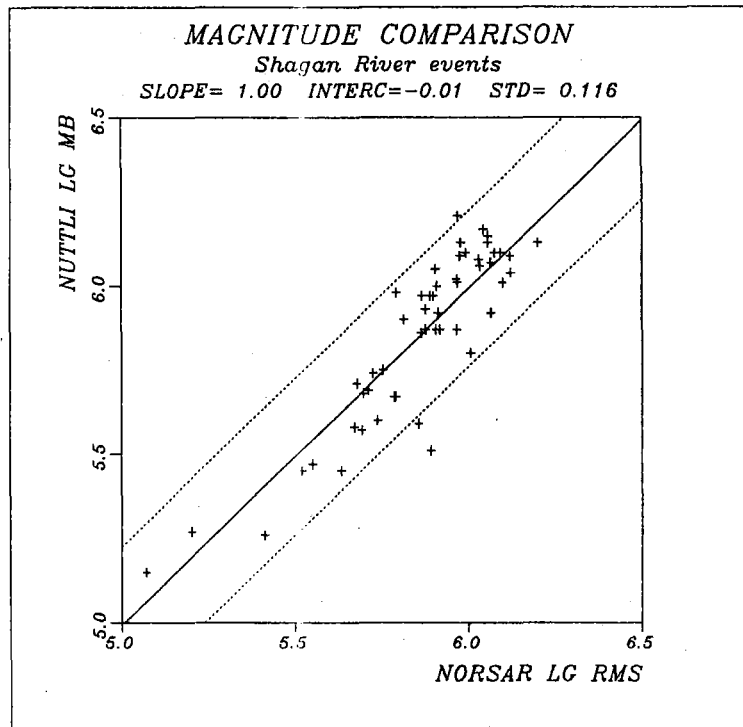
Fig. VII.5.6 Plot of Nuttli (1985) m_b (Lg) versus NORSAR Lg RMS magnitudes. The slope and dotted lines are defined as in Fig. VII.5.5. Note the significant scatter even at high magnitudes.

MAGNITUDE COMPARISON
Shagan River events
SLOPE= 1.00   INTERC=-0.05   STD= 0.092
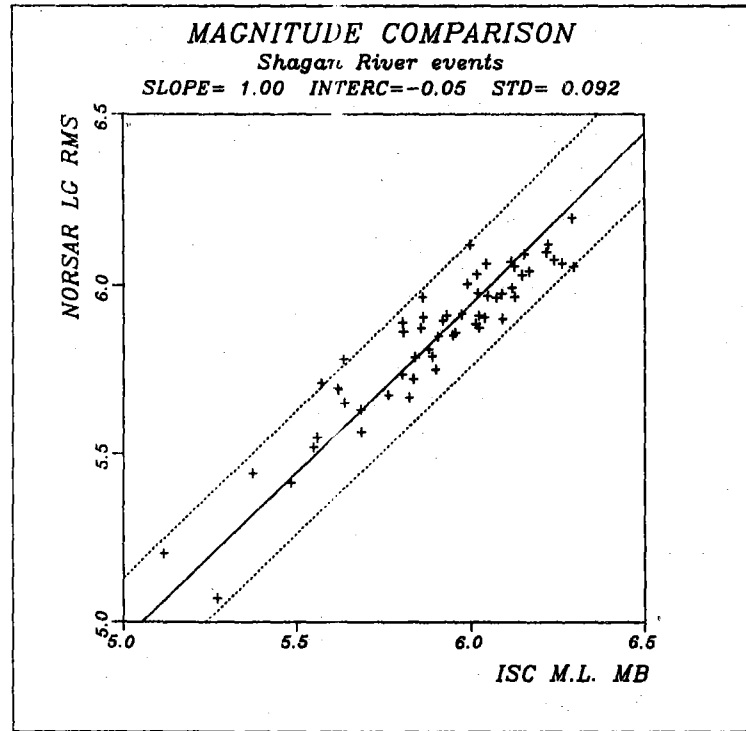
Fig. VII.5.7   Plot of ISC maximum likelihood m_b versus NORSAR Lg RMS
magnitudes. The slope and dotted lines are defined as in
Fig. VII.5.5.

MAGNITUDE COMPARISON
Shagan River events
SLOPE= 1.00   INTERC=-0.06   STD= 0.101
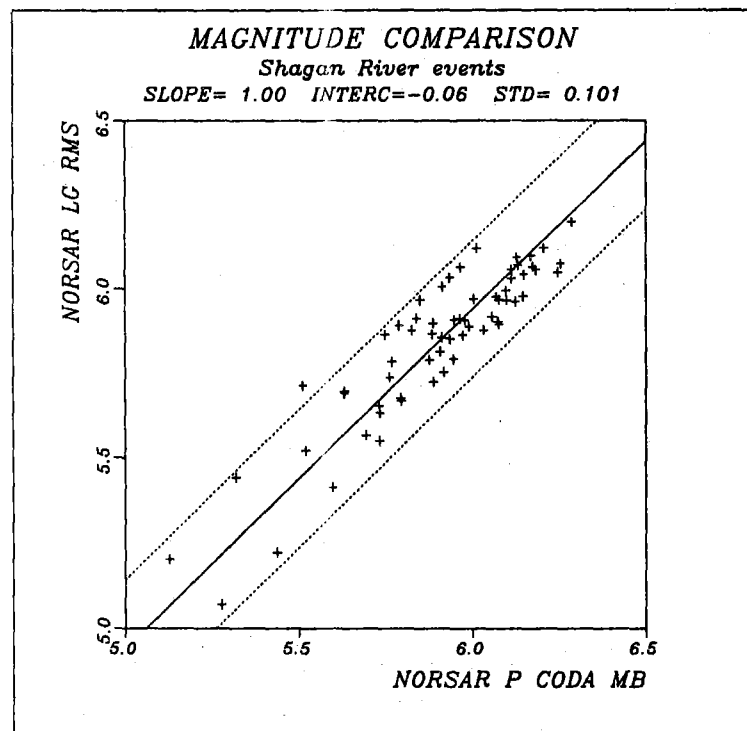
Fig. VII.5.8   Plot of NORSAR RMS P coda m_b versus NORSAR RMS Lg magni-
tudes. The slope and dotted lines are defined as in
Fig. VII.5.5.

NORSAR P CODA MB
SHAGAN RIVER EVENTS
BIAS RELATIVE TO NORSAR LG RMS
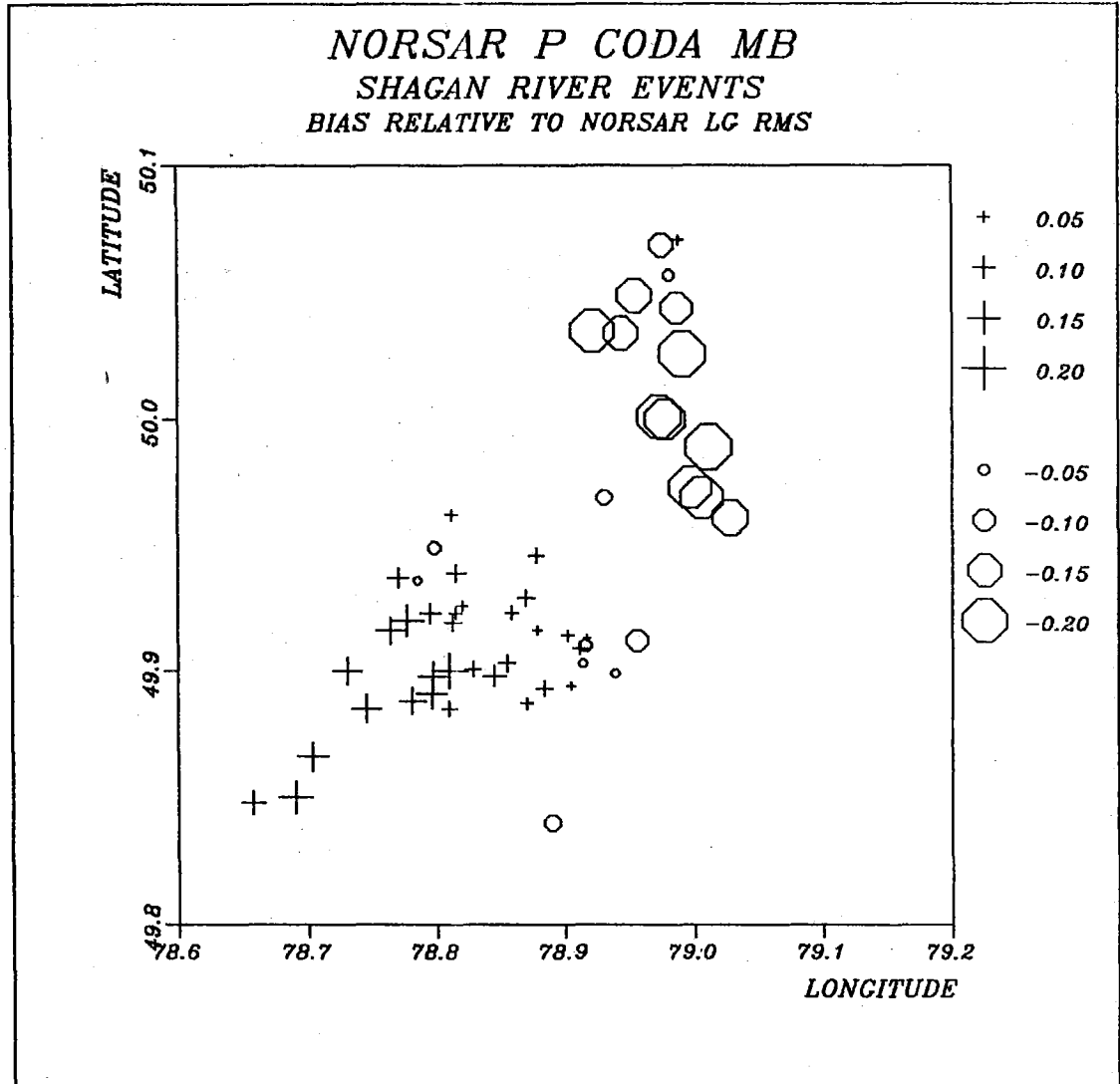
Fig. VII.5.9   Plot of magnitude residuals (NORSAR P coda minus NORSAR Lg RMS magnitudes) as a function of event location for events of $m_b > 5.60$. Plusses and circles correspond to residuals greater or less than the average, respectively, with symbol size proportional to the deviation. Location estimates are those of Marshall et al (1985) where available, otherwise NEIS estimates have been used. Note the systematic variation within the Shagan River area.
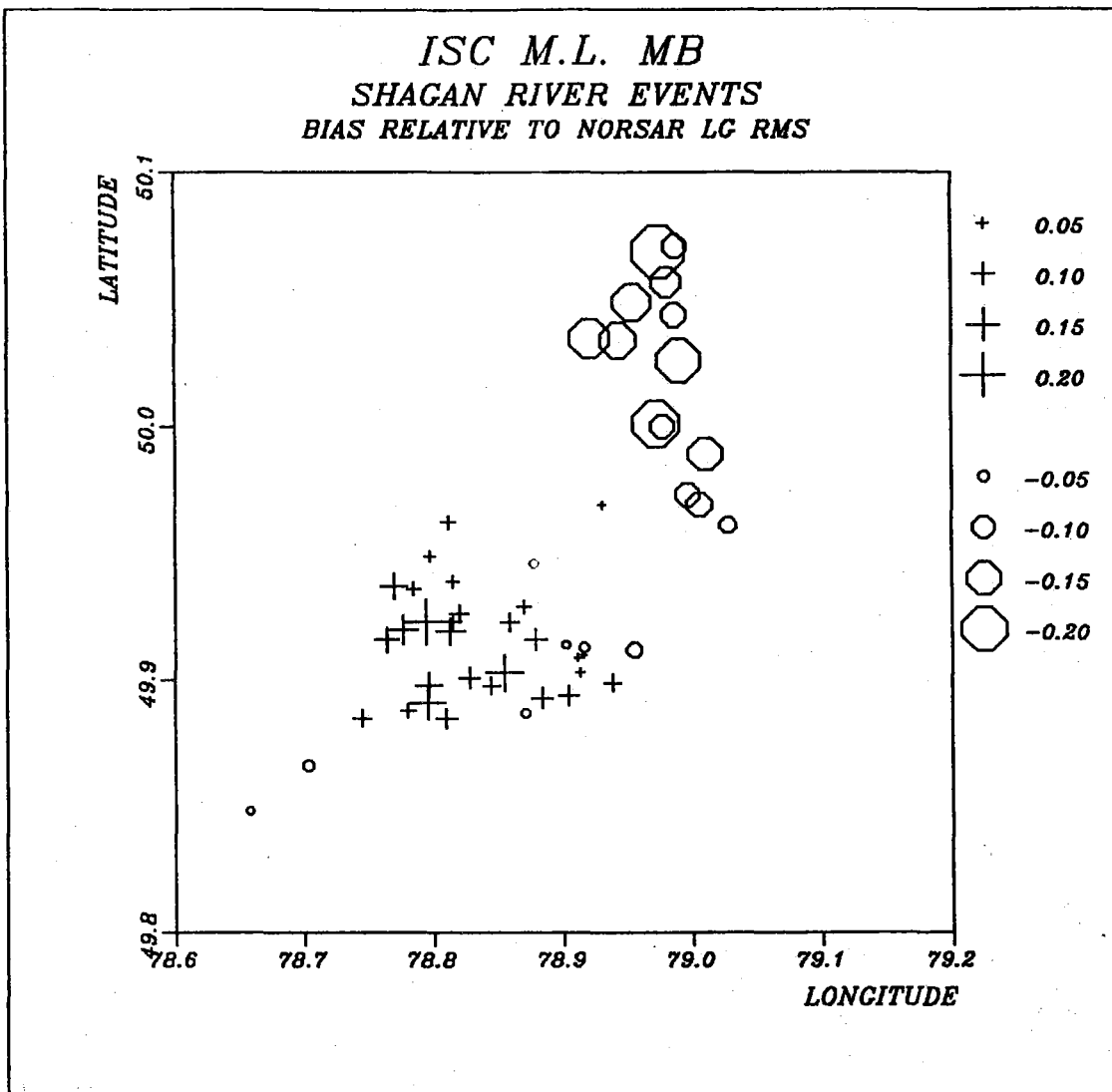
Fig. VII.5.10   Same as Fig. VII.5.9, except that the residual
corresponds to ISC maximum likelihood m_b minus NORSAR
Lg RMS magnitudes. Note the similarities with Fig.
VII.5.9.

MAGNITUDES
Shagan River events
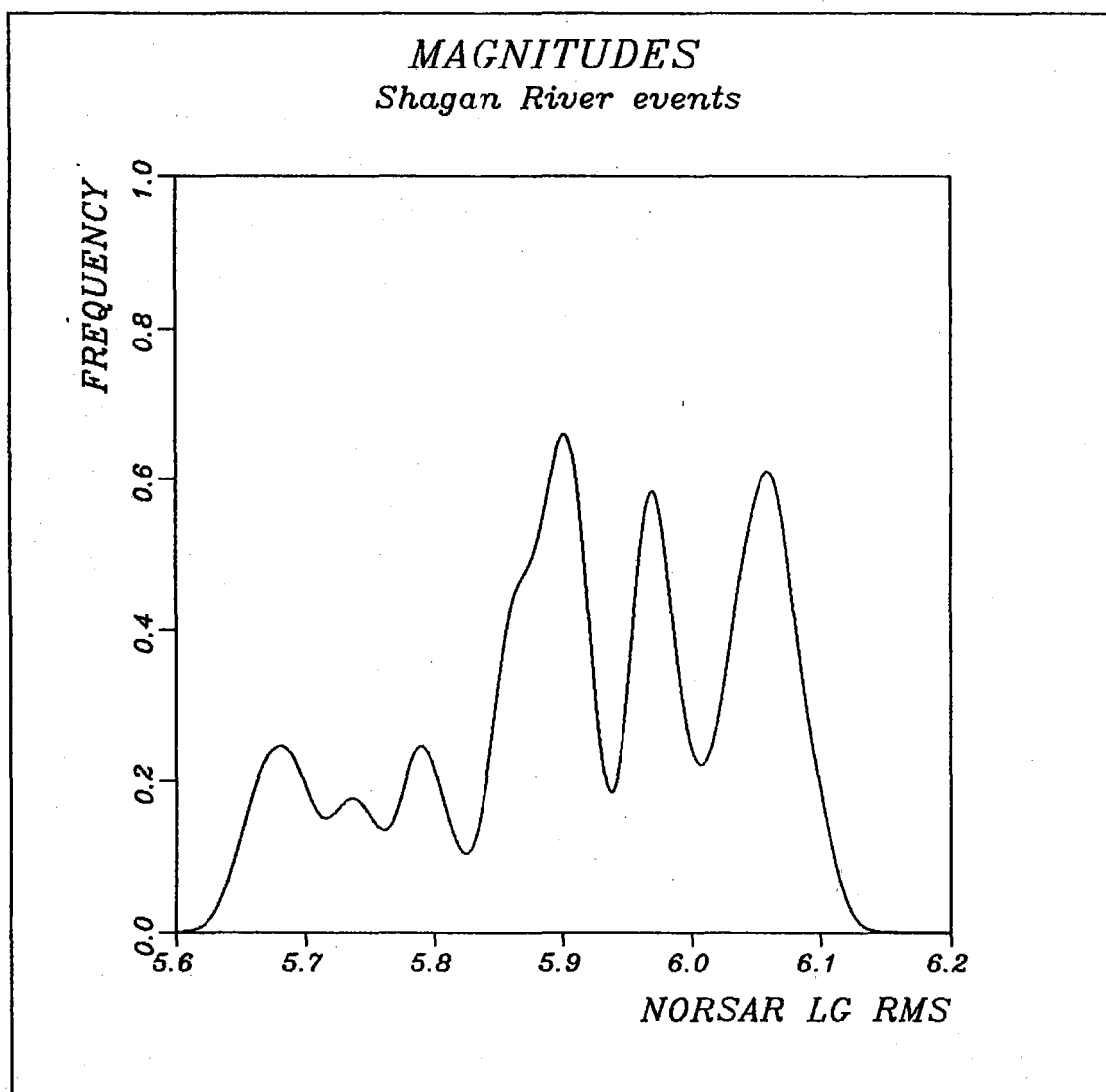
Fig. VII.5.11 Relative frequency of occurrence of large Shagan River
explosions after 1976, based on estimated NORSAR Lg RMS
magnitudes. The figure has been generated by adding
Gaussian probability density functions with standard
deviations of 0.015 centered at each magnitude value.
Note the three distinct peaks in the diagram.

VII.6   Towards an optimum beam deployment for NORESS;
experiments with a North Sea / western Norway data base

Several of our previous investigations have addressed the problem of determining the number and type of beams needed for adequate detection of signals recorded on NORESS. For example, Kværna and Mykkeltveit (1986) arrived at a recommendation for an optimum beam deployment for detection of regional and teleseismic P-waves.

As described in several papers, e.g., Mykkeltveit and Bungum (1984), automatic determinations of event epicenters using our on-line processing package requires detection and identification of both P- and S-arrivals from each event. This study utilizes data from a fairly extensive data base of regional events recorded at NORESS, and we attempt to determine an optimum beam deployment with respect to detection of all phases from these events.

Data base and detection processing

The data base comprises 101 events from the North Sea / western Norway region with locations as shown in Fig. VII.6.1. These events were located by the western Norway network and/or the network operated by the British Geological Survey. The epicentral distance range from NORESS is 250 - 1100 km, and the magnitudes are between 1.6 and 4.2.

This event data base comprises well located events for which it is possible to accurately define the types of observed phases and to read their onsets manually, as illustrated in Fig. VII.6.2.

All events were subjected to detection processing by a large beam set using a new program system developed at NORSAR (Fyen, 1987). Distributed among 12 different filter bands, this beam set contained 72

steered beams for detection of P-waves, 132 beams for detection of S-waves, 12 incoherent beams made from the vertical channels and 12 incoherent beams made from the horizontal channels. In selecting this beam set we attempted to include all candidates that could conceivably contribute to increasing the detection capability. A description of this beam set is given in section VII.3 of this report (Kværna et al, 1987).

The output from the detection analysis is a report containing parameters such as an identification of the detecting beam, detection time, STA, LTA and STA/LTA (SNR). For all events, the detection reports were divided into Pn, Pg, Sn and Lg detections. Table VII.6.1 shows an example of a report where the different detections are identified.

The essence of the following is a strategy for determination of a beam set that meets certain performance criteria and at the same time contains the lowest possible number of beams, selected from the set of 228 beams described above.

Analysis procedure

In the work presented in section VII.3 of this report (Kværna et al, 1987), we attempted to infer the STA/LTA (SNR) detection thresholds of the respective beams from noise statistics. For each phase detected in the present investigation, these thresholds were used to create a basis for comparison between the different beams. The procedure for comparing the maximum SNR values can be illustrated by the following example:

i)   Assume that a Pn phase is detected by three different beams,

by beam A, with a maximum SNR of 26.0 dB,
by beam B, with a maximum SNR of 23.5 dB and
by beam C, with a maximum SNR of 22.0 dB.

ii) Assume that the detection thresholds inferred from noise statistics are,

for beam A, 12.0 dB
for beam B, 10.0 dB and
for beam C, 6.0 dB

iii) If we take the detection thresholds to represent
a common basis for comparison, a unified quality measure
of the maximum SNR values will be the number of decibels
exceeding these thresholds. These quality measures, from now
on referred to as 'the adjusted SNR values', will for the
three beams in this example be:

Adjusted SNR value for beam A: (26.0 - 12.0) dB = 14.0 dB.
Adjusted SNR value for beam B: (23.5 - 10.0) dB = 13.5 dB.
Adjusted SNR value for beam C: (22.0 - 6.0) dB = 16.0 dB.

From this we conclude that beam C is the 'best' beam for detecting
this particular Pn phase.

Rather than progressing in our investigation with the concept of a
'best' beam, we introduce the concept of a 'valid' beam or 'valid'
detection: The maximum obtainable SNR value of a detection will be
reduced by phenomena like mis-steering of the coherent beams, random
increase in the noise level and lowered data quality on single chan-
nels. We therefore decided that all detections with adjusted SNR

values within 3 decibels of the best adjusted SNR for the phase, were
to be counted as 'valid' detections. This implies that each detected
phase will have several possible candidates for the 'best' beam.

The 3 decibels acceptance level is chosen rather subjectively,
however, the coherent beam deployment is sufficently dense that signal
losses due to mis-steering are within 3 decibels. In later analyses,
this acceptance level can of course be reduced or increased.

Table VII.6.2 shows the maximum SNR values and corresponding adjusted
SNR values for one of the Pn-phases in this investigation, for all 48
beam types.

Results

After finding the 'valid' detections for all phases in the data
base of 101 events, we were in a position to evaluate which beams
should be included in the optimum deployment. Tables VII.6.(3a-3d)
show the 'valid' detections for all Pn, Pg, Sn and Lg-phases,
respectively.

When considering the Pn phase in Table VII.6.3a, we found that beam
number 10 had the maximum number of 'valid' entries, 60 out of a total
number of 98. From this we concluded that this beam should obviously
be included in the final beam deployment. An interesting observation
was that many of the Pn phases from the North Sea / western Norway
region had dominant signal frequencies above 10 Hz.

Beam number 6 had the highest number of 'valid' detections for the Pg
phase, see Table VII.6.3b. For the Sn phase, (Table VII.6.3c), beam
number 45 or 46 was an obvious candidate. Beam number 46 had 66 'va-
lid' entries, which is about 80% of the total number of Sn detections.

Like the Pn phase, the Sn phases from this region contain much energy at high frequencies.

For the Lg phase (Table VII.6.3d) no specific beam is an obvious candidate for inclusion in the recommended beam deployment. Beam 42, however, exhibits the highest number of 'valid' entries.

In order to find the optimum beam deployment, we attempted to group the beams together in various ways. We required that all (or almost all) detected phases should be represented by at least one 'valid' beam in the final deployment. First, we attempted to do the grouping for each phase type individually.

For the Pn-phase, the number of 'valid' entries for the various beams are given in the last column of Table VII.6.3a. We first select the beam with the highest number of 'valid' entries, in this case beam number 10, and that beam handles 60 of the detected Pn-phases. Next, beam number 6 accommodates 22 of the remaining 38 beams, and so on. By iteration, we ended up with a priority list of beams as given in Table VII.6.4a.

From this we can infer that 8 beams are required to cover all Pn phases, but 5 beams alone cover 96% of the 'valid' entries. Note that, e.g., beam 10 (10.0 - 16.0 P) includes eight coherent beams with different steering delays. The actual azimuth range for this data base is 180-360 degrees, so it is sufficient to distribute about 4 coherent P-beams in each filter band to span this area. If we in addition accept that it is sufficient to cover 96% of the valid detections, the optimum beam deployment for detecting Pn-phases from this specific region will contain 16 coherent P-beams and one incoherent beam made from the vertical channels. If we require the coherent beam deployment to span all azimuth directions (symmetrically), about 32 coherent P-beams must be included.

The beam priority lists for the Pg, Sn and Lg phases are given
in Tables VII.6.4b-d, respectively.

An interesting observation is the large number of beams required
to cover the Pg detections. From Tables VII.6.4a-d we can infer the
beam deployment required for optimum detection under the given
requirements, when treating the phases individually; see Table
VII.6.5.

When recommending specific beam deployments, it is important to
keep in mind the implications on computational load for the
on-line processor. This load is primarily determined by the
total number of traces that must be bandpass filtered, and the
number of beams that are created.

For processing the data with the deployment of Table VII.6.5,
178 single channels must be filtered, and 55 beams must be formed,
each of which is subjected to STA/LTA-type detection processing.

These numbers can be considerably reduced if we apply an algorithm
where all phases are treated at the same time. We first include
the most obvious beam candidates (beams no. 46, no. 10, no. 42 and
no. 6), and then start the interative sorting procedure. The results
from this procedure are given in Table VII.6.6. Compared to the num-
bers in Table VII.6.5, the size of the beam deployment is reduced
by 30-40%.

As a final experiment, we decided to exclude the coherent S-beams
from the analysis. The results are given in Table VII.6.7.
Compared to the results given in Table VII.6.6, the number of beams to
be formed were marginally reduced, but the number of traces to be
filtered were increased due to including more incoherent beams made
from the vertical channels.

Conclusion

For detection of Pn-phases from the North Sea / western Norway region,
the high frequency coherent P-beams will contribute significantly to
an optimized beam deployment. For the more low frequency Pg phase,
the coherent P-beam filtered between 3.5 and 5.5 Hz seem to do best.

Including incoherent beams made from the horizontal channels, will
improve the detectability of Sn significantly. We also found that the
Sn phase in most cases had dominant frequencies around 10 Hz.

Like Pg, the Lg phase had maximum SNR in the range 1.5-4.5 Hz. Inco-
herent beams made from both the horizontal and vertical channels must
be included for optimum detection of the Lg phase.

A tool for determining the optimum beam deployment has been developed.
To validate the method and find a beam deployment that adequately
covers also other relevant regions, we plan to perform similar studies
for events from other areas, like the western USSR.

In our future work, then, we want to test whether the symmetric beam
deployment inferred from the North Sea/western Norway data base is
sufficient for optimum detection of events from other regions, or
if other beam types have to be added to the beam deployment.

T. Kværna
S. Kibsgaard
S. Mykkeltveit
F. Ringdal

References

Fyen, J. (1987): Improvements and modifications.
    Semiannual Technical Summary, 1 October - 31 March 1987,
    NORSAR Sci. Rep. No. 2-86/87, Kjeller, Norway.

Kværna, T. and S. Mykkeltveit (1986): Optimum beam deployment for
    NORESS P-wave detection. Semiannual Technical Summary, 1 April -
    30 September 1986, NORSAR Sci. Rep. No. 1-86/87, Kjeller, Norway.

Kværna, T., S. Kibsgaard and F. Ringdal (1987): False alarm
    statistics and threshold determination for regional event detection,
    Semiannual Technical Summary, 1 April - 30 September 1987,
    NORSAR Sci. Rep. No. 1-87/88, Kjeller, Norway.

Mykkeltveit, S. and H. Bungum (1984): Processing of regional
    events using data from small-aperture arrays, Bull. Seism. Soc.
    Am. 74, 2313-2333.

Manually read arrival times:

Pn: 14.11.56.4 Pg: 14.12.05.5 Sn: 14:12.39.0 Lg: 14.12.51.1

Detection results for steered P-beams.

Time interval subjected to detection processing:

017:14.09.46.0 - 14.13.46.0

Beam	Detection interval	STA	LTA	SNR	#detections
***> Pn					
I0906	017:14.11.56.6 - 12.03.9	827.01	18.52	44.661	1
H0807	017:14.11.56.9 - 12.06.4	647.98	12.91	50.173	4
J1006	017:14.11.56.9 - 12.04.9	543.86	11.58	46.969	9
E0505	017:14.11.57.1 - 12.03.4	318.56	26.33	12.099	2
F0607	017:14.11.57.1 - 12.03.4	454.06	26.09	17.406	5
G0707	017:14.11.57.1 - 12.03.6	793.77	30.41	26.106	5
D0408	017:14.11.57.4 - 12.03.4	263.52	23.11	11.403	9
C0308	017:14.11.57.6 - 12.03.1	279.83	30.10	9.297	13
B0201	017:14.11.58.4 - 11.58.9	112.92	27.44	4.116	1
***> Pg					
H0803	017:14.12.05.4 - 12.11.9	234.43	41.59	5.637	16
F0607	017:14.12.06.1 - 12.10.6	812.29	90.77	8.949	8
E0505	017:14.12.06.1 - 12.09.1	520.37	76.49	6.803	15
G0707	017:14.12.06.6 - 12.12.9	749.01	132.91	5.635	4
J1002	017:14.12.07.6 - 12.08.1	128.03	30.39	4.213	8
D0408	017:14.12.08.1 - 12.08.9	345.48	74.75	4.622	11
F0602	017:14.12.13.6 - 12.13.9	138.17	34.16	4.045	1
***> Sn					
H0805	017:14.12.40.1 - 12.42.1	318.42	77.59	4.104	2
D0402	017:14.12.40.4 - 12.40.9	231.42	55.96	4.136	2
G0702	017:14.12.40.4 - 12.41.4	516.81	98.40	5.252	3
C0302	017:14.12.40.4 - 12.40.9	253.58	57.01	4.448	2
***> Lg					
F0603	017:14.12.51.9 - 12.54.1	728.74	103.15	7.065	1
E0502	017:14.12.52.1 - 12.54.1	662.00	78.63	8.419	12
D0405	017:14.12.52.6 - 12.54.4	464.31	83.58	5.555	2
C0302	017:14.12.53.1 - 12.59.6	449.74	78.16	5.754	3
H0806	017:14.12.53.4 - 12.53.9	474.39	112.32	4.223	1
F0602	017:14.12.55.9 - 12.56.6	538.07	95.86	5.613	2
B0201	017:14.12.57.4 - 12.57.6	305.59	73.26	4.171	2
D0402	017:14.12.58.1 - 12.58.6	497.49	116.50	4.270	1

Table VII.6.1 The detection report shown in this table is the output
from detection analysis of the event displayed in Fig.
VII.6.2. We have here only given the results from pro-
cessing the 3-minute time interval containing the Pn,
Pg, Sn and Lg phases, with the 72 coherent beams with P-
wave velocities. The beam types are identified from the
first character of the beam name. The last two digits
of the beam name identify the coherent beam with maximum
SNR within that beam type. In the experiment outlined
in this paper, we give results for each coherent beam
type rather than for individual coherent beams. The last
column of the detection report gives the number of
detections for the beam type within the detection
interval, i.e., the time interval for which the SNR
values exceed the threshold.

Distance: 400.9 km.
Azimuth : 229.0 degrees
ML   :   2.7

Beam no.	Beam type	SNR in dB			Adjusted SNR in dB
1	1.0 - 3.0 P.	0.00	/		0.00
2	1.5 - 3.5 P:	12.30	/		1.29
3	2.0 - 4.0 P:	19.37	/		6.67
4	2.5 - 4.5 P:	21.14	/		8.74
5	3.0 - 5.0 P:	21.66	/		10.25
6	3.5 - 5.5 P:	24.82	/		13.91
7	5.0 - 7.0 P:	28.34	/		16.63
8	6.5 - 8.5 P:	34.01	/	*	22.51
9	8.0 - 16.0 P:	33.00	/	*	24.60
10	10.0 - 16.0 P:	33.44	/	*	24.94
11	1.0 - 2.0 P:	0.00	/		0.00
12	2.0 - 3.0 P:	0.00	/		0.00
13	1.0 - 3.0 S:	0.00	/		0.00
14	1.5 - 3.5 S:	0.00	/		0.00
15	2.0 - 4.0 S:	0.00	/		0.00
16	2.5 - 4.5 S:	0.00	/		0.00
17	3.0 - 5.0 S:	15.56	/		3.26
18	3.5 - 5.5 S:	19.41	/		7.41
19	5.0 - 7.0 S:	20.82	/		8.12
20	6.5 - 8.5 S:	26.52	/		14.72
21	8.0 - 16.0 S:	28.17	/		19.17
22	10.0 - 16.0 S:	31.88	/	*	22.88
23	1.0 - 2.0 S:	0.00	/		0.00
24	2.0 - 3.0 S:	0.00	/		0.00
25	1.0 - 3.0 V:	0.00	/		0.00
26	1.5 - 3.5 V:	7.24	/		0.64
27	2.0 - 4.0 V:	0.00	/		0.00
28	2.5 - 4.5 V:	0.00	/		0.00
29	3.0 - 5.0 V:	11.43	/		4.22
30	3.5 - 5.5 V:	14.12	/		7.32
31	5.0 - 7.0 V:	18.69	/		13.99
32	6.5 - 8.5 V:	23.17	/		18.67
33	8.0 - 16.0 V:	26.63	/	*	22.63
34	10.0 - 16.0 V:	27.94	/	*	23.94
35	1.0 - 2.0 V:	0.00	/		0.00
36	2.0 - 3.0 V:	7.60	/		0.00
37	1.0 - 3.0 H:	0.00	/		0.00
38	1.5 - 3.5 H:	0.00	/		0.00
39	2.0 - 4.0 H:	0.00	/		0.00
40	2.5 - 4.5 H:	0.00	/		0.00
41	3.0 - 5.0 H:	0.00	/		0.00
42	3.5 - 5.5 H:	17.13	/		11.84
43	5.0 - 7.0 H:	15.46	/		10.36
44	6.5 - 8.5 H:	19.34	/		14.54
45	8.0 - 16.0 H:	20.00	/		16.30
46	10.0 - 16.0 H:	20.82	/		17.12
47	1.0 - 2.0 H:	0.00	/		0.00
48	2.0 - 3.0 H:	0.00	/		0.00

Table VII.6.2 This table gives the maximum SNR values and the
corresponding adjusted SNR values for the Pn phase shown
in Fig. VII.6.2. The beam types with the characters 'P'
or 'S' are coherent beams with P- or S-wave velocities.
The character 'V' indicates incoherent beams made from
the vertical channels, whereas 'H' indicates incoherent
beams made from the horizontal channels. The beam types
with a star (*) in the column for adjusted SNR are
'valid' beams, i.e., within 3 decibels of the beam type
of highest SNR. Beam types with the value 0.0 have not
detected the phase.

No.	Beam type			#valid entries
1	1.0 -	3.0	P	0
2	1.5 -	3.5	P	0
3	2.0 -	4.0	P	5
4	2.5 -	4.5	P	12
5	3.0 -	5.0	P	22
6	3.5 -	5.5	P	32
7	5.0 -	7.0	P	23
8	6.5 -	8.5	P	23
9	8.0 -	16.0	P	55
10	10.0 -	16.0	P	60
11	1.0 -	2.0	P	0
12	2.0 -	3.0	P	0
13	1.0 -	3.0	S	0
14	1.5 -	3.5	S	0
15	2.0 -	4.0	S	0
16	2.5 -	4.5	S	0
17	3.0 -	5.0	S	2
18	3.5 -	5.5	S	0
19	5.0 -	7.0	S	0
20	6.5 -	8.5	S	0
21	8.0 -	16.0	S	0
22	10.0 -	16.0	S	9
23	1.0 -	2.0	S	0
24	2.0 -	3.0	S	0
25	1.0 -	3.0	V	0
26	1.5 -	3.5	V	0
27	2.0 -	4.0	V	1
28	2.5 -	4.5	V	1
29	3.0 -	5.0	V	1
30	3.5 -	5.5	V	3
31	5.0 -	7.0	V	6
32	6.5 -	8.5	V	7
33	8.0 -	16.0	V	11
34	10.0 -	16.0	V	27
35	1.0 -	2.0	V	0
36	2.0 -	3.0	V	1
37	1.0 -	3.0	H	0
38	1.5 -	3.5	H	0
39	2.0 -	4.0	H	1
40	2.5 -	4.5	H	1
41	3.0 -	5.0	H	0
42	3.5 -	5.5	H	0
43	5.0 -	7.0	H	0
44	6.5 -	8.5	H	0
45	8.0 -	16.0	H	0
46	10.0 -	16.0	H	0
47	1.0 -	2.0	H	0
48	2.0 -	3.0	H	0

Table VII6.3 a) The 'valid' detections for all Pn phases in the data base are in this table denoted by a star (*). If a Pn phase for one of the events is not detected by any beam, the coloum is marked with a period (.). In the last column, the total number of 'valid' entries for each beam type is given.

			10	20	30	40	50	60	70	80	90	100	#valid
No.	Beam type		!	!	!	!	!	!	!	!	!	!	entries
1	1.0 - 3.0	P											1
2	1.5 - 3.5	P											0
3	2.0 - 4.0	P											8
4	2.5 - 4.5	P											16
5	3.0 - 5.0	P											28
6	3.5 - 5.5	P											38
7	5.0 - 7.0	P											19
8	6.5 - 8.5	P											14
9	8.0 - 16.0	P											4
10	10.0 - 16.0	P											3
11	1.0 - 2.0	P											0
12	2.0 - 3.0	P											0
13	1.0 - 3.0	S											5
14	1.5 - 3.5	S											3
15	2.0 - 4.0	S											8
16	2.5 - 4.5	S											8
17	3.0 - 5.0	S											14
18	3.5 - 5.5	S											19
19	5.0 - 7.0	S											6
20	6.5 - 8.5	S											3
21	8.0 - 16.0	S											4
22	10.0 - 16.0	S											5
23	1.0 - 2.0	S											0
24	2.0 - 3.0	S											0
25	1.0 - 3.0	V											2
26	1.5 - 3.5	V											3
27	2.0 - 4.0	V											5
28	2.5 - 4.5	V											5
29	3.0 - 5.0	V											5
30	3.5 - 5.5	V											8
31	5.0 - 7.0	V											17
32	6.5 - 8.5	V											9
33	8.0 - 16.0	V											1
34	10.0 - 16.0	V											2
35	1.0 - 2.0	V											1
36	2.0 - 3.0	V											5
37	1.0 - 3.0	H											1
38	1.5 - 3.5	H											4
39	2.0 - 4.0	H											6
40	2.5 - 4.5	H											5
41	3.0 - 5.0	H											3
42	3.5 - 5.5	H											10
43	5.0 - 7.0	H											5
44	6.5 - 8.5	H											5
45	8.0 - 16.0	H											2
46	10.0 - 16.0	H											0
47	1.0 - 2.0	H											1
48	2.0 - 3.0	H											4

Table VII.6.3 b) This table shows the 'valid' detections for all Pg phases in the data base.

```
                            10        20        30        40        50        60        70        80        90       100    #valid
No.   Beam type             !         !         !         !         !         !         !         !         !         !     entries

  1   1.0 -   3.0  P              ... ..        ..             .        .    ...          .       . .  .      .       .   . .      0
  2   1.5 -   3.5  P              ... ..        ..             .        .    ...          .       . .  .      .       .   . .      0
  3   2.0 -   4.0  P              ... ..        ..             .        .    ...          .       . .  .      .       .   . .      0
  4   2.5 -   4.5  P              ... ..        ..             .        .    ...        . *       . .  .      .       .   . .      0
  5   3.0 -   5.0  P              ... ..        ..             .        .    ...        . *       . .  .      .       .   . .      1
  6   3.5 -   5.5  P              ... ..        ..             .        .    ....       . *       . .  .      .       .   . .      1
  7   5.0 -   7.0  P              ... ..        ..             .        .    ...        . *       . .  .      .       .   . .      1
  8   6.5 -   8.5  P              ... ..        ..             .        .    ...        . *       . .  .      .       .   . .      1
  9   8.0 -  16.0  P              ... ..        ..             .        .    ...        . *       . .  .      .       .   . .      1
 10  10.0 -  16.0  P              ... ..        ..             .        .    ....       . *       . .  .      .       .   . .      0
 11   1.0 -   2.0  P              ... ..        ..             .        .    ...          .       . .  .      .       .   . .      0
 12   2.0 -   3.0  P              ... ..        ..             .        .    ...          .       . .  .      .       .   . .      0
 13   1.0 -   3.0  S    *         ... .*..      ..             .        .    ...          .              *    . *     .   . .      3
 14   1.5 -   3.5  S    * *       ...:*:..      ..        *    .        . *  ...          .              *    . .     .   . .      6
 15   2.0 -   4.0  S    * *       * ...:*:..    ..        *    .        .    ...          .                   . .     .   . .      5
 16   2.5 -   4.5  S      *       * ...:*:..    ..        *    .        . *  ...          .                   . .     .   . .      0
 17   3.0 -   5.0  S              ... ..        ..             .        .    ...          .                   . .     .   . .      0
 18   3.5 -   5.5  S              ... ..        ..             .        .    ...          .                   . .     *   . .      1
 19   5.0 -   7.0  S              ... ..        ..             .        .    ...          .                   . .     .   . .      0
 20   6.5 -   8.5  S              ... ..        ..             .        .    ...          .                   . .     .   . .      0
 21   8.0 -  16.0  S              ... ..        ..             .        .    ...          .                   . .     .   . .      0
 22  10.0 -  16.0  S              ... ..        ..             .        .    ...          .                   . .     .   . .      0
 23   1.0 -   2.0  S              ... ..        ..             .        .    ...          .                   . .     .   . .      1
 24   2.0 -   3.0  S              ... ..        ..             .        .    ...          .                   . .     .   . .      2
 25   1.0 -   3.0  V              ... ..        ..             .        .    ...          .            *      . .     .   . .      3
 26   1.5 -   3.5  V              ... ..        ..             .        .    ...          .   *          *    . .     .   . .      4
 27   2.0 -   4.0  V    *         ...:*:..      ..             .        .    ...          .               *   . .     .   . .      1
 28   2.5 -   4.5  V    *         ...:*:..      ..             .        .    ...          .              *     . .    .   . .      0
 29   3.0 -   5.0  V              ... ..        ..             .        .    ...          .              *     . .    .   . .      1
 30   3.5 -   5.5  V              ... ..        ..             .        .    ...          . *                  . .    .   . .      2
 31   5.0 -   7.0  V              ... ..        ..             .        .    ...       *  . *                  . .    .   . .      2
 32   6.5 -   8.5  V              ... ..        ..             .        .    ...       *  . *                  . .    .   . .      2
 33   8.0 -  16.0  V              ... ..        ..             .        .    ...       *  . *                  . .    .   . .      0
 34  10.0 -  16.0  V              ... ..        ..             .        .    ...          . *                  . .    .   . .      4
 35   1.0 -   2.0  V    * *       ...:*:..      ..             .        .    ...          .          *         . .    .   . .      5
 36   2.0 -   3.0  V              ... ..        ..             .        .    ...          .                    . .    .   . .      6
 37   1.0 -   3.0  H              ... ..        ..             .      *  .    ..        **  . *    *  .** *     .      .   . .      9
 38   1.5 -   3.5  H    * *       ... ..        ..             .    *    .    ..        *   . *   * .  .** *    .      .   . .     12
 39   2.0 -   4.0  H    * *       ...:*:..      ..        *    .    *    .    ..        *   . *     .  .** *    .      .   * .     14
 40   2.5 -   4.5  H    * *       ... *...      ..        *    .    .  *  **  . *      ** * .*.    * .  .* *    .      . *  . .    22
 41   3.0 -   5.0  H    * *       ... *...      ..        *   *. ****  * *.  ** .*      *  .** *  *. *  .* *    .      . *   .  .   33
 42   3.5 -   5.5  H    ***       ***...      ..        * *  ** **** * .*   ** .*    * **. ** *  *. *  .* *    .      . * *   . **  42
 43   5.0 -   7.0  H   **** *  **** .*..       ..    *  ** **** *  .* **** ** .*  * **  * .** *. * *.  .** *   .   ** . *  *. * **  65
 44   6.5 -   8.5  H   ** *** ****:.  *. .  ******:. ***** ***** * ***** ** .*  ** * *  . ** *.* * *.  .*** ** *  *** .** *. * **   66
 45   8.0 -  16.0  H  *** ********:.  *. ******* ..* ***** ***** ***** ..  ** ** *  *. . *** .:* * *  .** *** .***** *.** * *       65
 46  10.0 -  16.0  H  *** ********:.  *. *******. .* ****** ***** ****** ..  ** *  *.  . ***.:* * *  .** ****.***** *.** * *        66
 47   1.0 -   2.0  H              ... ..        ..             .        .    ...          *         . *     .      .   . .         2
 48   2.0 -   3.0  H    *         ...:*:..      ..             .      *  .    ...          .          . * *   .      .   . .       5
```

Table VII.6.3 c) This table shows the 'valid' detections for all Sn phases in the data base.

Event number

No.	Beam type			10	20	30	40	50	60	70	80	90	100	#valid entries
1	1.0 -	3.0	P											0
2	1.5 -	3.5	P											2
3	2.0 -	4.0	P											21
4	2.5 -	4.5	P											10
5	3.0 -	5.0	P											18
6	3.5 -	5.5	P											34
7	5.0 -	7.0	P											3
8	6.5 -	8.5	P											0
9	8.0 -	16.0	P											2
10	10.0 -	16.0	P											2
11	1.0 -	2.0	P											0
12	2.0 -	3.0	P											0
13	1.0 -	3.0	S											4
14	1.5 -	3.5	S											18
15	2.0 -	4.0	S											35
16	2.5 -	4.5	S											48
17	3.0 -	5.0	S											39
18	3.5 -	5.5	S											40
19	5.0 -	7.0	S											7
20	6.5 -	8.5	S											11
21	8.0 -	16.0	S											5
22	10.0 -	16.0	S											2
23	1.0 -	2.0	S											0
24	2.0 -	3.0	S											0
25	1.0 -	3.0	V											30
26	1.5 -	3.5	V											40
27	2.0 -	4.0	V											45
28	2.5 -	4.5	V											43
29	3.0 -	5.0	V											36
30	3.5 -	5.5	V											40
31	5.0 -	7.0	V											22
32	6.5 -	8.5	V											11
33	8.0 -	16.0	V											2
34	10.0 -	16.0	V											1
35	1.0 -	2.0	V											26
36	2.0 -	3.0	V											33
37	1.0 -	3.0	H											23
38	1.5 -	3.5	H											28
39	2.0 -	4.0	H											24
40	2.5 -	4.5	H											32
41	3.0 -	5.0	H											38
42	3.5 -	5.5	H											49
43	5.0 -	7.0	H											23
44	6.5 -	8.5	H											23
45	8.0 -	16.0	H											17
46	10.0 -	16.0	H											9
47	1.0 -	2.0	H											19
48	2.0 -	3.0	H											17

Table VII.6.3 d) This table shows the 'valid' detections for all Lg phases in the data base.

a)

Beam 10	10.0 - 16.0 P	:	60 entries	
Beam 6	3.5 - 5.5 P	:	22 entries	
Beam 7	5.0 - 7.0 P	:	5 entries	96%
Beam 9	8.0 - 16.0 P	:	4 entries	
Beam 22	10.0 - 16.0 V	:	3 entries	

Beam 4	2.5 - 4.5 P	:	2 entries	
Beam 5	3.0 - 5.0 P	:	1 entry	4%
Beam 27	2.0 - 4.0 V	:	1 entry	

Total number of detected Pn-phases : 98

b)

Beam 6	3.5 - 5.5 P	:	38 entries	
Beam 4	2.5 - 4.5 P	:	8 entries	
Beam 16	2.5 - 4.5 S	:	6 entries	
Beam 8	6.5 - 8.5 P	:	4 entries	
Beam 31	5.0 - 7.0 V	:	4 entries	97%
Beam 13	1.0 - 3.0 S	:	3 entries	
Beam 25	1.5 - 3.5 V	:	3 entries	
Beam 18	2.5 - 5.5 S	:	2 entries	

Beam 3	2.0 - 4.0 P	:	1 entry	3%
Beam 20	6.5 - 8.5 V	:	1 entry	

Total number of detected Pg-phases : 70

c)

Beam 46	10.0 - 16.0 H	:	66 entries	
Beam 41	3.5 - 5.5 H	:	7 entries	
Beam 43	5.0 - 7.0 H	:	3 entries	96%
Beam 32	6.5 - 8.5 V	:	2 entries	
Beam 14	1.5 - 3.5 S	:	1 entry	

Beam 19	5.0 - 7.0 S	:	1 entry	
Beam 37	1.0 - 3.0 H	:	1 entry	4%
Beam 44	6.5 - 8.5 H	:	1 entry	

Total number of detected Sn-phases : 82

d)

Beam 42	3.5 - 5.5 H	:	49 entries	
Beam 25	1.0 - 3.0 V	:	19 entries	
Beam 35	1.0 - 2.0 V	:	7 entries	96%
Beam 16	2.5 - 4.5 S	:	6 entries	
Beam 27	2.0 - 4.0 V	:	3 entries	

Beam 20	6.5 - 8.5 S	:	2 entries	4%
Beam 37	10.0 - 16.0 P	:	1 entry	

Total number of detected Lg-phases : 87

Table VII.6.4 (a-d) In these tables we give the beam priority lists
for detection of Pn, Pg, Sn and Lg phases that result
from applying the iterative procedure to each phase
type individually.

			Number of traces to be filtered	Number of beams to be formed
Beam 46	10.0 - 16.0 H	:	8	1
Beam 10	10.0 - 16.0 P	:	4	4
Beam 42	3.5 - 5.5 H	:	8	1
Beam 6	3.5 - 5.5 P	:	4	4
Beam 41	3.5 - 5.5 H	:	8	1
Beam 35	1.0 - 2.0 V	:	17	1
Beam 16	2.5 - 4.5 S	:	6	6
Beam 7	5.0 - 7.0 P	:	4	4
Beam 9	8.0 - 16.0 P	:	4	4
Beam 8	6.5 - 8.5 P	:	4	4
Beam 31	5.0 - 7.0 V	:	22	1
Beam 22	10.0 - 16.0 V	:	22	1
Beam 13	1.0 - 3.0 S	:	6	6
Beam 25	1.5 - 3.5 V	:	17	1
Beam 43	5.0 - 7.0 H	:	8	1
Beam 18	2.5 - 5.5 S	:	6	6
Beam 32	6.5 - 8.5 V	:	22	1
Beam 14	1.5 - 3.5 S	:	8	8
			178	55
Symmetric deployment		:	222	99

Table VII.6.5 From the results produced by the iterative procedure with each phase type treated individually, the beam deployment given in this table was inferred. For each phase type, this beam deployment cover 96% of the 'valid' detections. We have also given the number of traces to be filtered and the number of beams to be formed. To cover the North Sea / western Norway region 178 traces must be filtered and 55 beams formed. To span all azimuth directions by the coherent beam deployment the numbers will be 222 and 99, respectively. Note that for incoherent beamforming, each individual trace must be filtered prior to the beamforming.

			Number of traces to be filtered	Number of beams to be formed
Beam 46	10.0 - 16.0 H	:	8	1
Beam 10	10.0 - 16.0 P	:	4	4
Beam 42	3.5 - 5.5 H	:	8	1
Beam 6	3.5 - 5.5 P	:	4	4
Beam 25	1.0 - 3.0 V	:	17	1
Beam 4	2.5 - 4.5 P	:	4	4
Beam 8	6.5 - 8.5 P	:	4	4
Beam 39	2.0 - 4.0 H	:	8	1
Beam 35	1.0 - 2.0 V	:	17	1
Beam 18	3.5 - 5.5 S	:	6	6
Beam 31	5.0 - 7.0 V	:	22	1
Beam 22	10.0 - 16.0 V	:	22	1
Beam 7	5.0 - 7.0 P	:	4	4
			128	33
Symmetric deployment		:	154	59

Table VII.6.6 The beam deployment of this table was produced by the iterative procedure when treating all phases at the same time, after first having required that beam nos. 46, 10, 42 and 6 should be included in the final deployment. Compared to the results presented in Table VII.6.5, the volume of the beam deployment is considerably reduced.

			Number of traces to be filtered	Number of beams to be formed
Beam 46	10.0 - 16.0 H	:	8	1
Beam 10	10.0 - 16.0 P	:	4	4
Beam 42	3.5 - 5.5 H	:	8	1
Beam 6	3.5 - 5.5 P	:	4	4
Beam 25	1.0 - 3.0 V	:	17	1
Beam 4	2.5 - 4.5 P	:	4	4
Beam 8	6.5 - 8.5 P	:	4	4
Beam 39	2.0 - 4.0 H	:	8	1
Beam 35	1.0 - 2.0 V	:	17	1
Beam 31	5.0 - 7.0 V	:	22	1
Beam 22	10.0 - 16.0 V	:	22	1
Beam 7	5.0 - 7.0 P	:	4	4
Beam 9	8.0 - 16.0 P	:	4	4
Beam 29	3.0 - 5.0 V	:	22	1
			148	32
Symmetric deployment		:	172	56

Table VII.6.7 The procedure for finding the results given in this table, is essentially the same as outlined for Table VII.6.6. The only difference is that we have not allowed any S-beams to be included in the final beam deployment.
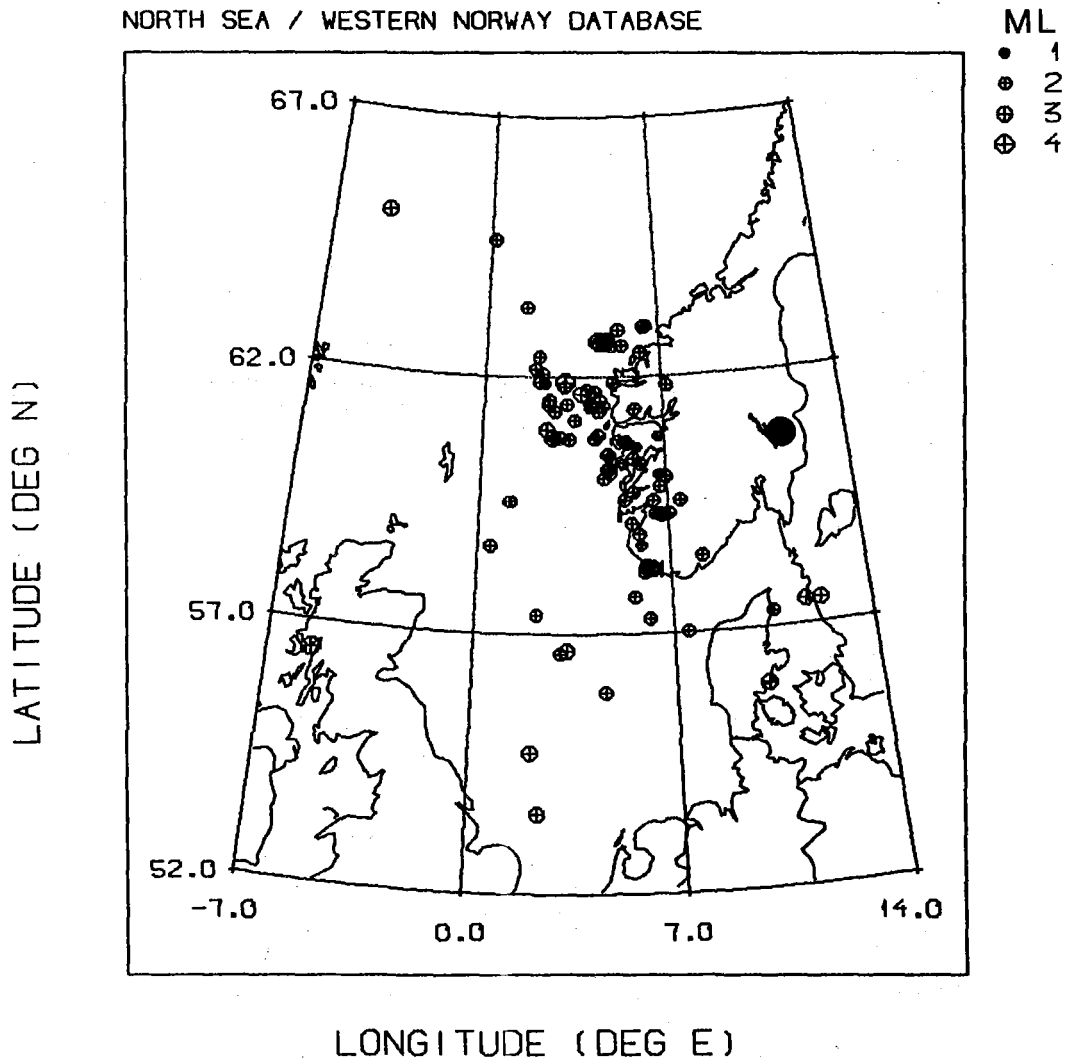
NORTH SEA / WESTERN NORWAY DATABASE

Fig. VII.6.1 The figure shows the locations of the 101 events in the North Sea / western Norway data base. The loaction of the NORESS array is indicated by a filled circle.
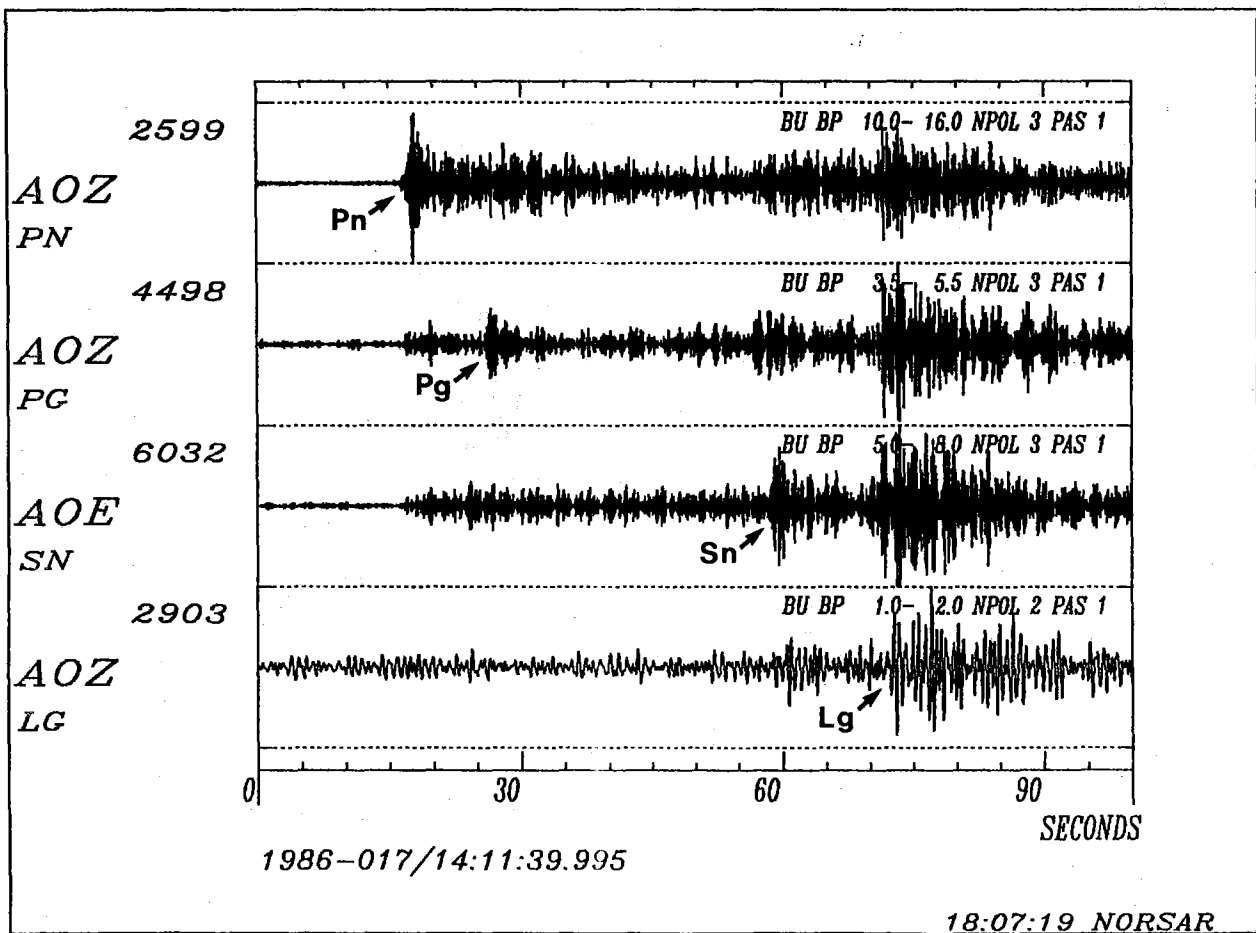
Fig. VII.6.2 To identify the different regional phases and pick
their arrival times, several filters were applied to
both the vertical and horizontal components. This
figure shows filtered NORESS recordings from an event in
southwestern Norway. The distance from NORESS is about
400 km and the local magnitude is 2.7.

VII.7   Local geology of the regional array sites in Norway

Information on local geological conditions at the NORESS and Finnmark array sites is available from various sources. In this contribution, we have attempted to compile information that is considered relevant from the seismological viewpoint. In particular, such information may be used to provide tentative explanations of certain observed features in the seismograms.

Local geology of the NORESS site

The NORESS site is located within the Precambrian (also referred to as pre-Eocambrian) rock complexes of southeastern Norway. Maps showing the local geology of the siting area have not yet been published. However, geologists of the Norwegian Geological Survey have conducted surveys in the area and have made available to us hand-colored maps of the local surface geology. These maps show that three different rock types are present at the array site, namely: (1) granite, (2) gabbro and (3) rhyolite. The information in these maps is transcribed onto the array configuration map of Fig. VII.7.1.

Johnson and Olheft (1984) and Bott (1982) give the following typical values for density and P-wave velocities (at a pressure of 0.3 Kbar, corresponding to a depth of 1 km) for these rock types:

	Density (g/cm^3)	Velocity (km/s)
Granite	2.66	5.91
Gabbro	2.99	6.74
Rhyolite	2.60	–

One should keep in mind that these values represent averages over a large number of samples from various geological environments. Wwe think, however, that these values could be used, with due care, for

the site considered here. For instance, such values can be used to
estimate reflection coefficients of possible subsurface interfaces.

The possible existence of such interfaces beneath the array can be
inferred from data from a reflection seismic survey that was carried
out in 1983. Reflection data were collected along the profiling line
shown in Fig. VII.7.1. The length of the line was approximately 2500 m
and charges of 1.4 kg of explosives were fired in 8 m deep boreholes
spaced at 40 m intervals along the profile. Each shot was recorded on
a spread of 24 geophones at 20 m intervals, with a constant distance
of 120 m between the shot and the nearest geophone. The data were
recorded using NORSAR's reflection profiling instrumentation (Texas
Instruments DFS-V). A sampling rate of 2 ms was chosen, and the analog
filters had cutoffs at 8 and 256 Hz. The recording interval was 20 s
for each shot. The field work and subsequent processing of the data
was organized and carried out by NORSAR personnel, notably Håvar
Gjøystdal, Paul W. Larsen and Ottar A. Sandvin.

The data were subjected to conventional CDP-stacking with a 10 m
interval between consecutive traces in the stacked section, giving a
6-fold coverage (except at the ends of the profile). The section shown
in Fig. VII.7.2 resulted from this processing and shows the data
filtered in the 100-250 Hz band. The section covers a two-way travel
time (TWT) of 0.0-1.0 s.

Several interesting features can be observed in the section of Fig.
VII.7.2. First of all, we see a dipping interface that appears to
intersect the surface near the southern end of the profile. The TWT of
0.37 s observed at the northern end of the profile indicates a depth
of roughly 1 km at that point, giving a dip of approximately 20°.
Based on the available information on the surface geology, we specu-
late that this horizon represents the interface between the granite

and the gabbro, which is outcropping near the southern end of the pro-
file, see Fig. VII.7.2. The reflection coefficient resulting from den-
sity and velocity changes across a granite/gabbro interface could
become significant and would be of the order of 0.12, using the values
given above.

In addition to this dipping interface, there are at least two clearly
observable events in Fig. VII.7.2. One of these is dipping across the
middle of the section at around 0.5-0.6 s TWT, and the other is an
apparently flat horizon at about 0.8 s TWT. Suffice it here to point
to these arrivals, without going any further into geological interpre-
tations.

The recording interval of 20 s for each shot made it possible to look
for coherent arrivals from depths even larger than the base of the
crust. Extensive plotting of sections for TWT intervals within the
1.0-20.0 s range only revealed one such arrival that could be traced
over any length of distance and tentatively attributed to a definite
structure at depth. This event is seen at about 5.5 s TWT in the
middle of the section of Fig. VII.7.3. The corresponding depth would
be approximately 18 km.

Local geology of the Finnmark array site

Only very limited information is yet available on the local geology of
the new regional array site in Finnmark, northern Norway. The Nor-
wegian Geological Survey has published a regional geological map of
the Karasjok, Finnmark area (Skålvoll, 1972). This map shows that all
seismometers of the new array are within an outcropping gabbro for-
mation approximately 4 x 10 km large. This gabbro window is located
within the Karasjok Group, which consists of metamorphic sedimentary
and igenous rocks of age 2000 million years. It is therefore reason-
able to assume the existence of high-density, high-velocity material

at the surface all across the new array. The possible existence of subsurface layering is, however, unknown at this time.

S. Mykkeltveit

References

Bott, M.H.P. (1982): The Interior of the Earth: Its Structure, Constitution and Evolution. Second Ed., Edward Arnold, London.

Johnson, G.R. and G.R. Olhoeft (1984): Density of rocks and minerals, In: CRC Handbook of Physical Properties of Rocks, Vol. III. R.S. Carmichael, ed., CRC Press, Boca Raton, Florida.

Skålvoll, H. (1972): Beskrivelse til geologisk kart over Norge 1:250 000, Karasjok. Norges Geologiske Undersøkelse.
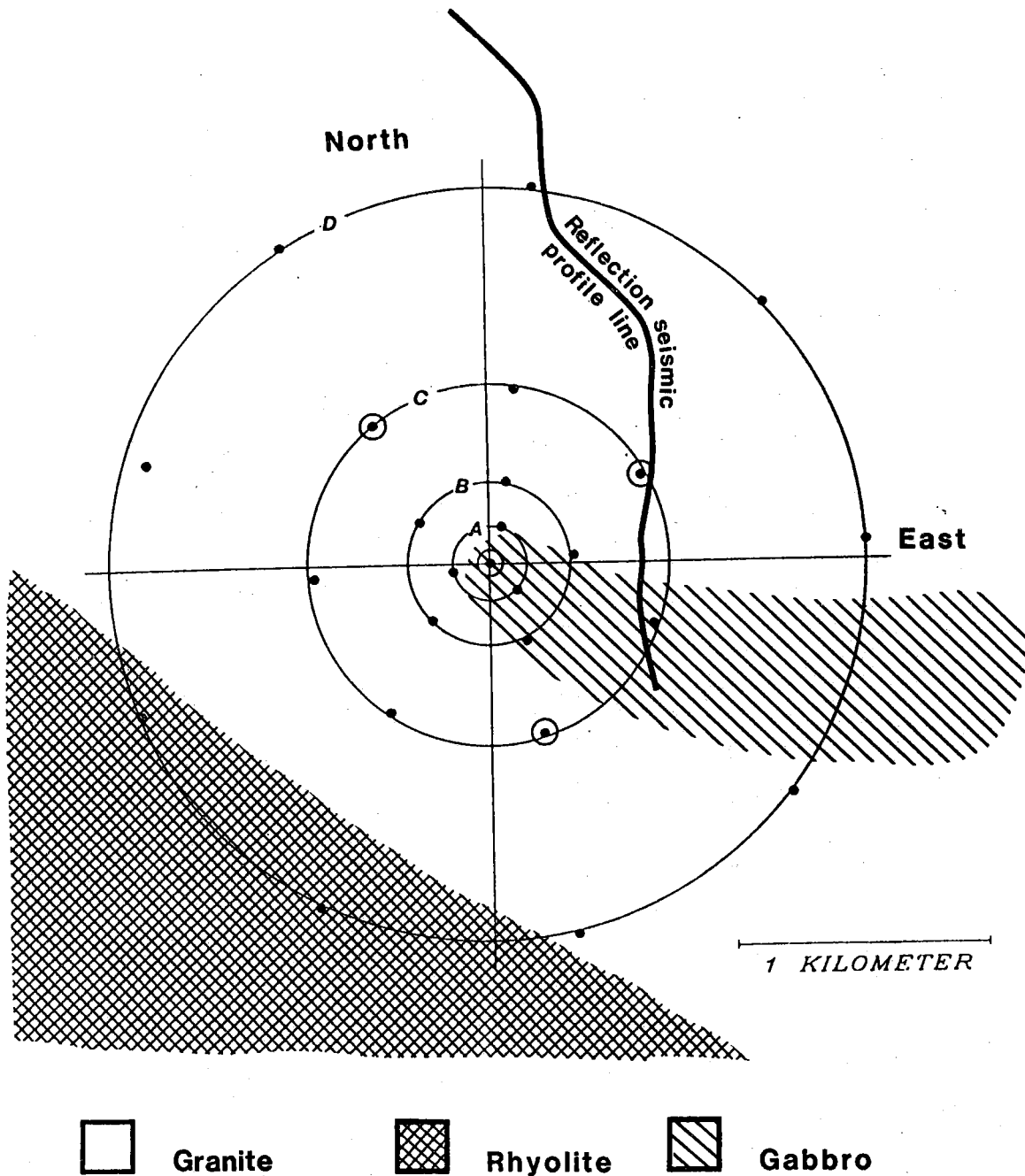
Fig. VII.7.1 Configuration and local geology of the NORESS array. The
four three-component stations are marked with special
symbols. The station at the center of the array is named
A0. The surface geology of the site is transcribed from
a map provided by the Norwegian Geological Survey. A 60
m deep borehole was drilled at site A0. According to the
drilling log, this hole was drilled in gabbro all the
way down to its bottom. A reflection seismic survey was
conducted with shots and geophones along the line
running into the array from the north.

Fig. VII.7.2 CDP-stacked section, for the TWT interval 0.0-1.0 s. The filter used was 100-250 Hz.

REGIONAL ARRAY EXPERIMENT

Fig. VII.7.3 CDP-stacked section, for the TWT interval 4.0-6.0 s. The filter used was 20-120 Hz.